THE UNIVERSITY OF MICHIGAN

THE MEASUREMENT AND USE OF SCATTERING MATRICES

by

J. W. Crispin, Jr., R. E. Hiatt, F. B. Sleator and K. M. Siegel

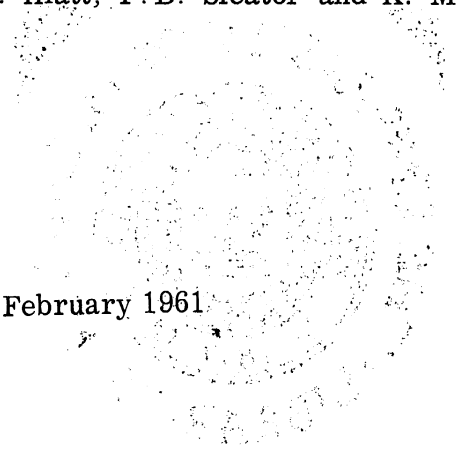

February 1961

2500-3-T

Aeronutronic
a division of
Ford Motor Company
Space Technology Operations
Newport Beach, California

The work reported in this document was performed under Contract AF 33(600)-39476. This work was completed in January 1960 .

TABLE OF CONTENTS

TABLE OF CONTENTS
(Continued)

LIST OF FIGURES

LIST OF FIGURES
(continued)

LIST OF TABLES

ABSTRACT

An experimental and theoretical investigation of the reflection characteristics of an IRBM type missile is described. The complete scattering matrix was determined for several aspects for the Jupiter C with and without the tail fins and for the Jupiter C nose cone. Good agreement was found between experimental and theoretical data. Experimental data from "unknown" models was analyzed to determine the possibility of identifying a target by means of scattering matrix data.

Section I

SUMMARY

Purpose

It is the aim of this program of study under contract AF 33(600)-39476 to investigate the feasibility of estimating, from radar data, the sizes and/or the configurations of the targets under observation as well as such characteristics of the target's motion as the angular velocities of axial rotation and tumbling and the inclination of the target axis relative to the mass-center trajectory.

Discussion

The general approach to be used in gleaning such information from radar data was presented in Reference 1: this material is reviewed in Section II. With the work being done currently by several organizations on the development of radar equipment appropriate for measuring scattering matrices, additional theoretical and experimental experience on scattering matrices of complex shapes has become highly desirable. The effort reported herein is for the most part devoted to the subject of getting this experience: that is, to the question of how and to what degree of accuracy one can predict the above target characteristics via scattering matrix measurements. We have concentrated on one complex shape, a Jupiter-type Missile.

As pointed out in Section II efficient use of matrix measurement techniques for estimating size and motion parameters requires simultaneous

measurements at several frequencies. It is pointed out, however, that often much can be learned from measurements at one or two frequencies, and we shall concentrate on this topic since in gaining experience one should start gradually. The experimental and theoretical analysis reported here has three primary aims: (1) to determine the precision with which one can measure the scattering matrix in the laboratory, (2) to obtain an estimate of the accuracy with which one can predict the experimental results using rapid optics-type approximation techniques, knowing the configuration and the aspect, and (3) to illustrate how one can determine size and shape information from experimentally measured values of the scattering matrix elements and to simultaneously obtain an estimate of how accurate such predictions of size actually are.

We have considered three sample target configurations: the Juptier Missile Nose Cone, a Jupiter-type Missile with fins, and the Jupiter-type Missile without fins. We also give some consideration to a few unknown shapes, (unknown to the individual studying the matrix data). The procedure we have followed has been to measure in the laboratory (laboratory wavelength was 1.22", i.e., the operating frequency was 9700 Mc) the return from models of these targets for six different polarization cases; both amplitude and phase were measured. This was done for a set of monostatic aspect situations with the return from a sphere of known

size being used for calibration purposes. These measured values were then analyzed to determine the degree of consistency in the measurements and the scattering matrix associated with each aspect. For convenience aspects were confined to the horizontal plane. While these quantities were being measured in the laboratory, theoretical calculations were also made, restricting attention to the range of aspects studied experimentally. Since our interest here deals primarily with the accuracy with which the matrix elements can be determined rather than full-scale data for these targets, we make no attempt to convert the cross section data to full-scale dimensions. Instead we shall work with the model data itself.

The experimental procedure and the techniques employed in reducing the data are discussed in detail in Section III while the theoretical approach is discussed in Section IV. Section V is devoted to the consideration of a few samples of what can be gleaned about size and shape from data obtained in the laboratory assuming no knowledge about the configuration itself.

Conclusions

We have observed that good matrix data can be obtained in the laboratory at target aspects corresponding to fairly strong signals. When attempting these matrix measurements in the laboratory at aspects where the reflected signal is relatively weak, it has been found that good data are difficult to obtain. This comes as no surprise because of the power limitations, etc., of our

laboratory equipment and does not present any serious obstacle to the plan of using matrix data to determine size and shape information, since we would expect to concentrate analysis on "strong-signal" data. Interest in weak-signal data can be centered on where they occur aspect-wise, rather than the actual amplitudes involved.

The methods employed to check the consistency of a set of matrix measurements in this study seem to be adequate; however it is felt that further study on this point would be desirable. That is, further investigation would be advantageous to optimize the methods used in reducing the raw matrix measurements. The work reported here indicated that theory and experiment for matrix determination are in good agreement for those cases in which both "good" experimental data are obtained and the theoretical technique employed is appropriate.

In order to develop this scattering matrix type of analysis further and to demonstrate its usefulness, it would be desirable to carry out relatively extensive detection and identification problems in the laboratory. This could be done in the form of "war games" between the experimental group and the theoretical group, the first making the measurements and the second analyzing the experimental data. A first step along these lines is discussed in Section V; the results of the "games" are sufficiently promising to indicate that additional study along these lines would be highly desirable.

The results of the studies reported here support the contention that this approach to the problem of determining size and shape information, as well as characteristics of the target's motion, can yield reliable information. The "games" discussed in Section V illustrate that reliable estimates of size and shape can often be obtained even though only limited data are available. It appears obvious that there is much to be gained by a continuation of an effort directed toward optimizing the methods of analyzing the measurements.

Section II

GENERAL COMMENTS ON THE DETERMINATION OF SIZE AND MOTION RELATIVE TO MASS-CENTER TRAJECTORY

2.1 No Intervening Magneto-Ionic Medium

The problem of determining configuration and motion relative to the center of mass of an arbitrary object traveling at orbital altitude and velocity, e.g. an artificial earth satellite, by analyzing radar returns is discussed in this Section. It is assumed that the orbit or trajectory of the center of mass is known.

To explain the procedure used to develop this information in general, the simpler problem in which electromagnetic radiation suffers no rotation of electric (or magnetic) vector as it traverses its path to and from the target, i.e., with no intervening magneto-ionic medium (the ionosphere), is considered first. The cas of an intervening medium of this type is discussed in Section 2.2. The problem of determining the size and shape of the object as well as its spin and tumbling rates remains, as expected, quite a sizeable one. Ideally, the problem can be solved by providing a sufficient amount of radar data. This would include measurement of the complete scattering matrix continuously at at least four frequencies simultaneously. In this section, however, a more modest approach is considered; ways in which spin rates, tumbling rates, and size and shape information may be

deduced from less than ideal amounts of radar data are considered.

In essence, the procedure is based on the following: If the field scattered by a target is specified completely at all points in space, for any one instant in time, then the target size and shape is completely determined.* Since, however, many of the bodies of interest are satellites or missiles which are restricted to certain physical shapes, it is not necessary to know the scattered field everywhere; in fact a few measured values of radar cross section may suffice to provide a gross picture. By measuring the variation in cross section with time, the motion of the body (motion relative to the trajectory of the center of mass**) can be determined. These same data can be used to refine the original picture as described below.

In order to investigate systematically the scattering properties of the target, the formalism of scattering matrices is employed. The scattered electric far field can be formally expressed in terms of the incident electric field as

$$\vec{E}^s = \left[A\right] \vec{E}^i, \tag{2-1}$$

where the superscript "s" indicates scattered, and "i", incident. When, for

* In fact, the system is over-determined; that is, there will be a large amount of redundant information.

** The use of radar to provide trajectory information is standard procedure and cannot rightfully be included in this report.

any incident direction and polarization, this relation determines $\vec{E}^s$ for all field points, then $[A]$ is called the complete scattering matrix. In this treatment only backscattering is considered; hence the elements of the scattering matrix for a particular incident field and target orientation are constant. $[A]$ in general is a 3 x 3 matrix, but because the radial component of the far field behaves like $1/r^2$, compared with the components in the plane perpendicular to the direction of propagation which behave like $1/r$, $[A]$ is thus made 2 x 2 for simplicity. In order to specify $\vec{E}^s$ for an arbitrary incident polarization (i.e., direction of $\vec{E}^i$) the elements of the scattering matrix $[A]$ must be specified. This involves evaluating eight quantities, since these elements are, in general, complex numbers. The number of quantitites can be reduced immediately to seven since absolute phase is not of importance. It is necessary to consider only relative phases; thus any one of the four elements can be taken to be real.*

If the z-axis is taken along the direction of incidence, the equations for the field components can be written in the form

$$E_x^s = A_{11} E_x^i + A_{12} E_y^i$$

$$E_y^s = A_{21} E_x^i + A_{22} E_y^i \qquad (2\text{-}2$$

It is the set of complex numbers A_{ij} that must be determined. For the case in which

* The reader is referred to References 2 and 3 for additional discussions on the subject of scattering matrices.

there is no rotation of the $\vec{E}$ vector, reciprocity dictates that $A_{12} = A_{21}$; for the case under discussion this means that only five quantities need be evaluated rather than the seven mentioned above.

It can readily be shown that the scattering matrix can be determined by measuring $\sigma(AA)$, $\sigma(AB)$, $\sigma(BB)$ and any two of the three phases associated with these amplitudes, where $\sigma(IJ)$ denotes the cross section measured when the transmitted energy has the polarization J and the receiver polarization is along the direction I, and the symbols A and B designate two mutually orthogonal directions in the HV-plane with H used to indicate the horizontal direction and V the vertical direction (perpendicular to the horizontal and the direction of incidence). This is not, however, the only way one can determine the matrix. For convenience we might take A = H and B = V. Making this set of measurements for the body as it passes by the radar enables one to determine a scattering matrix (as a function of time) from which a considerable amount of data can be obtained. As stated previously, a first approximation to the size and shape of the target can be obtained from these measured values at one instant in time, when considered together with a knowledge of the target's physical limitations.

By analyzing the variation of these measured values with time, the motion of this first approximation to the configuration is determined so as to be compatible with the measured variations. The measured values at another instant of time are then examined, and the approximation to the configuration

modified accordingly. This, of course, may alter the postulated motion. As more and more of the data are thus employed, the picture of the object and its motion becomes more refined. With a judicious initial estimate of size and motion parameters, this refinement will occur quite rapidly.

This process can be illustrated by considering a few special cases. As a first example, these data can be used to distinguish between elongated bodies and bodies which are essentially spherical, since a long, thin body exhibits a cross section which is quite polarization-dependent while a body which is essentially spherical does not exhibit a polarization-dependent cross section. Consider a measurement in which, for example, σ(HH) is fairly large with respect to σ(VV). This indicates that the body is long and narrow with the length of the body (in the horizontal direction) large in comparison with the wavelength, and the diameter of the body (in the vertical direction) not large in comparison with the wavelength. In order to discriminate between cylinders and spheroids it may be necessary to measure returns at more than one frequency or to obtain the scattering matrix for 30^{o} in aspect (not a hard requirement if the body is tumbling). This is discussed more fully below, but for the present example consideration is confined to the case in which measurements are obtained at one frequency and the large values of σ correspond to broadside looks.

Measured values of σ(HH), σ(VV), σ(HV), etc., all plotted as a function of time would be available. Assume that σ(HH) takes on a peak value at $t = t_1$

and that σ(VV) is relatively small at $t = t_1$; assume further that at $t = t_2$, σ(VV) is relatively large with respect to σ(HH), and that this value of σ(VV) is the same as the value of σ(HH) obtained at $t = t_1$. The fact that the two relative peak values were the same would suggest that the body was broadside at both $t = t_1$ and $t = t_2$ and tumbling in a plane normal to the direction of incidence. Taking $t_2 - t_1 = \Delta t_1$ (particularly if this pattern of variation in σ(HH) and σ(VV) is continued), it is implied that the body makes one complete revolution in $4 \Delta t_1$ seconds, and thus that the tumbling rate is $1/(4\Delta t_1)$ revolutions per second.

Assume, for the purpose of a second example, that σ(HH) takes on relative peak values at regular intervals equal to $\Delta t'$ but that σ(VV) does not take on any of these relative peak values. If these peak values of σ(HH) are all about the same, it would be reasonable to assume broadside aspect at the times these peak values were obtained. The fact that no equal peak values of σ(VV) were obtained would indicate that the body was tumbling in a plane which was <u>not</u> normal to the direction of incidence. In conjunction with size and shape estimates obtained from other time segments of the data it would be possible to estimate the aspect angle (angle off nose) by studying the magnitudes of σ(VV) at those times at which peak values would have been anticipated had it been assumed the body was tumbling in a plane normal to the direction of incidence. From the

data it would be concluded that the tumbling rate was $1/(2\Delta t')$ revolutions per second.

It should be noted that in the second example σ(HH) and σ(VV) were chosen as an illustration. The same argument would apply if σ(AA) attained relative peak values but σ(CC) did not attain these values, where A is any direction and C is any other direction. Thus a knowledge of σ(II) for many values of I is necessary for this kind of analysis. However, such values can be computed from the five measured quantities.

The above two examples serve to illustrate how size information and estimates of the tumbling rate can be obtained if it is determined that the body is long and thin. This is due to the fact that such a body yields a relatively large cross section if the $\vec{E}$ vector is parallel to the long axis of the body, but a relatively small cross section if the $\vec{E}$ vector is normal to the long axis of the body. Of course, if the body were spherical, then this approach would not yield any information about tumbling rates although it would yield information relative to the size of the body.

It is important to note that in the examples above, polarization dependence of cross sections would not be exhibited if the body were elongated and the diameter of the body were large in comparison with the wavelength* (in this case the

---

* In considering radar cross sections it is convenient to consider the wavelength spectrum as consisting of three regions: Rayleigh, Optics, and Resonance. The Rayleigh region is that region in which the wavelength is large in comparison to the characteristic dimensions of the body, the Optics region is that region in which the wavelength is very small in comparison to the dimensions of the scatter ing body, and the Resonance region is the region intermediate to the other two.

difference in peak cross sections due to polarization effects would be very small). Thus, in this case it is important to use another wavelength which can be expected to be comparable to or larger than the diameter of the body. Data gathered at wavelengths much smaller than the diameter of the body, however, can be used to study the wavelength dependence of the cross section and for this purpose it is convenient to have the wavelength small enough to permit application of the physical optics approximation. An upper limit on this range of wavelengths is obtained by requiring the wavelength to be smaller than the gross body dimensions (i.e., length, width, etc.). A lower limit is obtained from practical power limitations. An estimate of minimum dimensions can be obtained, in the case of missiles, from state-of-the-art limitations. It would be advisable to have sets of these data from at least two different frequencies in this range (taken simultaneously) so that the wavelength dependence of the cross section could be used to estimate size and shape.

To illustrate the use of wavelength dependence, it can be noted that the broadside cross section of a cylinder in the optics region varies like $1/\lambda$ while the broadside return from a spheroid or an ogive is relatively independent of the wavelength. Also, since the broadside cross section of an elongated body is a non-decreasing function of $1/\lambda$ while the off-broadside cross sections are oscillatory, aspect information can be gained.

Summarizing briefly, the advantages of measuring cross section at three frequencies - one in the resonance region (at the optics end) to determine

polarization dependence and two in the optics region to determine wavelength dependence - have been illustrated. This is not meant to imply that three is an optimum number of frequencies.

Considerable information can be obtained with measurements at only two frequencies, although the analysis becomes more complex. Similarly, with data at many frequencies a very complete picture can be determined without measuring all the elements of the scattering matrix. For example, in the Rayleigh region, the volume of the body can be determined from the dipole pattern and, if it is "fat", an idea of its length-to-width ratio obtained. Also, in the resonance region, length can be determined quite accurately by noting the number of maxima and minima which occur over a range in wavelength. If different frequency measurements are made simultaneously then the width could be determined by the length of the resonance region. In the optics region, singularities in the illuminated region could be determined from frequency data.

Concerning now the question of determining spin rates: If the body is a surface of revolution, it would be impossible to gain any information about spin by use of radar alone, since the body looks the same at all spin angles. Actually, sufficient knowledge of the configuration and precession would enable one to estimate the spin rate, even for a body of revolution. In order to determine the

spin rate directly, it is necessary that the body have some protuberances, e.g., fins, which in themselves will yield a measurable return.

Consider, as an example, the existence of fins. First consider the nose-on case (and the similar tail-on case). If the body has three or four fins symmetrically placed around the body, spin rates cannot be determined at this aspect by measuring σ(AA) since the return is independent of polarization. If the body should have only two fins, then the best estimates of spin rates are obtained at this aspect since the return from the fin edges would be highly dependent upon polarization. Thus if there was reason to believe that the aspect was essentially nose-on to the body, and the cross section was polarization dependent, it might be concluded that there were two fins. If no polarization dependence was exhibited at this nose-on aspect, it might be concluded that the body did not have two fins (it might have three or four or none). However, if σ(HV) shows no sensible variation there cannot be four, but there could be three or none. If, on analyzing σ(HA) for all directions A, no minimum appears, there are no fins. If three or four rectangular shaped fins were assumed, it would be possible to obtain an estimate of the lengths of the leading edges of these fins for the nose-on returns. To do this, use would be made of the fact that the returns from the three or four fins are all in phase, and thin-wire theory could be employed as the basis for investigating the return from these edges.

Where the body has three or four fins the best estimates of spin rates can be obtained at aspects which are close to broadside, since as the body

spins, the direction of incidence will be normal to the flat plate portion of a fin at certain intervals of time (which depend upon the spin rate). If the spin rate is greater than the tumbling rate the effect of spin (oscillations in the cross section) will be superimposed on the slower tumbling rate effect. To determine the spin rate and the area of each fin, those periods of time at which the data indicate broadside aspect would be concentrated upon. Suppose that σ(HH) was at an extreme maximum in the vicinity of $t = t''$ and that the remainder of the data in the vicinity of $t = t''$ indicates that the direction of incidence is essentially broadside. The faster spin effect would superimpose an oscillation on top of this peak and, by determining the difference between the maximum value and the average value in the vicinity of $t = t''$, an estimate of the return from a single fin (if there are three fins), or a pair of fins (if there are four fins) would be obtained. Then knowing how the cross section of a flat plate varies with area and wavelength, it would be possible to estimate the area of a fin. The spin rate could be determined by noting the number of times a small relative maximum superimposed on the tumbling rate effect occurs in each cycle of the latter and compensating this count by knowledge of the number of fins.*

---

* This problem could, of course, be more complicated if the fins were big enough to allow double reflections; the use of circular polarizations would determine the possible existence of double reflections.

The foregoing discussion has been an attempt to indicate how considerable information can be obtained about the body under investigation by measuring the scattering matrix. It is important to note that if this approach were used, σ(HH), σ(VV), σ(HV), etc., as functions of time and measured at (at least) two different frequencies would be necessary. One segment of data, by itself, could be made to yield estimates (or rather, ranges of estimates) relative to size, etc. Other segments of the data would either confirm or reject these estimates or, at least, serve to narrow down the range of estimates to be considered. If all that is available is, say, σ(HH) at one frequency, then it would be possible only to limit the discussion to various classes of bodies or ranges in size and shape.

2.2 With An Intervening Magneto-Ionic Medium

If an intervening magneto-ionic medium is present, the problem discussed in Section 2.1 becomes more difficult since now the $\vec{E}$ vector would have experienced a rotation. In this case seven independent measurements rather than five are needed to determine the scattering matrix, since σ(HV) and σ(VH) will now yield different results, i.e., reciprocity no longer holds. We might note that this can be used as a means of detecting the presence of the magneto-ionic medium

Essentially the same technique as described in Section 2.1 is to be applied; however, more measurements are required to gain the necessary

information. The problem of measuring the scattering matrix when the electric vector is rotated as it passes through the ionosphere is discussed in References 3 and 4. The fact that the amount of rotation, the Faraday angle, varies as the target moves introduces complications. The amount of rotation must be measured at each instant or an accurate picture of the variation in Faraday rotation with time and with target direction devised.

A discussion of various methods for determining the amount of Faraday rotation could be quite extensive. For our purposes here it will suffice to indicate but a few. [The British, for example, (Ref. 5) have utilized the signals from 1957 Alpha to obtain a measure of the Faraday rotation.] One method of determining the angle of rotation, independent of target emission, would place the energy sources with the receiver, i.e., monostatic radar. Electromagnetic energy could be transmitted at three or more frequencies and received at each frequency with two orthogonal antennas. This measurement of the rotation of the polarization direction would allow a determination of the integrated electron density of the ionosphere. If the measurement were repeated for several transits of the satellite, this would provide a measure of the variation of the integrated electron density with time. If the satellite is followed as it descends, it might be possible also to extract information as to the height distribution of the electrons. Operation at several frequencies is advantageous in order to

overcome the ambiguity in the rotation angle (which is measured only modulo π); certainly, tracking information would also help in this respect.

A possible alternative to the measurement of the rotation angle would be the measurement of the time delay between the arrival of left- and right-circularly polarized pulses. However, this time delay would probably be of the order of one period at radar frequencies.

In continuing this discussion of the analysis of radar data we shall assume that the Faraday angle is known for each measurement of the scattering matrix. With this angle known, operations can proceed in the manner outlined in Section 2.1, making sure in all considerations that this rotation is compensated for.

Suppose that the Faraday angle were 45°, then a case in which the return is dominated by σ(HV) would correspond to σ(HH) dominating in the "no rotation" case. If it were known that the Faraday angle was 30°, then it would be advisable to make the "A" polarization one which is inclined at an angle of 60°. This would make it possible to set up a correspondence between the σ(HA) measurement of this case and the σ(HH) value in the "no rotation" case. Of course with total scattering matrices available these other cases could be quickly computed.

Thus it is seen that if the Faraday angle and its variation are known, they can be compensated for in the analysis of the data obtained and, as in

Section 2.1, information concerning the size and shape of the object, tumbling rate, and, if there are measurable protuberances (like fins), its spin rate, derived.

In the procedure for investigating a satellite or missile with radar briefly outlined above, it has been indicated how information could be gained from specific radar measurements. In the ideal case, there is a sufficient amount of data, i.e., continuous measurements of the scattering matrix at many frequencies, to determine all of the size, shape, and motion parameters. In those cases for which there are not enough data to accomplish this, a technique for utilizing the available data together with other knowledge of the target to yield a partial picture of the situation has been outlined. Isolated measurements of the cross section at a given frequency and at a given polarization will yield some information about the target, but usually such information can only yield ranges of values of size and shape parameters.

Fortunately, in studying a satellite or a missile, information on the motion of such a body obtainable from sources other than the radar data can be used. For example, use can be made of the results obtained from a theoretical analysis of the mechanics of satellite motion. What is important here is to note that the results of the "non-radar" investigations can serve to limit the ranges

of the size and motion parameters which are to be determined from the radar data. It should also be noted that other information of a "radar type" is available such as range, velocity, trajectory, etc.

2.3 The Case Under Study

In the present analysis we are dealing with the measurement of scattering matrices in the laboratory and thus we assume the "no rotation" case of Section 2.1. Adopting the notation of Equation (2-2) where the direction of propagation is along the z-axis, we find that if the electric polarization vector of the incident field is denoted by $(\hat{x} \cos \phi_i + \hat{y} \sin \phi_i)$ and the polarization of the receiver is given by $(\hat{x} \cos \phi_r + \hat{y} \sin \phi_r)$, the field measured at the receiver will be given by

$$E^r/E^i = A_{11} \cos \phi_i \cos \phi_r + A_{22} \sin \phi_i \sin \phi_r + A_{12} \sin (\phi_i + \phi_r) , \tag{2-3}$$

(Ref. 3).

The geometry of the cases studied under the present program is somewhat restricted. The general case is shown in Figure 2-1 in which the coordinate systems of the target and the transmitter-receiver are displayed. We see that in general there are three angles of concern which correspond to azimuth, elevation, and roll. For the cases studied here we have taken $\gamma = 0^o$ and $\alpha = 0^o$ which implies that the y-axis is always normal to the x'y'-plane.

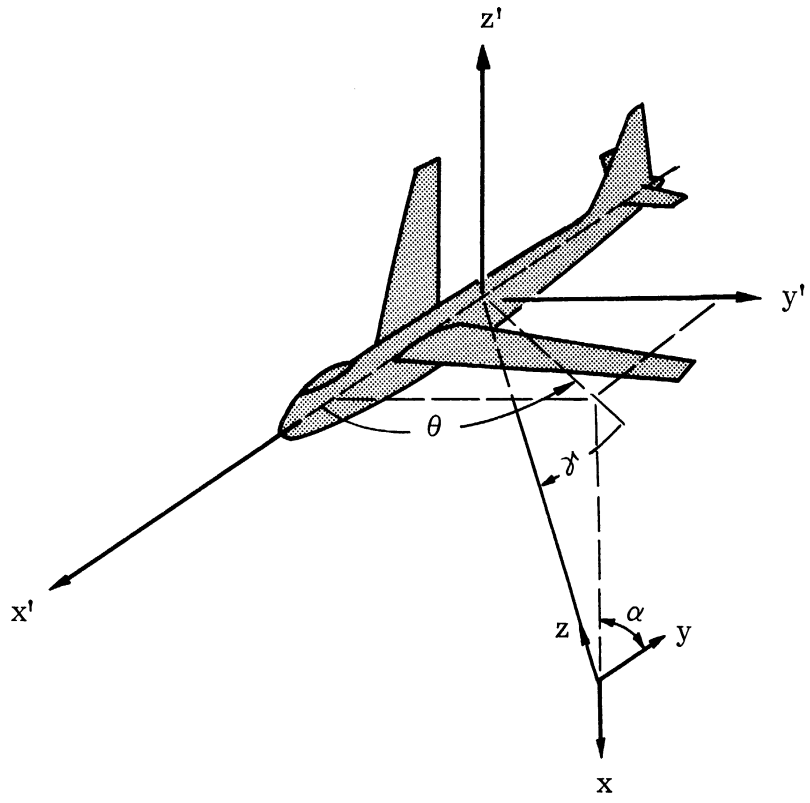

FIGURE 2-1: GEOMETRY FOR THE GENERAL CASE

Measurements of both amplitude and phase* have been made at various values of θ for the following six pairs of values for ϕ_i and ϕ_r

$$
\begin{aligned}
&(1) \quad \phi_i = \pi/2, \quad \phi_r = \pi/2 \\
&(2) \quad \phi_i = \pi/2, \quad \phi_r = \pi/4 \\
&(3) \quad \phi_i = \pi/4, \quad \phi_r = \pi/4 \\
&(4) \quad \phi_i = 0, \quad \phi_r = \pi/4 \\
&(5) \quad \phi_i = 3\pi/4, \quad \phi_r = 3\pi/4 \\
&(6) \quad \phi_i = 0, \quad \phi_r = \pi \quad .
\end{aligned}
\tag{2-4}
$$

If we denote E^r/E^i by $S(\phi_i, \phi_r)$ and the A_{ij} by $a_{ij} e^{i\Phi_{ij}}$ we thus see that we are obtaining the following for each value of θ selected:

$$
\begin{aligned}
&(1) \quad S(\pi/2, \pi/2) = a_{22} e^{i\Phi_{22}} \\
&(2) \quad S(\pi/2, \pi/4) = \frac{1}{\sqrt{2}} \left\{ a_{22} e^{i\Phi_{22}} + a_{12} e^{i\Phi_{12}} \right\} \\
&(3) \quad S(\pi/4, \pi/4) = \frac{1}{2} a_{11} e^{i\Phi_{11}} + \frac{1}{2} a_{22} e^{i\Phi_{22}} + a_{12} e^{i\Phi_{12}} \\
&(4) \quad S(0, \pi/4) = \frac{1}{\sqrt{2}} \left\{ a_{11} e^{i\Phi_{11}} + a_{12} e^{i\Phi_{12}} \right\}
\end{aligned}
\tag{2-5}
$$

---

* Obviously the phase measurements yield values of the relative phase since a movement of the target by 0.1 inch toward (or away from) the antennas would alter the measured phase angles by 60° at the frequency employed in these experiments.

$$(5) \qquad S(3\pi/4,\ 3\pi/4) = \frac{1}{2}\, a_{11}\, e^{i\Phi_{11}} + \frac{1}{2}\, a_{22}\, e^{i\Phi_{22}} - a_{12}\, e^{i\Phi_{12}}$$

$$(6) \qquad S(0,\ \pi) = -\, a_{11}\, e^{i\Phi_{11}} = a_{11}\, e^{i(\pi + \Phi_{11})} \quad .$$

In each case both the amplitude and phase of the $S(\phi_i,\ \phi_r)$ are measured.

The measurement procedures and the methods employed in reducing the data are discussed in the next section.

Section III

MEASUREMENT OF SCATTERING MATRICES IN THE LABORATORY

3.1 Instrumentation and Measurement Procedure

The number and nature of measurements which are sufficient to determine the scattering matrix have been discussed in Section II. The requirement of measuring both amplitude and phase placed two unusual demands on our equipment for measuring radar scattering characteristics. First, in the approach we employed, one must be able to adjust polarization quickly and easily. The direction of the new polarization must be known and any phase change introduced by the polarization change must be accurately known. Secondly, one must be able to measure the relative phase of the scattered signal to within a few degrees.

Other known experimental work on the measurement of scattering matrices of laboratory models include that of M. J. Ehrlich of the Microwave Radiation Company, Inc. (reported in Reference 6) and that of E. M. Kennaugh and associates at Ohio State University Research Foundation (see, for example, Ref. 7.) These investigators determined scattering matrix elements by the measurement of the amplitude of the scattered return for several combinations of linear and circular polarization. Scattering matrix measurements have also been made by the Dalmo Victor Company (see, for example, Reference 8,

This list is not intended to be exhaustive, but only representative. In the University of Michigan system, both amplitude and relative phase of the scattered signal were measured for six combinations of linear polarization. In this system, standard waveguide components and antennas were used throughout. The polarizations of the transmitter and receiver horns were changed by rotating them about their axes. A coaxial rotating joint supporting the horns made this rotation possible. The phase shift due to the rotating joints measured less than $\pm 2^{o}$. The attenuation change due to the rotating joints measured less than ± 0.2 db. In the experimental work reported here, twelve measurements (six phases and six amplitudes) were made. This gives much more than is required to determine the matrix. The extra measurements were made to check out this measurement procedure. Experience with our laboratory equipment showed that the amplitudes should be correct to within 1 db for strong signals, 2 db for moderately strong signals, and 3 db for weak signals; the phases should be measurable within 5^{o} for the strong signals and within 10^{o} for the moderately strong signals, while errors of 30^{o} or more might be noted for the weak signals. Thus, if scattering matrices are to be determined from values measured in the laboratory, it is advisable to avoid aspects at which nulls in the pattern appear; this is readily observable from some of the data obtained.

A photograph of the equipment used is shown in Figure 3.1-1 and it is shown in block diagram form in Figure 3.1-2. An examination of Figure 3.1-2 should indicate how the system works. With no target on the support column, the effect of the comparison signal through phase shifter and attenuator No. 2 is eliminated by cranking in about 90 db of attenuation. The unwanted signals due to horn-to-horn coupling, background return, etc., are then balanced out by adjusting attenuator and phase shifter No. 1 to produce a null at the receiver. The receiver signal resulting from the placement of the target on the pedestal is nulled out by adjusting precision phase shifter and attenuator No. 2. (Since a larger signal requires the removal of a larger amount of attenuation, a lower db reading indicates a stronger target return.)

In practice, the settings of attenuator and phase shifter No. 1 for balance conditions for the six polarization combinations were determined before the target was placed in position. Once the target was in place, its return for the six polarization settings was found with the proper balance conditions having been set beforehand. Errors due to change in target range or aspect were thus eliminated by completing the data for a particular aspect without movement of the target. This, and the fact that all readings were taken within a period of a few minutes tended to minimize errors due to change in oscillator frequency or output power. A typical set of raw data is shown in Table 3.1 showing

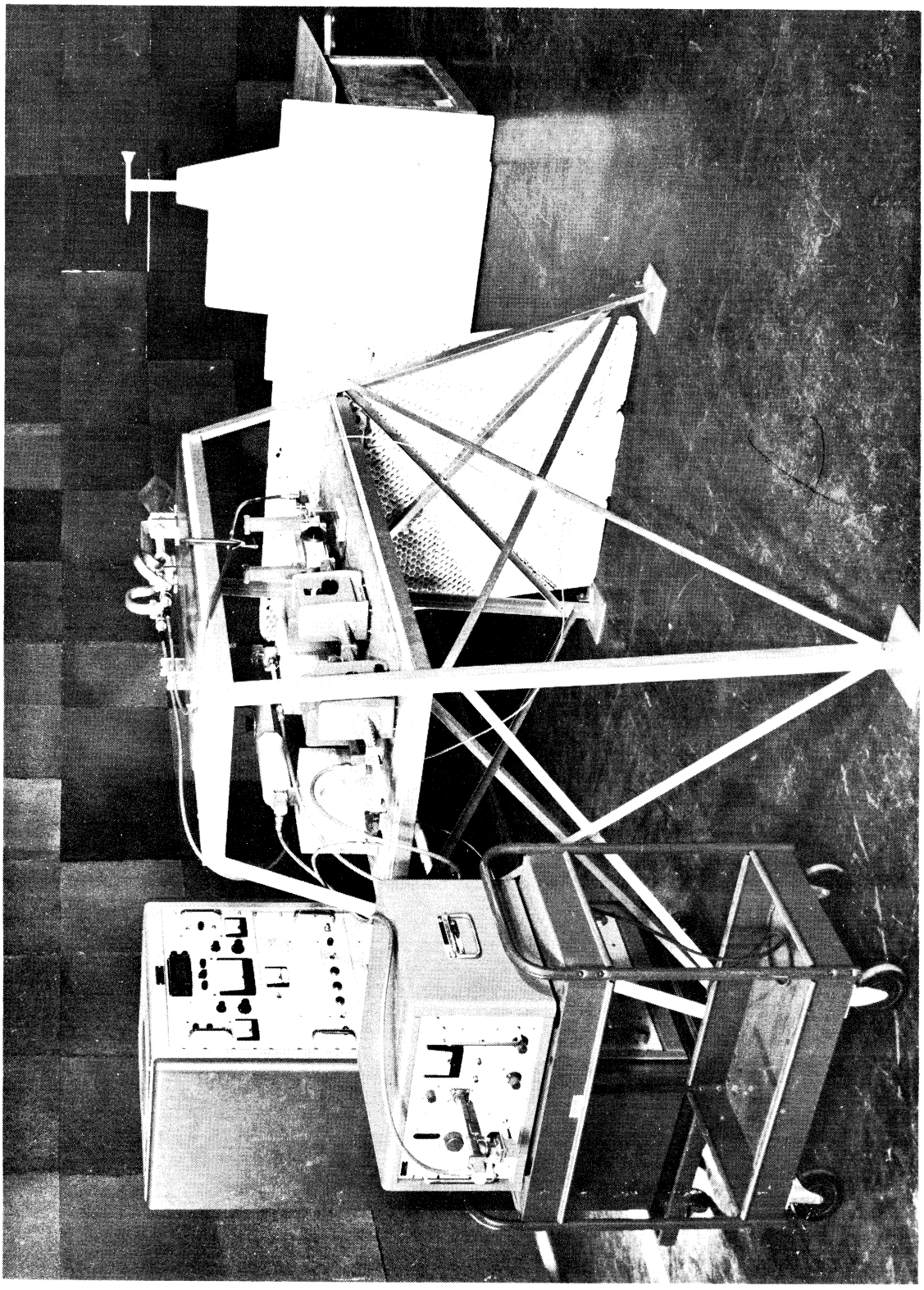

FIGURE 3.1-1: PHOTOGRAPH OF EQUIPMENT

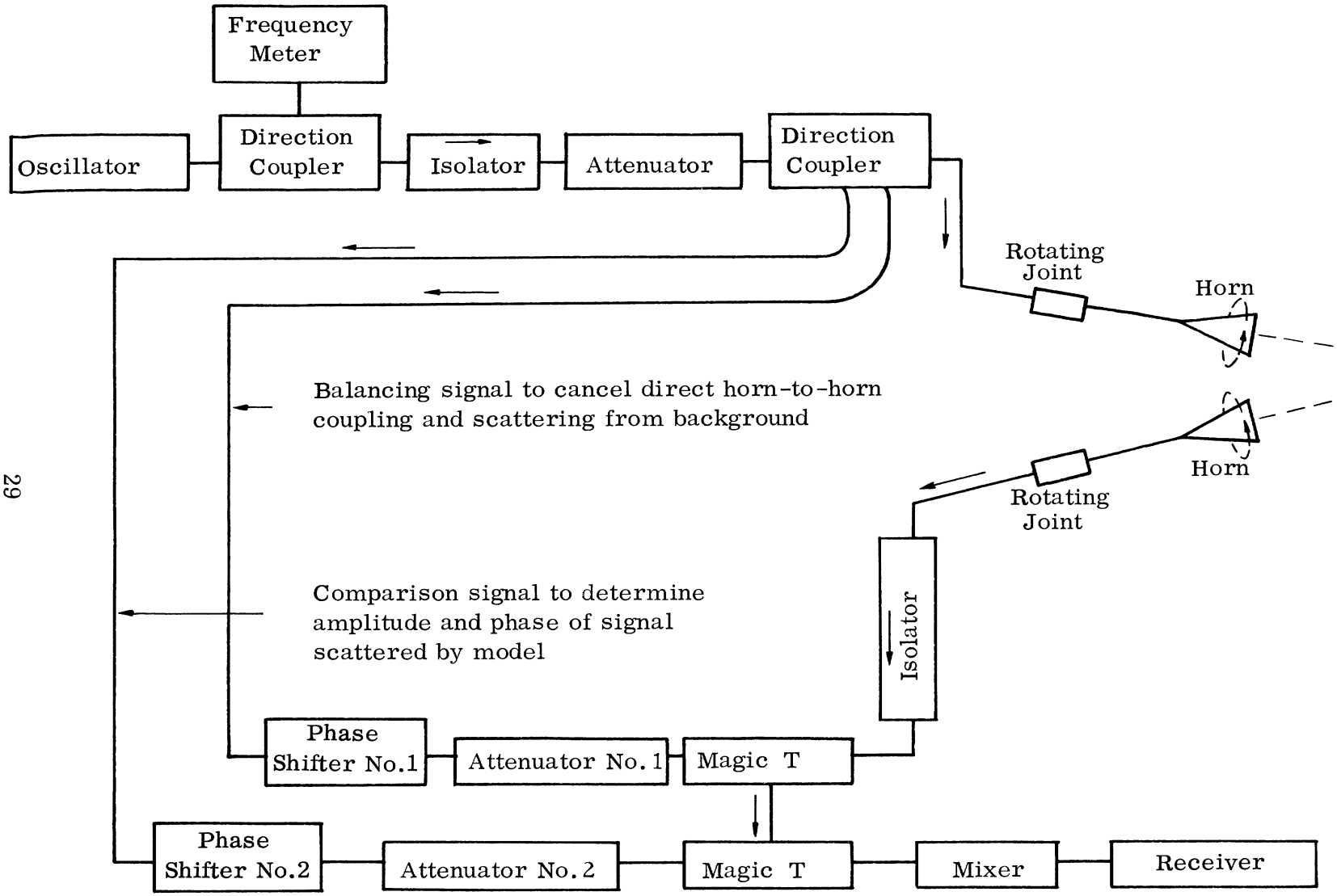

FIGURE 3.1-2: SCHEMATIC OF EQUIPMENT FOR MEASURING PHASE AND AMPLITUDE OF BACKSCATTERED SIGNAL AT ANY COMBINATION OF LINEAR POLARIZATIONS

the order in which data were taken and the repeatability of balance data and target return data. The data repeatability for all aspects giving a relatively strong return was found to be good. Aspects near the nulls in the scattering patterns generally resulted in poor data.

The range, R, separating the antennas from the target was D^2/λ, where D is the maximum dimension of the target, for all measurements. The bistatic angle between the horns was 3^o or less. The oscillator used in the system was the cavity stabilized model 814-X-21 manufactured by Laboratory for Electronics. The superheterodyne receiver used was Scientific Atlanta Model 402B. Hewlett Packard Model X382A attenuators and Model X885A phase shifters were used.

The absolute magnitude of the scattered cross section is obtained by relating the returns from all polarizations to the vertical-vertical return from a standard sphere.

Test runs were made on three targets: (1) a one-foot model of a Jupiter-type Missile, (2) the one-foot Jupiter model without fins, and (3) a $\frac{1}{10}$ - scale model of the Jupiter Nose-cone.

To be precise the missile model employed in these tests was patterned from a missile model purchased from a local hobby shop - the Revell model

TABLE 3.1 - SAMPLE OF RAW DATA

Aspect	Target	Date:	Operators
$\theta = 76^{o}$	Scattering Matrix (Nose Cone)	12-21-59	Hon - Siegman

Direction of Polarization [1]	ϕ_2 balance	db [3]	ϕ sphere	db	ϕ target	db	ϕ target	db	ϕ sphere	db	ϕ balance	db
↑ ↑	209	30.6	232	27.8	248	6.55	248	6.6	234	27.9	209	30.6
↑ ↗	274	29.5			248	9.3	248	9.3			274	29.5
↗ ↗	331	22.4			250	6.5	250	6.5			330	22.1
→ ↗	22	23.6			250	10.1	250	10.1			22	23.3
↖ ↖	340	25.2			249	6.6	250	6.7			341	25.1
→ ←	205	20.5	56	283	71	6.6	70	6.6	56	28.3	204	20.5

1) notation for ϕ_T and ϕ_R, ↑ is $\pi/2$, → is 0, ← is π, etc.

2) relative phase, in degrees

3) relative cross section in db (recall that a lower db reading indicates a stronger target return)

kit of the Jupiter C.* The nose-cone configuration data were supplied to us by C. W. Williams of the Chrysler Missile Division and describe the Jupiter Nose-cone.

Cases (1) and (2) were studied first and measurements were made at regular intervals in θ. This resulted in many runs in which the amplitudes of the returns were quite small, resulting usually in inconsistent data. In case (3) measurements were made at values of θ at which relative peaks in σ(VV) were observable; the troublesome cases of small amplitudes were thus usually avoided.

3.2 Reduction of Experimental Data

The experimental data were analyzed in two different ways. The first was essentially a "check by inspection" approach, in which a "measurement" was discarded if the two recorded values of phase differed by more than six degrees or if the two recorded values of intensity differed by more than two db. This led to the discarding of complete runs in some cases and to the reduction of the amount of useable data in other runs to the point that the calculation of scattering matrices was not possible. The other approach was of a more analytic nature but also furnished an estimate, in many cases, of which measurements were the more reliable in a given run.

* This is the satellite-launching version of the Jupiter C used in the launching of the Explorer satellite in January of 1958.

This analytic test for consistency ran as follows: (a more detailed discussion will be found in the Appendix.): For the purpose of determining the scattering matrix of a given target at a given aspect we are at liberty to choose that basis which is of most convenience. In terms of the measurements made, two such bases immediately suggest themselves, as can be seen from Equation (2-4). One set would be the $(0, \pi/2)$ basis and the other the $(\pi/4, 3\pi/4)$ basis. Considering these two bases for the matrix analysis and considering relationships existing between any four of the measured quantities, we obtained the following set of 13 relations

$$
\begin{aligned}
&1.\quad Q = S_{ah} - S_{av} - \frac{\sqrt{2}}{2} S_{hh} + \frac{\sqrt{2}}{2} S_{vv} \\
&2.\quad Q = S_{aa} - \frac{\sqrt{2}}{2} S_{ah} - \frac{\sqrt{2}}{2} S_{av} \\
&3.\quad Q = S_{aa} + S_{bb} - S_{hh} - S_{vv} \\
&4.\quad Q = S_{ah} - \frac{\sqrt{2}}{2} S_{bb} + \frac{3\sqrt{2}}{4} S_{hh} + \frac{\sqrt{2}}{4} S_{vv} \\
&5.\quad Q = S_{av} + \frac{\sqrt{2}}{2} S_{bb} - \frac{\sqrt{2}}{2} S_{hh} - \frac{3\sqrt{2}}{4} S_{vv} \\
&6.\quad Q = S_{aa} - 2\sqrt{2}\, S_{ah} - S_{bb} + 2 S_{hh}
\end{aligned}
\qquad (3\text{-}1)
$$

7. $Q = 3S_{aa} - 2\sqrt{2}\, S_{ah} + S_{bb} - 2\, S_{vv}$

8. $Q = 3\, S_{aa} - 2\sqrt{2}\, S_{av} + S_{bb} - 2\, S_{hh}$

9. $Q = S_{aa} - 2\sqrt{2}\, S_{av} - S_{bb} + 2\, S_{vv}$

10. $Q = 3\sqrt{2}\, S_{ah} - \sqrt{2}\, S_{av} + 2\, S_{bb} - 4\, S_{hh}$

11. $Q = -\sqrt{2}\, S_{ah} + 3\sqrt{2}\, S_{av} + 2\, S_{bb} - 4\, S_{vv}$

12. $Q = S_{aa} - \sqrt{2}\, S_{ah} + \frac{1}{2}\, S_{hh} - \frac{1}{2}\, S_{vv}$

13. $Q = S_{aa} - \sqrt{2}\, S_{av} - \frac{1}{2}\, S_{hh} + \frac{1}{2}\, S_{vv}$

in which Q represents the total (experimental) discrepancy, and

$$S_{\alpha\beta} = \rho_{\alpha\beta} \exp\left[i\Phi_{\alpha\beta}\right] \quad \text{for } \alpha, \beta = a, b, h, v .$$

The theoretical maximum of fifteen such relations is reduced by the vanishing of certain coefficients in three of the equations. This is also the reason why Equation (2) involves only three terms. The four-term relations were selected in preference to three-term ones because not enough of the latter are available. In the above the a, b, h, and v subscripts indicate

the directions $\pi/4$, $3\pi/4$, 0 (or π), and $\pi/2$ respectively. We thus observe, via Equation (2-5), the relations between the above notation and that of the discussion of Section II.

These thirteen equations are neither all independent nor are they unique but they do provide a set of check equations. Each Q should be zero, but the various errors which are inherent in any experimental work tend to make these Q's deviate from zero. By calculating Q in each case and considering the magnitude of $|Q - \tilde{\rho}|^2 / \tilde{\rho}^2$ where $\tilde{\rho}$ is the smallest term involved in the equation, one can obtain an idea of the consistency of the measurements. It was necessary to adopt some criterion of "goodness of fit" and the somewhat arbitrary selection of 2 db was made, that is, for example, if $20 \log_{10} |Q/\tilde{\rho} - 1| < 2$, then the consistency of the quantities involved was deemed adequate. By examining those equations for which the above criterion was not satisfied it was possible in certain cases to estimate which of the measured values were unreliable.

This procedure combined with the "check by inspection" approach led to the selection of certain runs which were considered sufficiently consistent to warrant matrix calculations. Tables 3.2 through 3.4 summarize the results of this investigation.

In these tables the code classification of runs, A, B, C, and D, has the following meaning:

A: the run was sufficiently consistent to be considered good in all measurements

B: the run contained a few questionable measurements but was deemed such that tentative matrix element calculation could be made

C: the run was sufficiently inconsistent to make matrix element calculation inadvisable

D: run chosen for matrix element calculation.

One will observe that the matrix element calculations were not performed for all of the "good" runs, it being considered unnecessary to perform calculations for two runs at the same aspect if there was no significant difference in the data measured.

We would also like to point out that when measurements are restricted to aspects in the vicinity of relative peaks in σ, one finds fewer inconsistent runs. That is, in the measurements on the full missile (with and without fins) where aspect was altered in 10 degree steps there were many more runs in the "C" category than in the other experiments, where measurements were made for the most part only at relative peaks.

In Tables 3.5 through 3.7 we present the experimental data for those runs which received an "A" classification on the basis of the consistency

check. It will be noted in these tables that with but few exceptions a "good" run has a fairly strong signal. This is what was anticipated in the discussion of Section 3.1. Given good measurements the calculation of the remaining elements in the scattering matrix is quite straightforward and therefore we shall not discuss it here.

Tables 3.8 - 3.10 contain some of the calculated matrix elements. Figures 3.2-1 through 3.2-3 are included to display the continuous variation of the cross section with changes in aspect. Only σ(VV) was measured in this way.

For those cases in which the 1.98" sphere was used for calibration it was found that the noise level was about 22 db below the sphere. When the 2.95" sphere was employed the noise level was about 19 db below the sphere. Thus we note that in many of the cases shown in Tables 3.8 - 3.10 the values of σ(HV) calculated from the experimental data are "in the noise". In the cases of the nose cone and the missile without fins, theory indicates that σ(HV) should be zero; with the value determined by experiment in the noise we thus observe agreement between theory and experiment within the limits governed by the experimental equipment. Further comparisons between theory and experiment are given in the next section.

The data given in Tables 3.8 - 3.10 represent the elements of the matrix written in the form

$$\begin{pmatrix} \sqrt{\sigma(HH)}\, e^{i\phi_{HH}} & \sqrt{\sigma(HV)}\, e^{i\phi_{HV}} \\ \sqrt{\sigma(VH)}\, e^{i\phi_{VH}} & \sqrt{\sigma(VV)}\, e^{i\phi_{VV}} \end{pmatrix}$$

where the $\sigma(IJ)$ are the cross section values given in db relative to the sphere return and the ϕ_{IJ} in degrees. Recall that the ϕ_{IJ} are known only in a relative sense and that for this case $\sigma(VH) = \sigma(HV)$ and $\phi_{HV} = \phi_{VH}$.

Run No	Date	θ (deg.)	A	B	C	D
1	11/12/59	0			x	
2	"	10		x		x
3	"	20		x		
4	11/13/59	30			x	
5	"	40			x	
6	11/19/59	0		x		
7	"	10			x	
8	12/2/59	0			x	
9	"	0		x		x
10	12/3/59	0		x		x
11	"	0			x	
12	"	90	x			
13	"	50			x	
14	"	50			x	
15	"	40			x	
16	"	0			x	
17	12/4/59	90	x			x
18	"	90	x			
19	12/7/59	90	x			
20	"	100	x			x

Run No	Date	θ (deg.)	A	B	C	D
21	12/7/59	100	x			
22	"	110	x			x
23	"	110	x			
24	"	120	x			x
25	"	120	x			
26	"	130		x		x
27	12/8/59	20		x		x
28	"	30		x		x
29	"	30			x	
30	"	130		x		
31	"	130		x		
32	"	140		x		x
33	"	140		x		
34	"	150		x		x
35	"	150		x		
36	12/8/59	160		x		x
37	"	170		x		x
38	"	180		x		x
38.1	12/18/59	50	x			x

TABLE 3.2: MISSILE MODEL WITH FINS - RUN CLASSIFICATION

Run No	Date	Q (deg.)	A	B	C	D
39	12/9/59	0		x		x
40	"	0		x		
41	"	20		x		x
42	"	20		x		x
43	"	40			x	
44	12/10/59	40		x		x
45	"	60			x	
46	"	60			x	
47	"	70	x			x
48	"	80	x			
49	"	80	x			x
50	"	90	x			x
51	"	100			x	
52	"	100		x		x
53	"	100			x	
54	"	120			x	
55	"	120			x	
56	"	140			x	
57	"	160		x		x
58	"	180	x			x
59	12/11/59	10	x			x
60	"	10	x			
61	"	50		x		x
62	"	77.7	x			x
63	12/12/59	110		x		x
64	12/11/59	30			x	
65	"	50		x		x

TABLE 3.3: MISSILE MODEL WITHOUT FINS - RUN CLASSIFICATION

Run No	Date	θ (deg.)	A	B	C	D
1	12/21/59	0		x		
2	"	0	x			x
3	"	9.5	x			
4	"	9.5	x			x
5	"	26		x		x
6	"	42.7	x			x
7	"	62.7	x			x
8	"	77.7	x			x
9	"	180	x			x
10	"	180	x			x
11	12/22/59	96	x			x
12	"	108		x		x
13	"	125.5		x		x
14	"	134	x			x
15	"	172	x			x

TABLE 3.4: MISSILE NOSE CONE - RUN CLASSIFICATION

Run No.	θ (deg.)	σ (in db rel. to sphere)*						Relative Phase Angle (deg.)					
		VV	VA	AA	HA	BB	HH^-	VV	VA	AA	HA	BB	HH^-
12	90	18	15	18	15	18	18	4	4	-1	-4	-4	174
17	90	21	18	21	18	21	21	1	4	0	-4	-2	177
18	90	22	19	21	18	21	21	3	4	1	-1	-3	187
19	90	21	17	21	18	21	21	3	3	1	-5	-1	174
20	100	8	5	8	7	8	10	120	128	161	184	151	0
21	100	8	4	8	7	8	10	122	130	165	187	153	0
22	110	3	0	3	2	2	5	110	115	154	176	151	0
23	110	2	-2	2	2	2	5	114	120	157	180	150	0
24	120	-4	-5	1	1	0	4	0	18	8	1	-21	178
25	120	-4	-5	2	1	0	4	0	15	6	0	-18	179
38.1	50	0	-4	-10	-7	-6	-4	237	229	268	9	290	176

* Sphere diameter = 1.98".

TABLE 3.5: DATA FOR THE MISSILE-WITH-FINS EXPERIMENT

Run No.	θ (deg.)	σ (in db rel. to sphere)*						Relative Phase Angle (deg.)					
		VV	VA	AA	HA	BB	HH^-	VV	VA	AA	HA	BB	HH^-
47	70	-3	- 6	0	-1	0	2	150	149	132	116	119	292
48	80	3	0	2	-2	1	0	220	219	215	201	215	18
49	80	4	1	4	0	3	3	192	192	195	191	193	10
50	90	18	15	19	16	19	19	114	114	107	99	104	278
58	180	6	3	6	3	6	6	87	87	88	89	86	266
59	10	-6	-10	-6	-7	-4	-2	72	61	93	116	115	300
60	10	-6	-10	-6	-7	-5	-3	71	66	100	128	119	309
62	77.7	0	- 2	2	0	0	4	98	100	84	75	76	255

* Sphere diameter = 1.98"

TABLE 3.6: DATA FOR THE MISSILE-WITHOUT-FINS EXPERIMENT

Run No.	θ (deg.)	σ (in db rel. to sphere)*						Relative Phase Angle (deg.)					
		VV	VA	AA	HA	BB	HH^-	VV	VA	AA	HA	BB	HH^-
2	0	5	1	4	0	3	3	- 4	- 2	3	7	-3	186
3	9.5	1	-1	0	-5	-1	-1	- 9	-10	4	12	5	193
4	9.5	2	-1	1	-4	1	1	- 4	- 9	-1	8	5	196
6	42.7	1	-2	2	-2	2	1	5	3	-1	-6	-3	175
7	62.7	3	0	4	2	4	5	- 7	- 7	2	6	4	188
8	77.7	22	19	22	18	22	22	- 1	- 1	1	1	1	181
9	180	15	12	14	10	14	13	- 1	- 1	0	2	3	183
10	180	15	12	15	10	15	14	- 1	- 1	0	0	3	181
11	96	-1	-3	-1	-4	-1	0	0	- 8	-2	6	8	189
14	134	0	-3	-1	-4	-1	-2	-20	-13	0	19	-1	196
15	172	18	16	18	14	18	16	0	0	0	0	0	179

* Sphere diameter = 2.945"

TABLE 3.7: DATA FOR THE MISSILE NOSE CONE EXPERIMENT

Aspect	Run No	σ(HH)	σ(HV)	σ(VV)	ϕ_{HH}	ϕ_{VV}
		(in db rel. to sphere)			(in deg. rel. to ϕ_{HV})	
0°	2	3.1	-24.4	4.6	203.5	193.5
9°30'	4	0.5	-14.9	2.1	-170.2	-156.2
26°	5	3.6	-16.1	2.8	128.0	121.0
42°45'	6	1.2	-29.5	1.2	65.1	75.6
77°42'	8	21.5	-18.8	21.5	-8.3	-10.8
96°	11	-0.5	-22.1	-0.8	-36.0	-45.5
108°	12	-23.2	-24.8	-5.1	108.3	-162.2
125°30'	13	-1.4	-28.5	0.6	-22.9	-60.4
172°	15	17.3	-15.2	18.4	-133.4	-131.4
180°	10	13.8	-19.6	15.3	166.2	163.7

TABLE 3.8: SCATTERING MATRIX ELEMENTS - NOSE CONE

Aspect	Run No	σ(HH)	σ(HV)	σ(VV)	ϕ_{HH}	ϕ_{VV}
		(in db rel. to sphere)			(in deg. rel. to ϕ_{HV})	
0^o	10	-7.2	-26.1	-5.1	92.7	87.7
10^o	2	-10.3	-32.5	-15.7	-17.0	-93.8
20^o	27	-5.7	-23.4	-6.2	-147.7	-78.5
30^o	28	-9.3	-20.5	-0.8	98.6	159.3
50^o	38.1	-2.8	-17.9	-0.8	-137.6	98.3
90^o	17	21.3	-1.7	21.1	-53.5	-49.5
100^o	20	9.8	-8.8	8.1	-61.8	-121.3
120^o	24	3.5	-10.3	-4.3	-59.9	-57.9
140^o	32	-0.7	-12.0	5.1	-9.1	-16.3
160^o	36	-17.5	-30.6	3.9	18.2	69.2
180^o	38	2.1	-21.9	2.1	0.5	0

TABLE 3.9: SCATTERING MATRIX ELEMENTS - MISSILE WITH FINS

Aspect	Run No	σ(HH)	σ(HV)	σ(VV)	ϕ_{HH}	ϕ_{VV}
		(in db rel. to sphere)			(in deg. rel. to ϕ_{HV})	
0°	39	-16.4	-26.6	-15.2	-104.1	-109.5
10°	59	-2.0	-20.6	-6.3	-156.7	251.3
20°	41	-22.3	-29.2	-27.8	-8.1	123.4
40°	44	-22.5	-20.7	-14.8	137.5	-99.0
70°	47	2.4	-30.3	-2.8	-118.6	156.6
90°	50	19.2	-15.7	18.1	-41.6	-25.6
100°	52	-9.7	-20.9	-4.7	32.5	110.5
110°	63	-8.6	-20.9	-5.8	-100.0	0
160°	57	-2.0	-19.4	1.0	78.5	99.0
180°	58	5.9	-30.0	6.3	34.5	35.0

TABLE 3.10: SCATTERING MATRIX ELEMENTS - MISSILE WITHOUT FINS

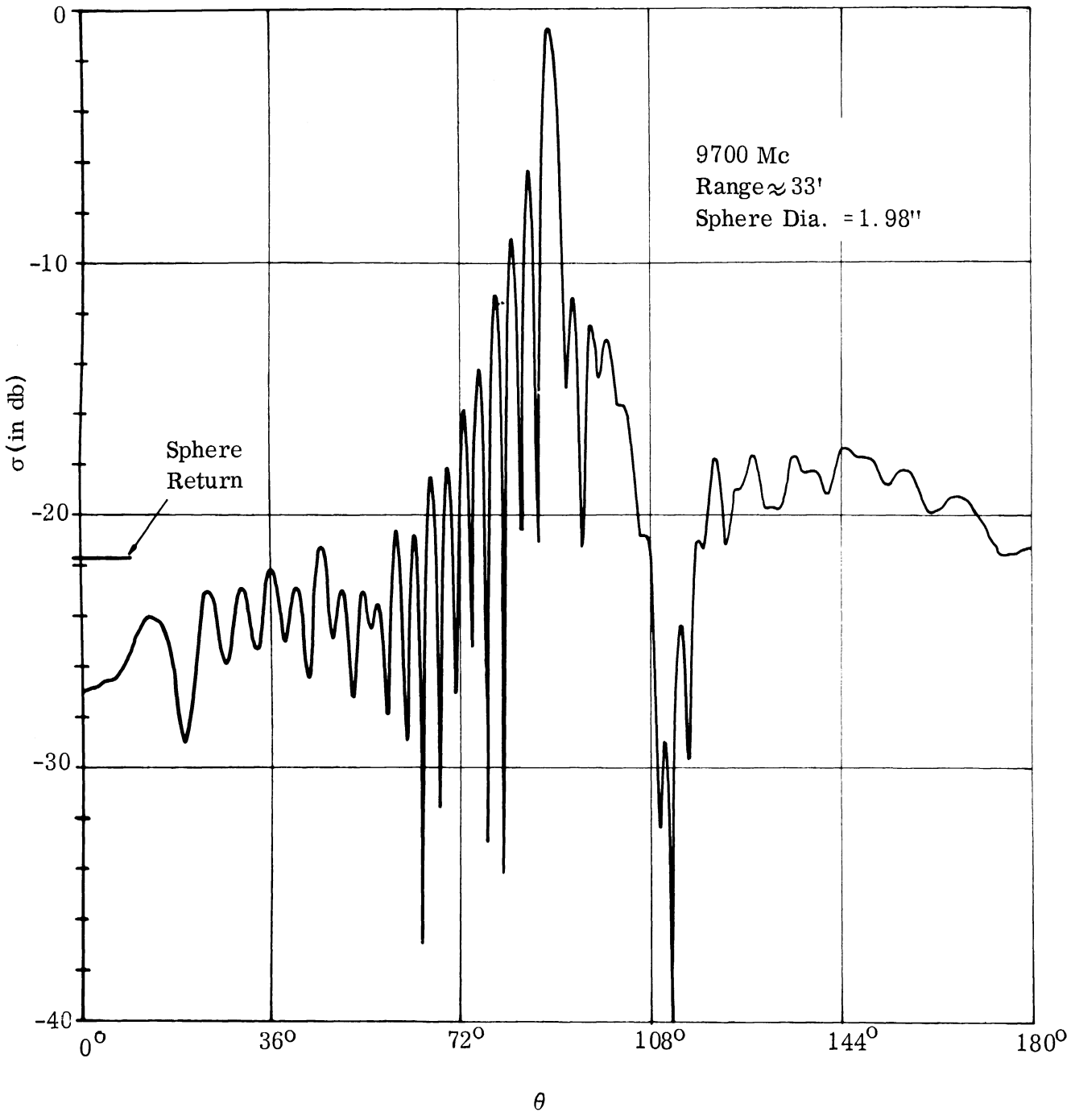

FIGURE 3.2-1: $\sigma(V, V)$ VS. θ FOR MISSILE MODEL WITH FINS

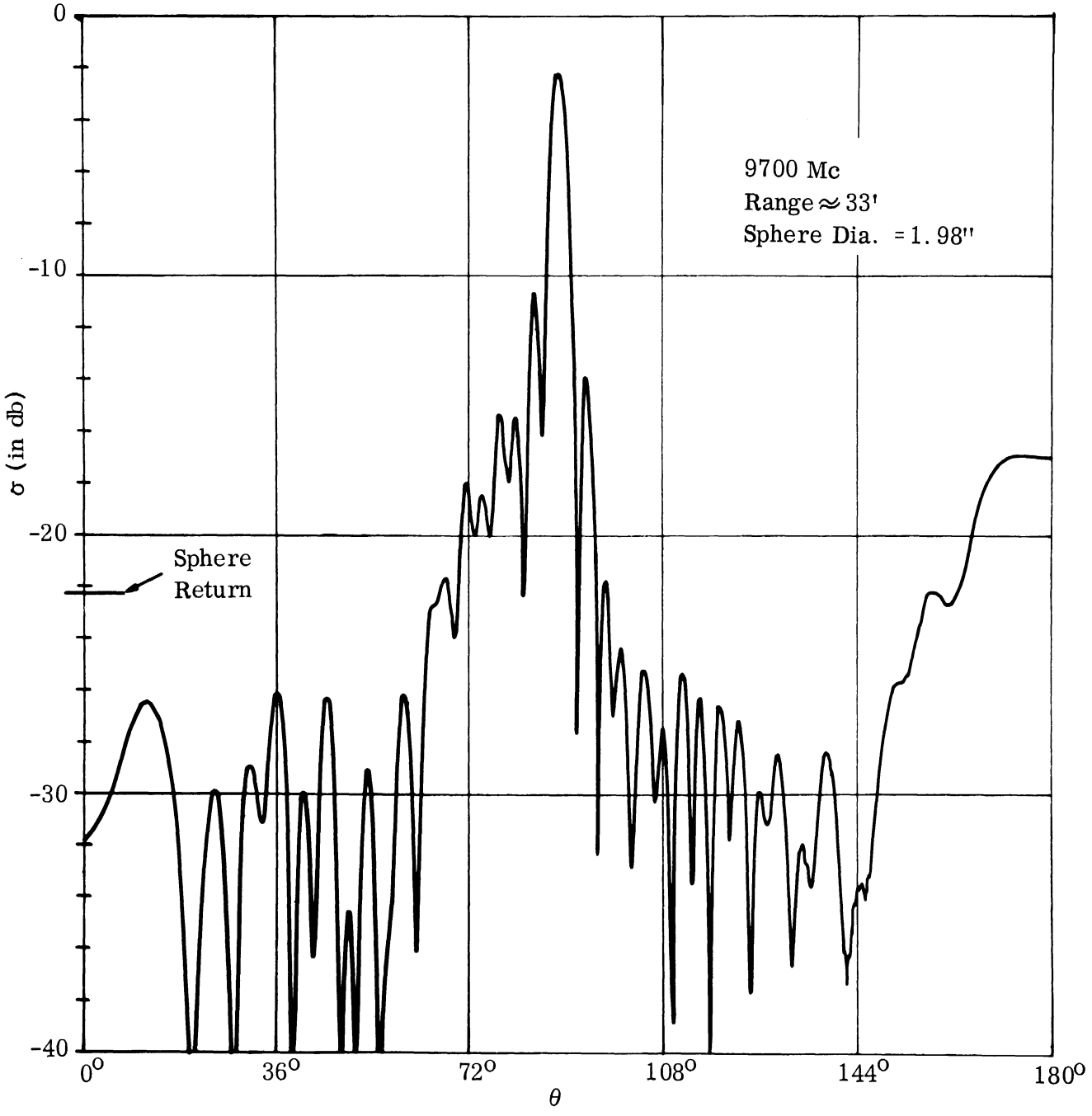

FIGURE 3.2-2: $\sigma(V, V)$ VS. θ FOR MISSILE MODEL WITHOUT FINS

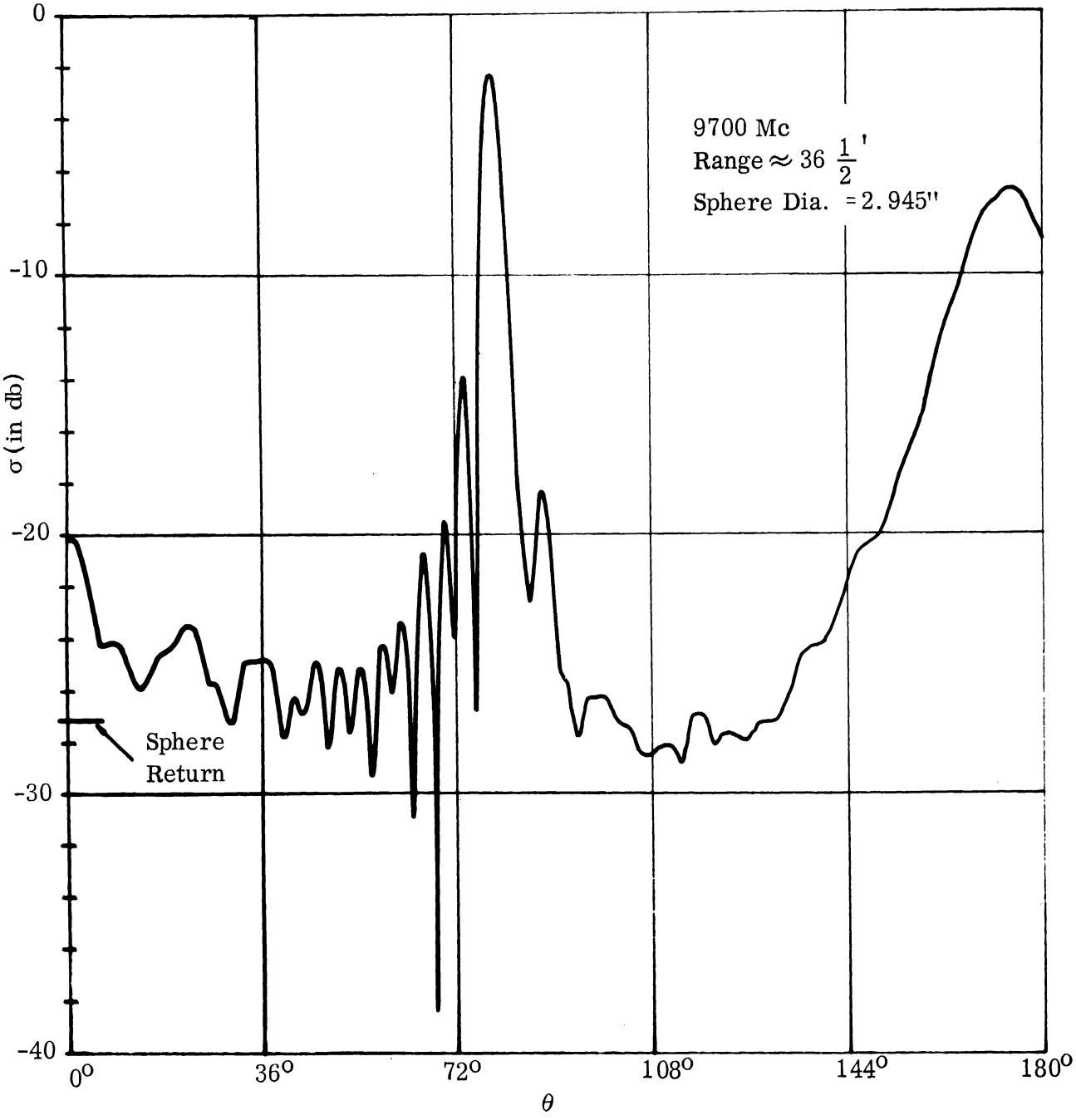

FIGURE 3.2-3: σ(V, V) VS. θ FOR NOSE CONE MODEL

Section IV

THEORETICAL CALCULATIONS AND COMPARISONS WITH EXPERIMENT

4.1 Procedure and Methods

In performing the theoretical calculations of the scattering matrices of the targets studied in the laboratory it was decided to concentrate on the cross sections involved. Thus the radar cross sections have been computed as functions of the aspect angle θ ($\alpha = \gamma = 0^o$ - see Figure 2-1) for each of the six polarization cases studied experimentally (see Equation (2-4)). The relative phase angles to be expected in each measurement are estimated only at isolated aspects. In addition, as mentioned in Section I, we shall concentrate on the model cross sections rather than the full-scale data. A modified version of Figure 2-1 is presented in Figure 4.1-1 to clarify the geometry employed in this analysis.

The calculation procedures will be based on the material of Reference 9 and we shall discuss the approach in detail for each of the targets studied. A special case of interest is the situation which occurs when the cross section is independent (or at least essentially so) of polarization. Here, we would have $\Phi_{11} = \Phi_{22}$, $a_{11} = a_{22}$, and $a_{12} = 0$ and the six measured quantities of Equation (2-5) would be

$$(1) \quad S(\pi/2, \pi/2) = a_{11} e^{i\Phi_{11}}$$

$$(2) \quad S(\pi/2, \pi/4) = \frac{1}{\sqrt{2}} a_{11} e^{i\Phi_{11}}$$

$$(3)\quad S(\pi/4,\ \pi/4) = a_{11}\, e^{i\Phi_{11}}$$

$$(4)\quad S(0,\ \pi/4) = \frac{1}{\sqrt{2}}\, a_{11}\, e^{i\Phi_{11}}$$

$$(5)\quad S(3\pi/4,\ 3\pi/4) = a_{11}\, e^{i\Phi_{11}}$$

$$(6)\quad S(0,\ \pi) = a_{11}\, e^{i\left[\Phi_{11} + \pi\right]}.$$

Thus in such a case we would expect the measured values of phase to be the same in the first five cases (of the form ϕ_0) and for the sixth to be of the form $(\phi_0 + \pi)$. The amplitudes of the returns for the second and fourth cases can be expected to be a factor of two (3 db) less than in the remaining cases. We shall give particular attention to these cases in our analysis of the targets of interest and in the analysis of Section V.

It should be pointed out in connection with these calculations that it is not our intent to strive for extreme precision. We shall, rather, attempt to obtain estimates which we feel will be accurate to within 2 to 6 db at most aspects. From time to time we will be confronted with a component shape which we know is such that for this wavelength $\sigma(H, H)$ and $\sigma(V, V)$ differ by about 1 to 3 db; in such a case we will not employ the refined techniques taking this into account. In Section V, however, where we attempt to reconstruct size and shape information from the radar data alone, we shall make use of such differences in cross section. The body of the Jupiter Missile is such

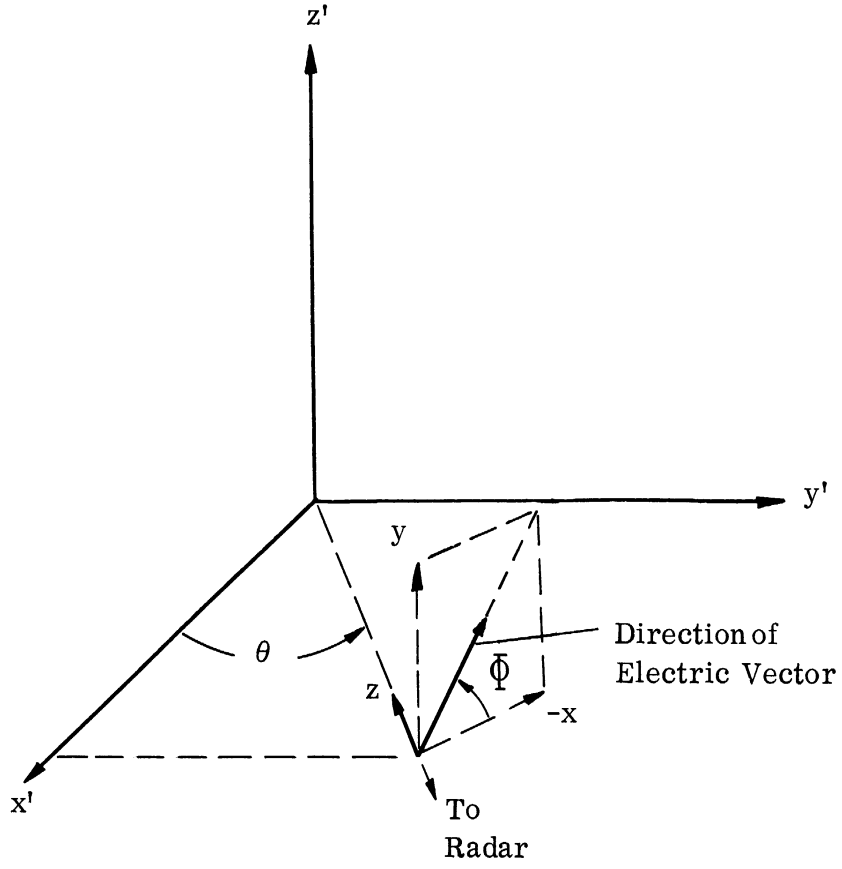

FIGURE 4.1-1: GEOMETRY FOR CROSS SECTION STUDY

a case, as we shall see in Section 4.3.*

Although we are aware that some of the experimental data are in error (in particular, some of the measurements of the amplitudes of weak signals) as noted in Section III, we include almost all of the amplitude data here in our comparisons between theory and experiment. This will explain some of the apparent inconsistencies in the comparisons. Measurements made at different dates at nominally the same aspect can lead to appreciably different results. This could occur, for example, in the vicinity of a deep null in the pattern where small changes in θ result in appreciable changes in the cross section.

4.2 The Jupiter Nose Cone

The model of the Jupiter Nose Cone studied is shown in Figure 4.2-1; this is a 1/10-scale model. (Thus the analysis performed for $\lambda = 1.22''$ corresponds to a full scale analysis in the vicinity of 1000 Mc). We observe that the configuration consists of a sphere faired into a truncated circular cone with a sphere sector "cap" at the rear. For the purpose of estimating the radar cross section we note that a specular-reflection type contribution can be expected for aspects out to $\sim 77^{\circ}$ off nose-on from the spherical cap in the front. The magnitude of this contribution is given by $\sigma = \pi r^2$ with $r = 1.21''$, i.e., this nose contribution is about 4.6 in^2. A similar contribution can be

* Also we shall concentrate on "relative peak" data at the expense of precision for the relatively weaker signals since we know that for the latter the experimentally measured values are less reliable.

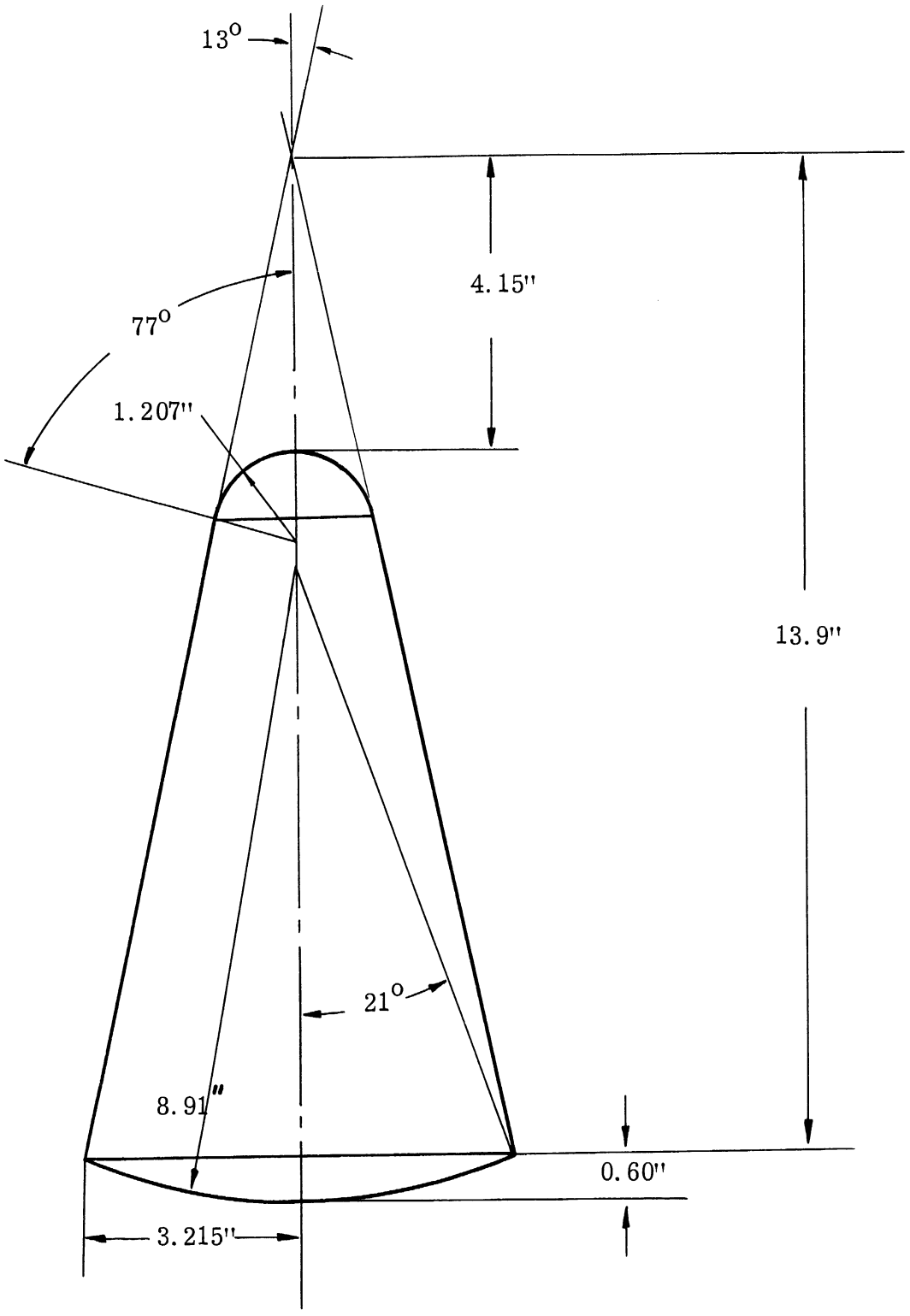

FIGURE 4.2-1: NOSE CONE MODEL

expected for aspects within about 21^o of the tail-on aspect due to the rear spherical cap; here again the contribution is given by an expression of the form $\sigma = \pi r^2$ where r in this case is 8.91", i.e., this "tail" contribution is about 250 in^2. The remaining contributions stem from the truncated cone and the ring-like singularity which exists at the juncture of the cone and rear "cap".

For $\theta = 77^o$ we anticipate a large return since the aspect is normal to the slant side of the cone. From Equation (4.3.14) of Reference 9 we estimate this cross section contribution to be about 930 in^2. The ring singularity is treated as the base of a thin cone for $\theta = 0^o$ as discussed in Appendix B of Reference 9 (p. 256) using the wedge segment approach. For other values of θ this ring is treated as a wire loop (see Section 4.5 of Reference 9) for values of θ appreciably different from 77^o, and as the end of the truncated cone (Equation (4.3.15) of Reference 9) for θ within about 50 degrees of 77^o.

This approach leads to the conclusion that the cross section should be essentially independent of polarization for $\theta = 0^o$, $\sim 20^o < \theta < \sim 80^o$, and $\sim 160^o < \theta \leqslant 180^o$. Polarization dependence of a moderate degree can be expected around $\theta = 10^o$ and of a strong degree for $\sim 100^o < \theta < \sim 150^o$ due to the fact that the wire loop contribution is highly dependent on polarization. Since the experimental measurements were made at aspects at which relative peaks occurred we can expect, in general, that the experimental data will run to larger values of cross section than those predicted by the average,

or random phase method, the approach used for most of the calculations. The results of these calculations are displayed in Figures 4.2-2 through 4.2-4; to facilitate comparison with experiment all values of σ have been computed relative to the return from a 2.945" diameter sphere, the one used in the experimental measurements.

The results corresponding to $\phi_i = \pi/2$, $\phi_r = \pi/4$ and $\phi_i = 0$, $\phi_r = \pi/4$ are not presented graphically. It will suffice to note that the theoretical approach indicates that $\sigma(\pi/2, \pi/4)$ should be 3 db below that of $\sigma(\pi/2, \pi/2)$ and $\sigma(0, \pi/4)$ should be 3 db below that of $\sigma(0, \pi)$. This was observed in the experimental data as indicated in Table 4.1.

It will also be of interest to check the phase angles measured experimentally to see if for the aspects mentioned above the relative phase angles were as predicted. (It will be recalled that in Section 4.1 we concluded that at aspects for which the cross section was independent of polarization the measured phase angles should be of the form ϕ_0 in the first five cases and $\phi_0 + \pi$ in the sixth case.) This is displayed, for those runs having values of θ in the ranges given above, in Table 4.2. We observe from the table that to within a possible error of about 10^o, the measured relative phase angles agree with those predicted.

In reviewing the material shown in Figures 4.4-2 through 4.4-4 and in Tables 4.1 and 4.2 we observe that the estimated values of cross section

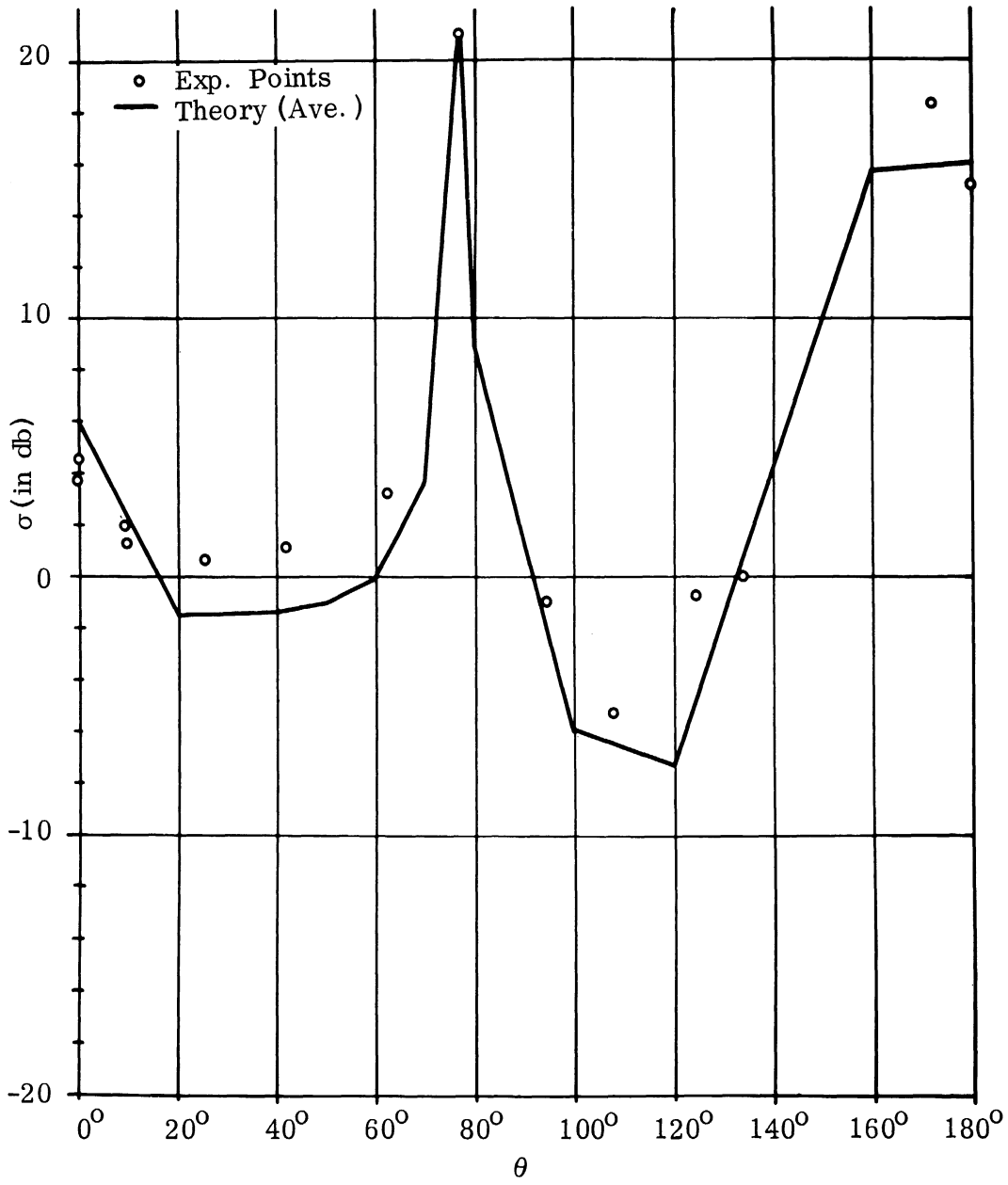

FIGURE 4.2-2: RADAR CROSS SECTION OF NOSE CONE MODEL FOR $\phi_i = \pi/2$ AND $\phi_r = \pi/2$

($\lambda = 1.22''$ and 0 db $\rightarrow$ 6.8 in^2)

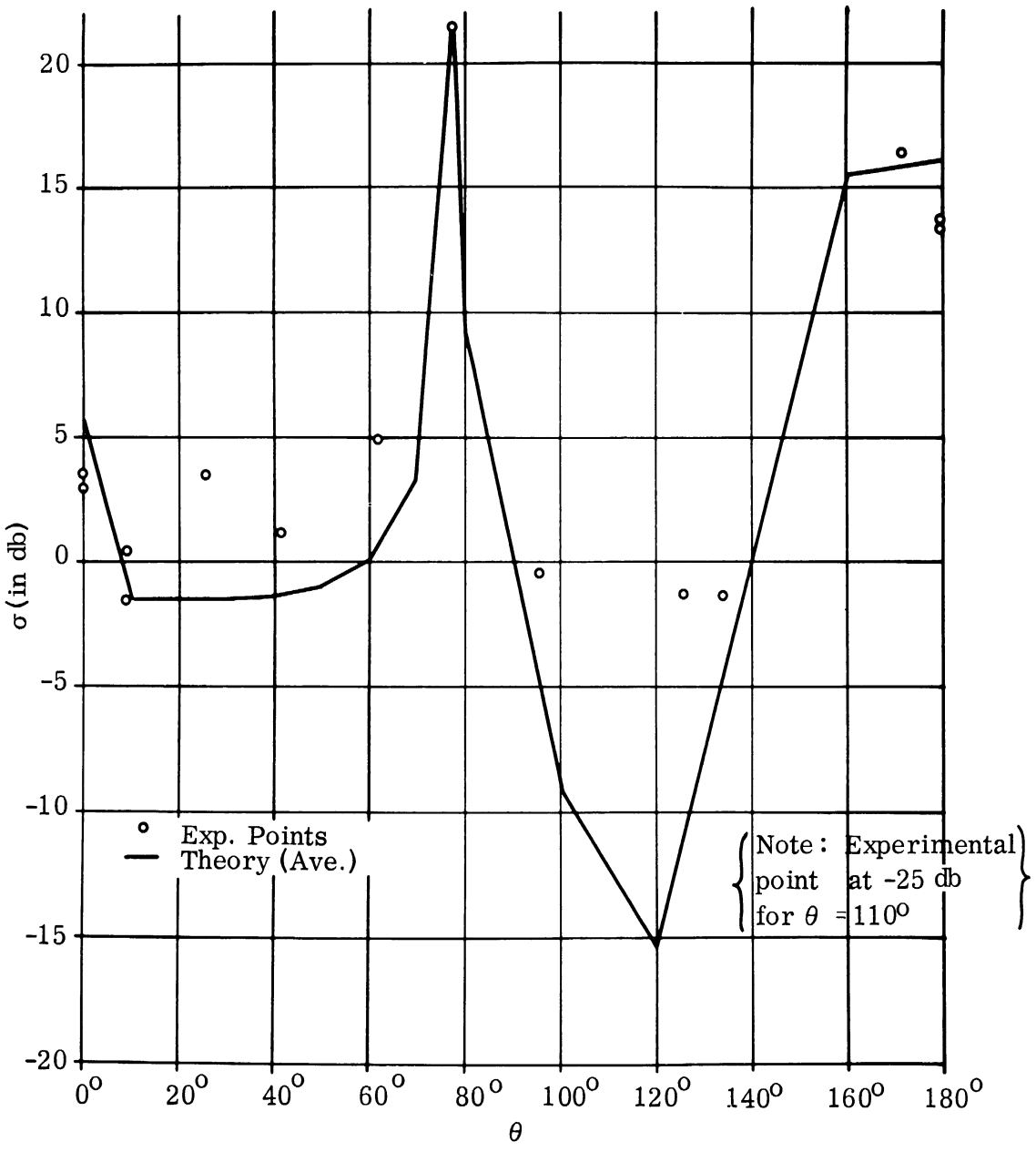

FIGURE 4.2-3: RADAR CROSS SECTION OF NOSE CONE MODEL FOR $\phi_i = 0$ AND $\phi_r = \pi$

($\lambda = 1.22''$ and 0 db $\rightarrow 6.8$ in^2)

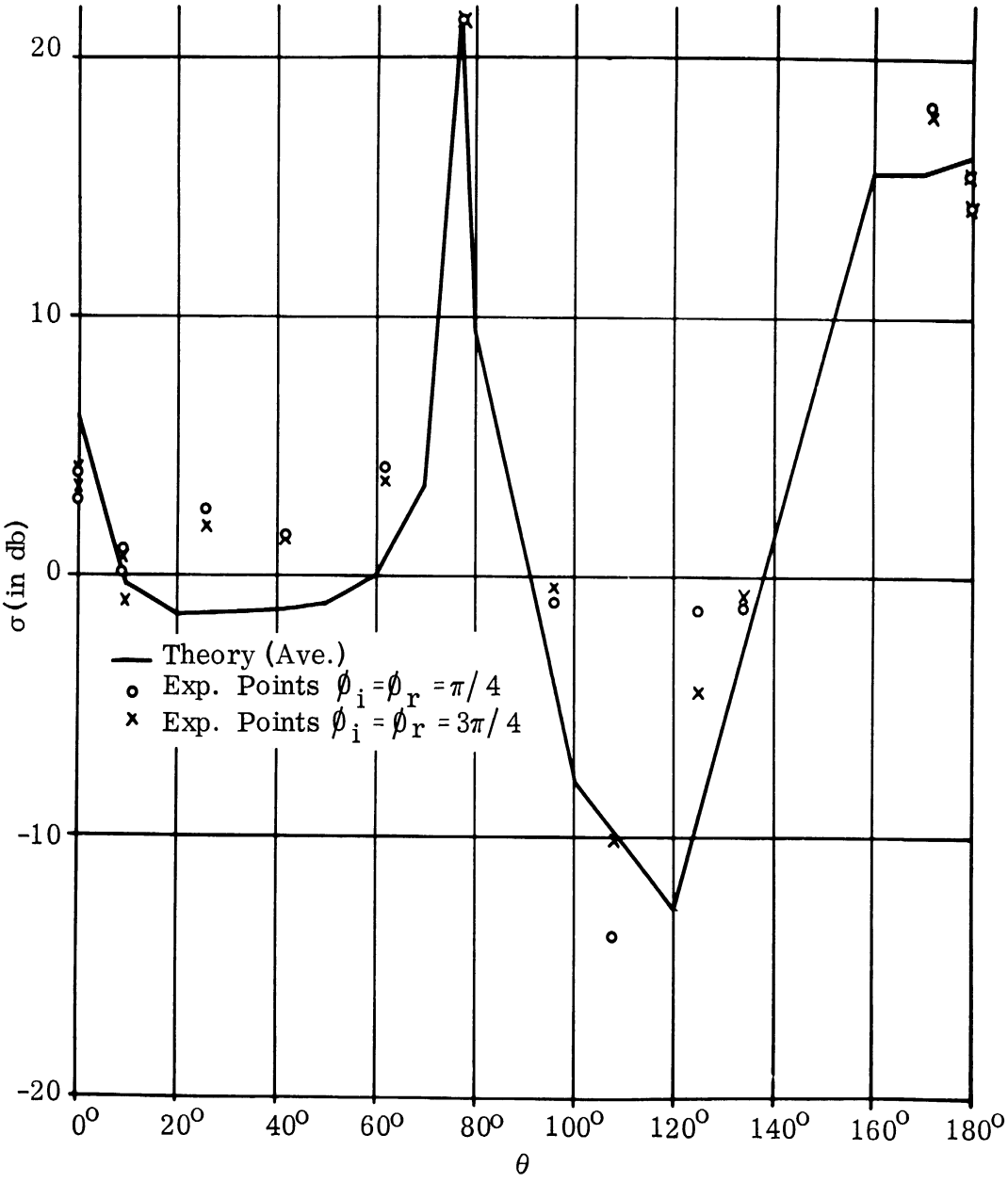

FIGURE 4.2-4: RADAR CROSS SECTION OF NOSE CONE MODEL FOR $\phi_i = \phi_r = \pi/4$ AND $\phi_i = \phi_r = 3\pi/4$

($\lambda = 1.22''$ and 0 db $\longrightarrow$ 6.8 in^2)

Aspect	$\sigma(\pi/2, \pi/4) \Big/ \sigma(\pi/2, \pi/2)$ (in db)	$\sigma(0, \pi/4) \Big/ \sigma(0, \pi)$ (in db)
0^o	-3.3	-4.4
0^o	-3.1	-3.4
$9^o 30'$	-2.2	-3.4
$9^o 30'$	-2.7	-4.6
26^o	-2.1	-3.6
43^o	-2.7	-2.9
63^o	-3.1	-3.4
78^o	-2.7	-3.5
96^o	-2.6	-3.6
108^o	-3.9	+0.6*
125^o	-2.4	-3.0
134^o	-3.1	-2.2
172^o	-2.7	-1.9
180^o	-2.9	-3.6
180^o	-2.9	-3.6

* Note that very weak signals (relatively speaking) were obtained here.

TABLE 4.1: $\sigma(\pi/2, \pi/4) \Big/ \sigma(\pi/2, \pi/2)$ AND $\sigma(0, \pi/4) \Big/ \sigma(0, \pi)$ IN DB - MEASURED VALUES FOR THE NOSE CONE

Theory or Experiment	Aspect (θ) ϕ_i = ϕ_r =	Measured Phase Angle (Relative) in Degrees					
		$\pi/2$ $\pi/2$	$\pi/2$ $\pi/4$	$\pi/4$ $\pi/4$	0 $\pi/4$	$3\pi/4$ $3\pi/4$	0 π
Theory	all	0	0	0	0	0	180
Experiment	0^o	-9	-9	-1	9	-3	182
"	0^o	-4	-2	3	7	-3	186
"	26^o	-3	-4	-1	-1	7	185
"	43^o	5	3	-1	-6	-3	175
"	63^o	-7	-7	2	6	4	188
"	78^o	-1	-1	1	1	1	181
"	172^o	0	0	0	0	0	179
"	180^o	-1	-1	0	2	3	183
"	180^o	-1	-1	0	0	3	181

TABLE 4.2: RELATIVE PHASE ANGLES FOR THE NOSE CONE

and the estimated values of the measured phase angles agree reasonably well with the experimental data, the agreement between theory and experiment being as desired except for aspects in the interval $\sim 110^{o} < \theta < \sim 150^{o}$ where it appears that a more refined approach is required for theoretically estimating the return from the warhead.* The data for the aspect range from $\theta = 0^{o}$ out to $\theta \approx 100^{o}$ are summarized in Figure 4.2-5. In this figure we display the theoretical "in-phase" estimate while in the preceding figures we used the average or "random phase" estimates. Since the experimental measurements were made at the relative peaks, the former is considered to be a more appropriate comparison of theory and experiment.

4.3 The Entire Missile (without Fins)

A sketch of the missile model used in the experiments is displayed in Figure 4.3-1; the model "with fins" is shown in the figure although measurements were made on the model both with and without fins. (We shall discuss the "with fins" case in Section 4.4.) It is readily seen that the configuration's body (i.e., the missile without fins) consists of a circular cylinder (length = 10.60 in. and diameter = 1.06 in.) with a truncated circular cone mounted at the front. This "nose cone" is cut from a circular cone of half-angle equal to approximately 13^{o}. For the purpose of these calculations we shall neglect the small protuberance at the nose, since the magnitude of the contribution to the cross section

* Such a more refined approach could have been made but the purpose here is to check out the relatively simple method of approach.

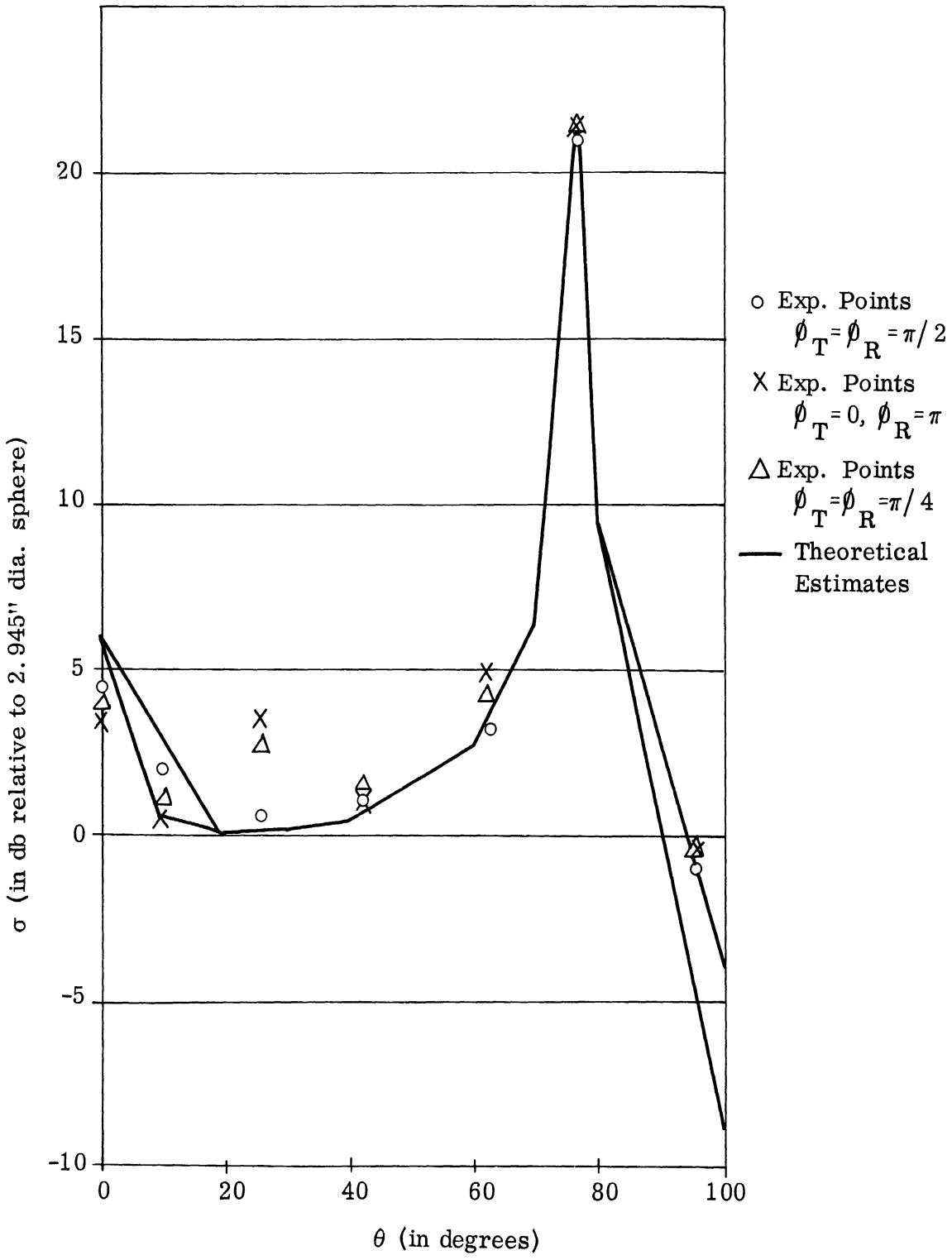

FIGURE 4.2-5: RADAR CROSS SECTION OF $\frac{1}{10}$ - SCALE MODEL FOR $\lambda = 1.22$ in.

(The Nose Cone)

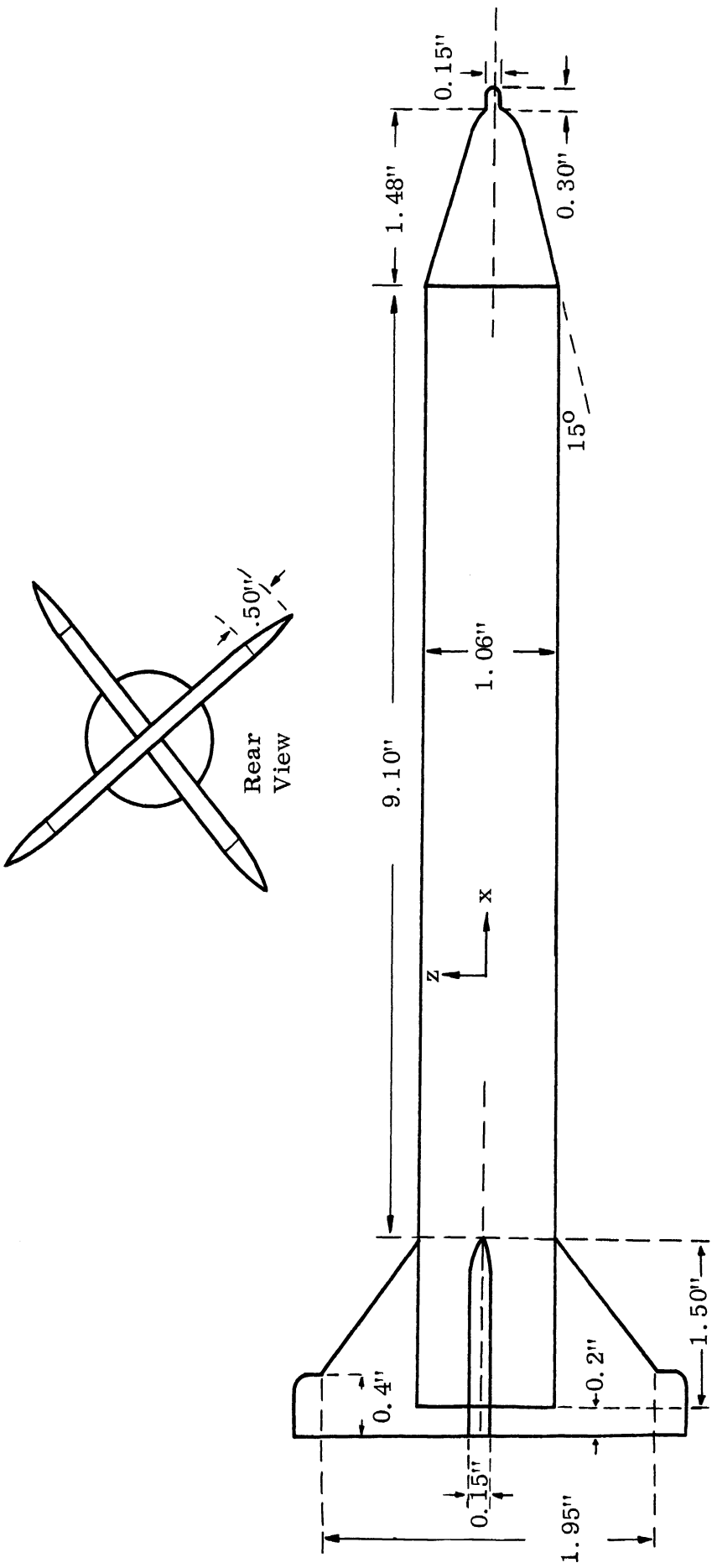

FIGURE 4.3-1: SKETCH OF MISSILE MODEL (Showing Fins)

of the missile stemming from this part of the body can be expected to be negligible in comparison to the other contributions.

The fins are taken as flat plates of the shape shown in the figure with the edges assumed to be sufficiently sharp that they can be modeled by thin wires. For the purpose of our calculations for the finless missile we shall restrict our attention to the truncated cone nose, the cylinder body, and the flat plate rear section. The missile model employed in the experimental tests differed in its warhead section from the nose cone configuration studied in the preceding section. This requires a slightly different approach from that used in the analysis of the nose cone alone. We should like to point out again (as noted in Section III) that the missile model used in these tests was patterned after a model obtained from a local hobby shop.

Restricting our attention for the moment to the broadside case we note that the cross section will be dominated by the cylinder response. With $\lambda = 1.22$ in. we observe that we are dealing with a value of $2\pi a/\lambda$ of about 2.73 (a = radius of cylinder). We note from Mentzer (Ref. 10, page 64) that we can expect $\sigma(0, \pi)$ and $\sigma(\pi/2, \pi/2)$ to differ by less than 2 db for $\theta = \pi/2$. Thus, optics techniques should suffice. Using optics techniques throughout as outlined in Reference 9 we thus obtain an estimate which implies that at each θ:

$$\sigma(\pi/2, \pi/2) = \sigma(\pi/4, \pi/4) = \sigma(3\pi/4, 3\pi/4) = \sigma(0, \pi)$$

and

$$\sigma(0, \pi/4) = \sigma(\pi/2, \pi/4)$$

with $\sigma(0, \pi/4)$ being 3 db below $\sigma(\pi/2, \pi/2)$.

For the nose-on case we employ the rough approximation method used in Reference 11 for the 7-0C Modified Warhead (flat stern), i.e., for example at $\theta = 0^o$, $\sigma(\pi/2, \pi/2) = 1.03(ka)^{-5/2} \pi a^2$ with a = the radius of the cylinder.

At the tail-on aspect we consider a circular flat plate to estimate the cross section. The radius is 0.53 in and we employ the material of Section 4.7.2 of Reference 9 to obtain the cross section estimate.

The optics methods are inadequate to indicate the expected oscillatory nature of the cross section for aspects which are off nose-on and off tail-on. Thus, we also consider the "thin body" approach as outlined in Section 5 of Appendix B of Reference 9. For aspects in the region $0^o < \theta < \sim 60^o$ we consider the body to be a thin rod while for $\sim 120^o < \theta < 180^o$ we consider the body to be essentially ogival. The results obtained by this procedure are shown in Figure 4.3-2; for the purpose of easy comparison with the experimental data all cross sections are shown in db relative to the return from a sphere of diameter 1.98" (the one used in the experimental work). The cases in which $|\phi_i - \phi_r|$ is either zero or π are displayed; the cross sections for those cases in which $|\phi_i - \phi_r| = \pi/4$ are expected to be 3 db below those shown in the figure.

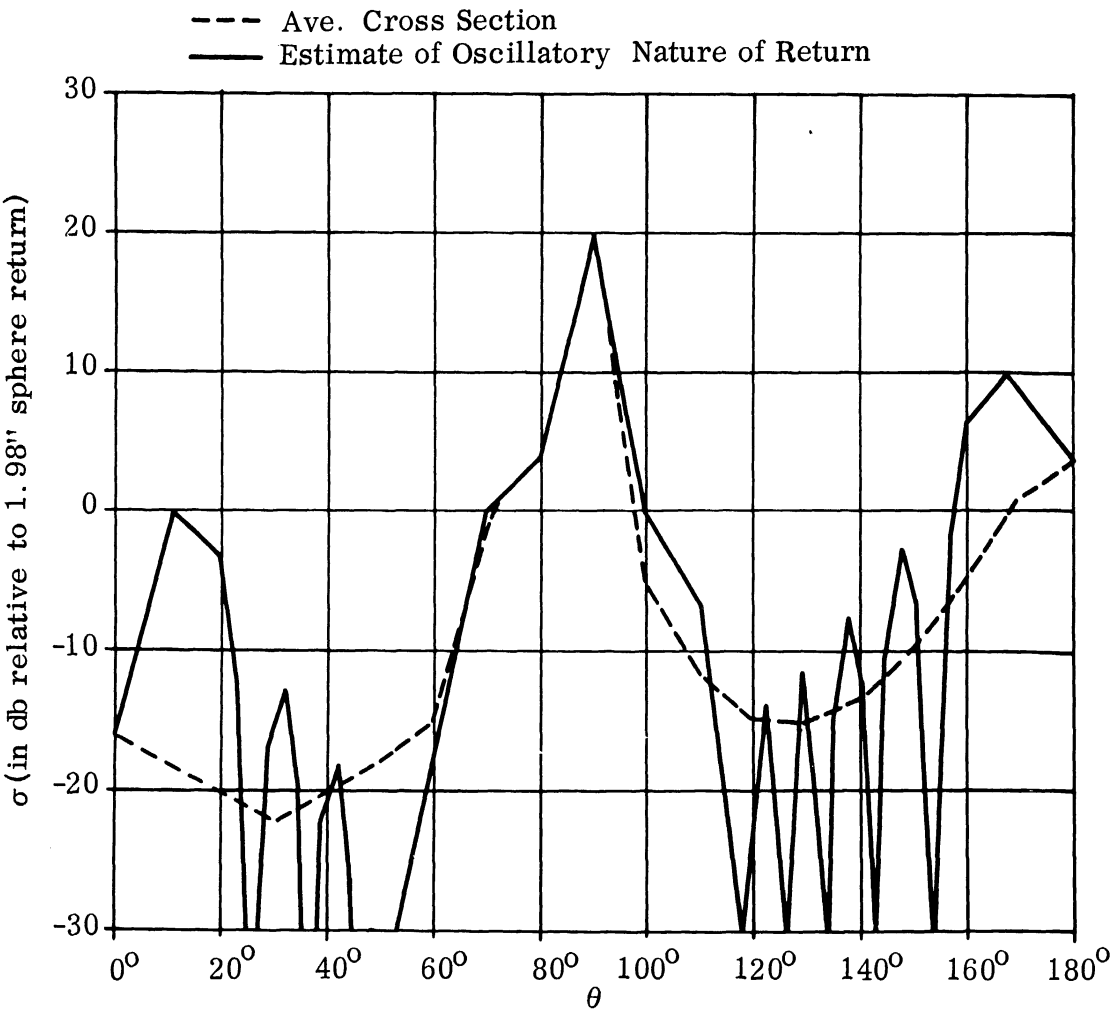

FIGURE 4.3-2: RADAR CROSS SECTION OF MISSILE WITHOUT FINS - THE MODEL FOR $\lambda = 1.22''$ (0 db $\rightarrow 3$ in^2)
(cases of $\phi_i = \phi_r$ (or $|\phi_i - \phi_r| = \pi$))

These theoretical estimates are compared with the experimental data in Figures 4.3-3 through 4.3-8. Taking into consideration the highly oscillatory nature of the cross section of the target and the fact that no attempt was made to measure (in the laboratory) at aspects at which relative peaks in σ would occur the agreement between theory and experiment shown in these figures appears to be reasonably good.

As an additional check on the method of approach in calculating the cross sections and on the behavior of the cross section as a function of θ, additional measurements of the cross section were made at one degree steps from $\theta \approx 8^{\circ}$ to $\theta \approx 25^{\circ}$ for the $\phi_i = \phi_r = \pi/2$ case. These results together with the theoretical estimate are displayed in Figure 4.3-9 where we note that the trends appear to have been predicted quite well although discrepancies of about 5 db in amplitude and about 5° in location of the null are apparent.

With regard to the phase angles which were measured we shall restrict our attention to the nose-on, broadside and tail-on cases where we would expect the first five to be of the form ϕ_0 with the sixth of the form $\pi + \phi_0$. Table 4.3 displays the measured values compared with this estimate. The large differences which seem to exist for the nose-on case are undoubtedly due to the fact that the amplitude is very small at this aspect and as noted in Section 3.1 possible errors in phase of up to 40° or more were anticipated for signals of this small amplitude.

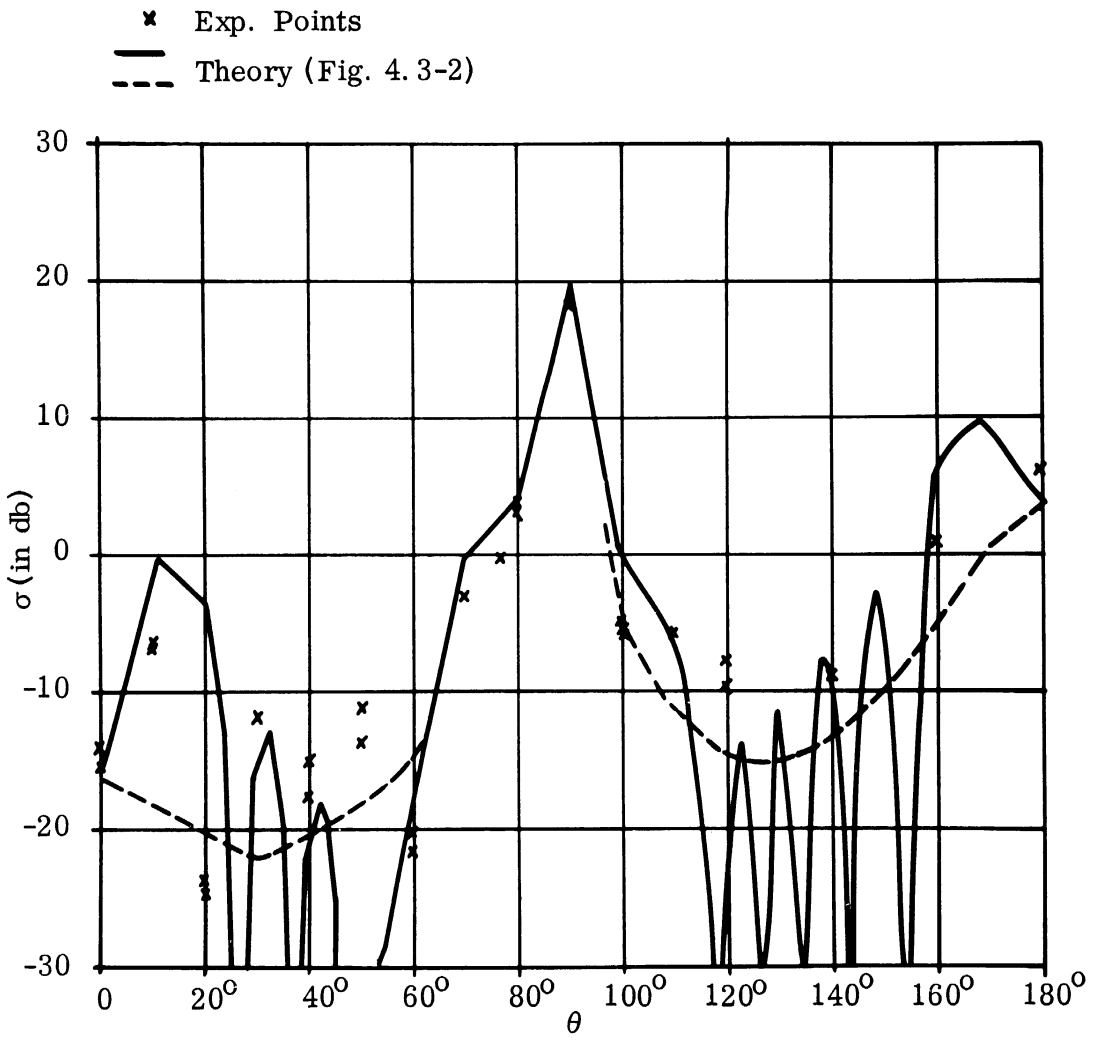

FIGURE 4.3-3: MISSILE WITHOUT FINS - THEORY VS. EXPERIMENT
($\phi_i = \pi/2$, $\phi_r = \pi/2$)

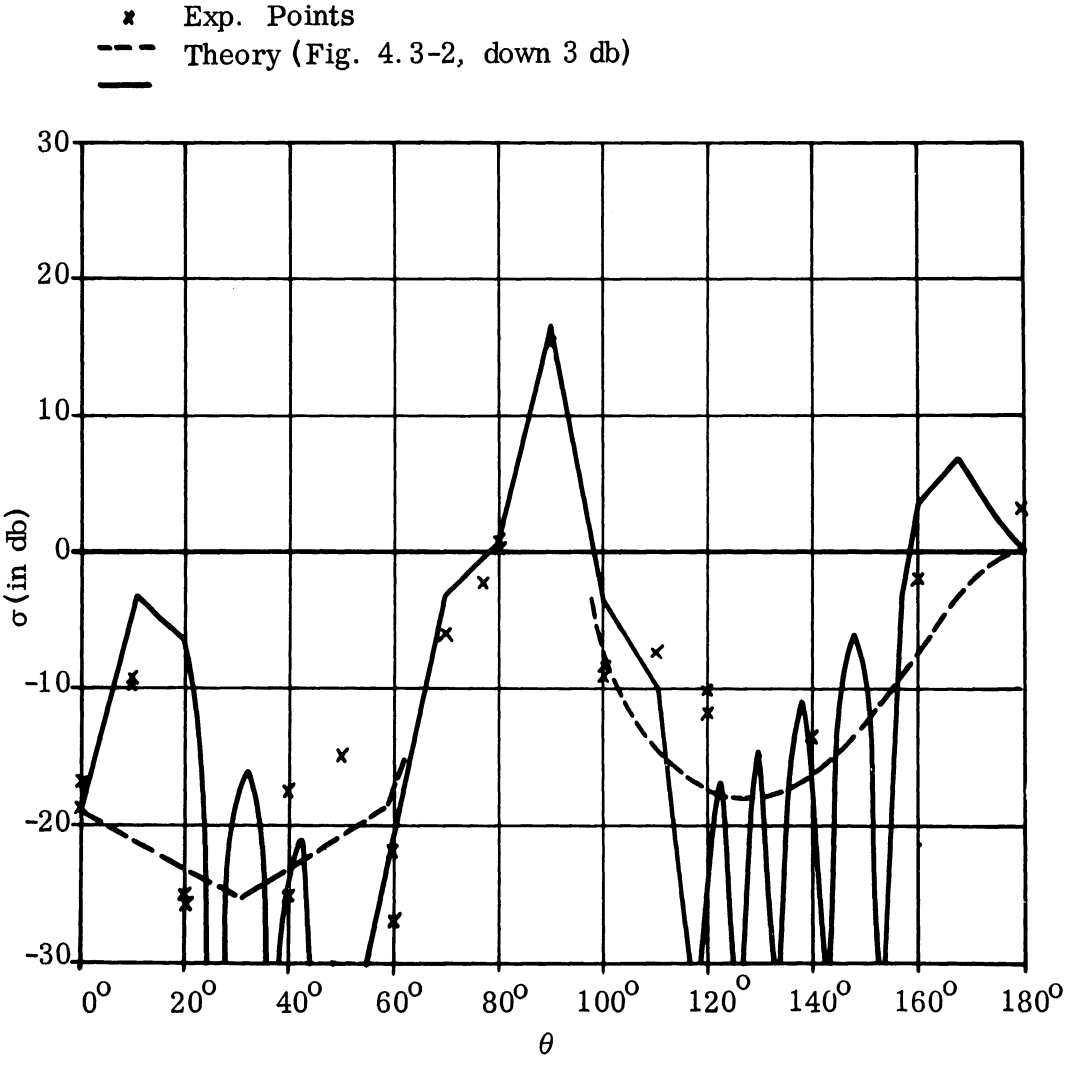

FIGURE 4.3-4: MISSILE WITHOUT FINS - THEORY VS. EXPERIMENT
($\phi_i = \pi/2$, $\phi_r = \pi/4$)

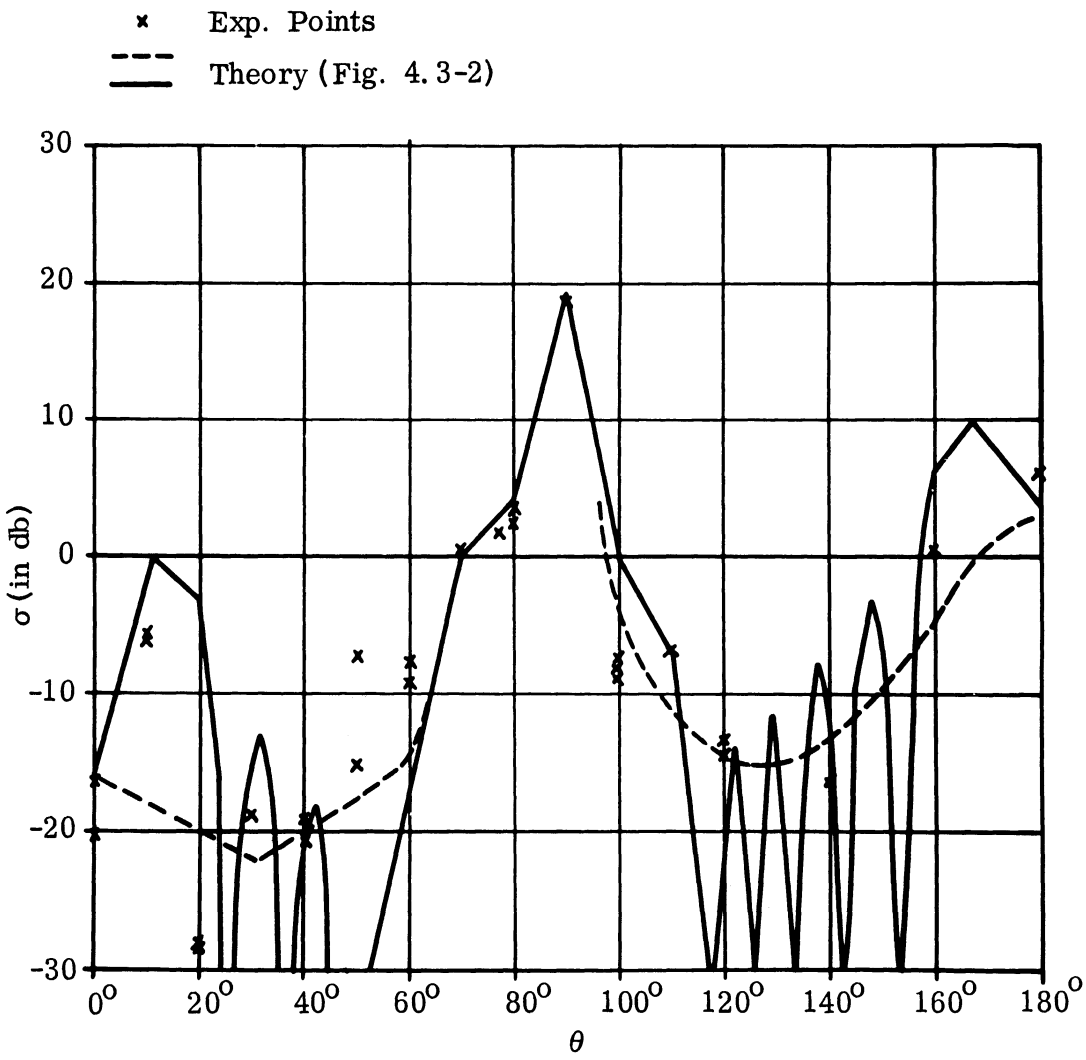

FIGURE 4.3-5: MISSILE WITHOUT FINS - THEORY VS. EXPERIMENT
($\phi_i = \pi/4$, $\phi_r = \pi/4$)

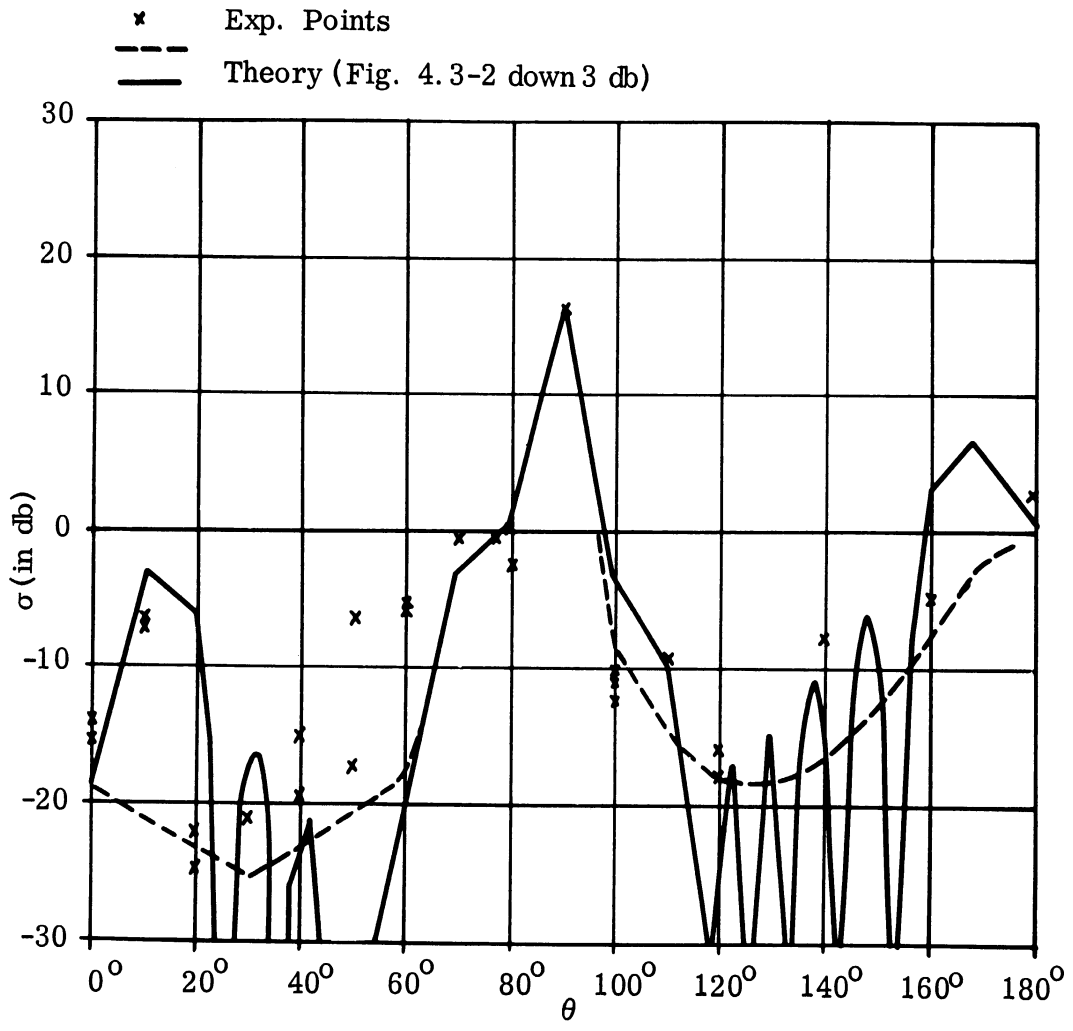

FIGURE 4.3-6: MISSILE WITHOUT FINS - THEORY VS. EXPERIMENT
($\phi_i = 0$, $\phi_r = \pi/4$)

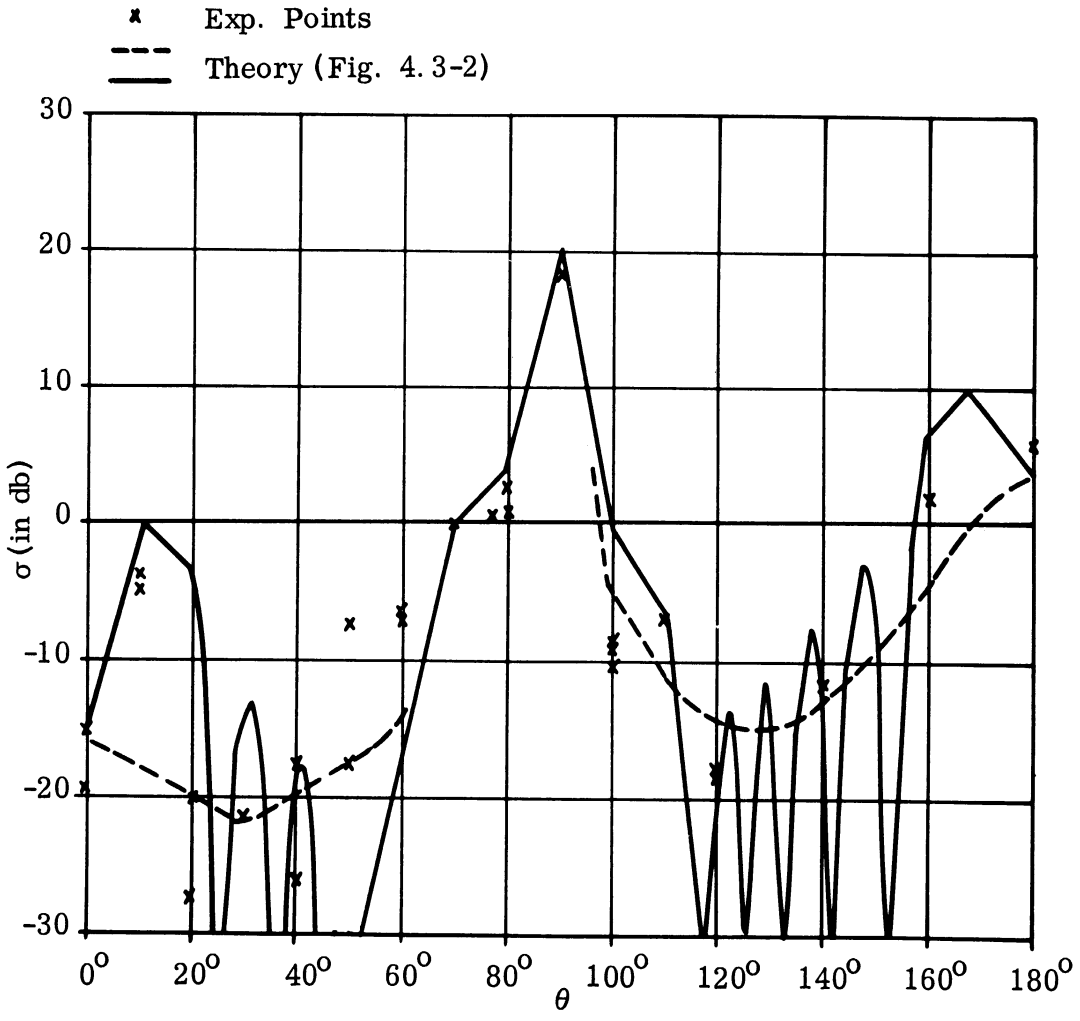

FIGURE 4.3-7: MISSILE WITHOUT FINS - THEORY VS. EXPERIMENT
($\phi_i = 3\pi/4$, $\phi_r = 3\pi/4$)

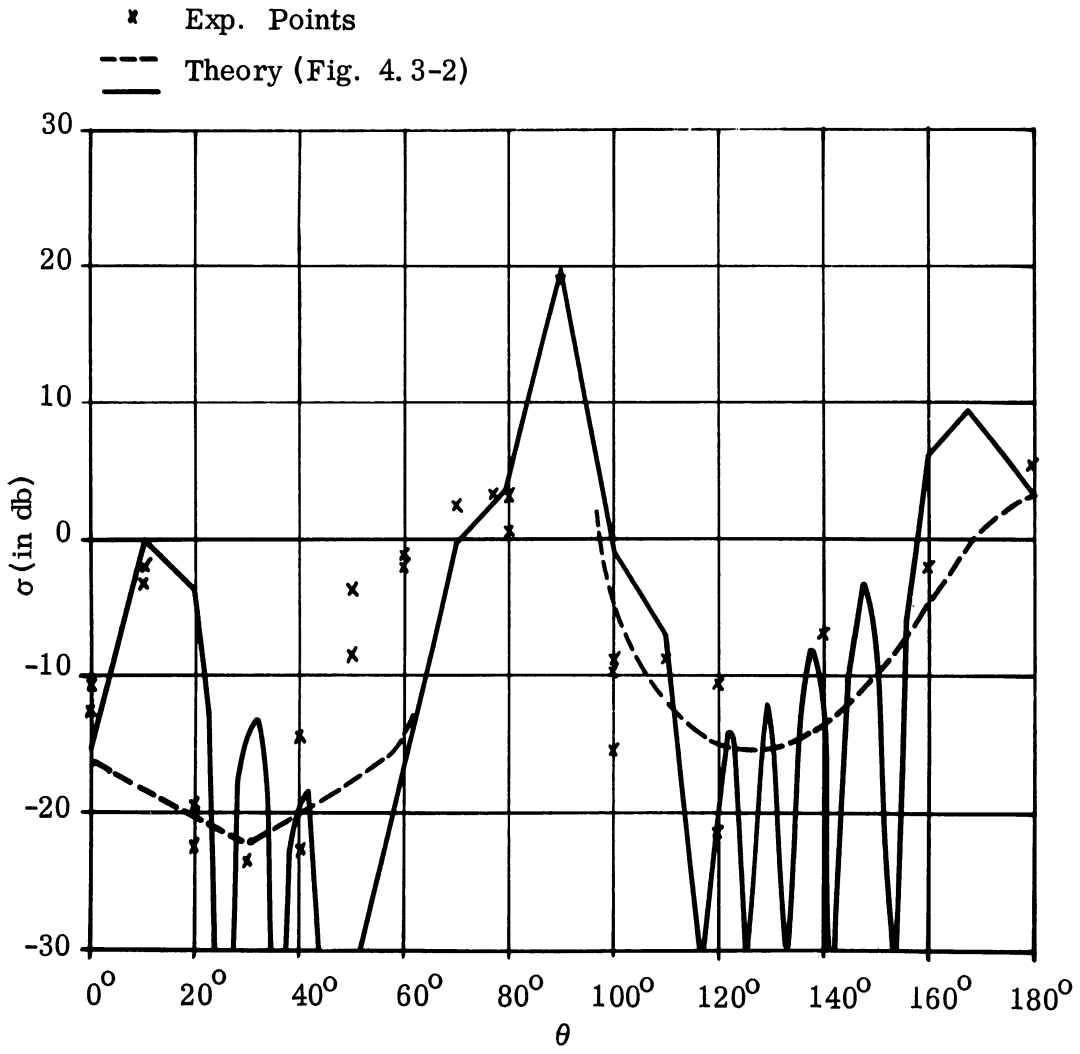

FIGURE 4.3-8: MISSILE WITHOUT FINS - THEORY VS. EXPERIMENT
($\phi_i = 0$, $\phi_r = \pi$)

$\left\{\begin{array}{l} 0 \text{ db} \longleftrightarrow 3 \text{ in}^2 \\ \lambda = 1.22'' \end{array}\right\}$

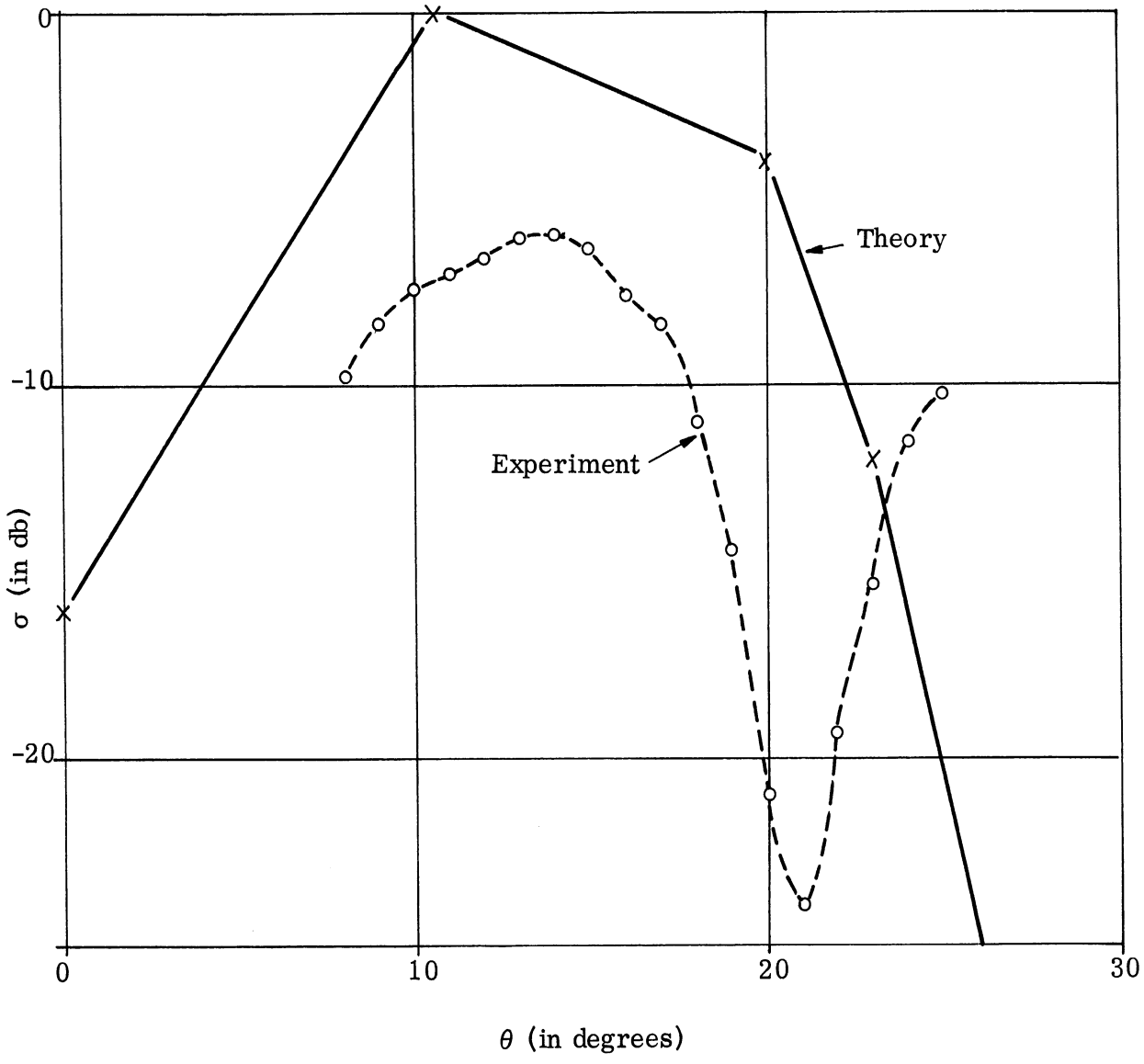

FIGURE 4.3-9: MISSILE WITHOUT FINS - THEORY VS. EXPERIMENT FOR $\phi_i = \phi_r = \pi/2$

Run No	Aspect θ	ϕ_i =	Relative Phase Angle (in Degrees)					
		ϕ_r =	$\pi/2$	$\pi/2$	$\pi/4$	0	$3\pi/4$	0
			$\pi/2$	$\pi/4$	$\pi/4$	$\pi/4$	$3\pi/4$	π
39	0^o		-16	-1	-5	-12	-8	+199
40	0^o		-45	-55	-13	+11	-3	+233
50	90^o		8	8	1	-7	-2	+172
58	180^o		0	0	1	2	-1	+179
--	Theory		0	0	0	0	0	+180

TABLE 4.3: MEASURED PHASE ANGLES - MISSILE WITHOUT FINS - THEORY AND EXPERIMENT

4.4 The Entire Missile (with Fins)

The missile model is displayed in Figure 4.3-1 and the basic assumptions relative to how the missile is to be modeled for the purpose of the calculations were presented in the preceding section. We find that there are six cross section contributions to be considered:

σ_1 = the contribution of the fuselage,

σ_2 = the contribution from the leading edges of the vertical fins,

σ_3 = the contribution from the leading edges of the horizontal fins,

σ_4 = the contribution from the trailing edges of the vertical fins,

σ_5 = the contribution from the trailing edges of the horizontal fins, and

σ_6 = the "flat plate" contributions from the fins and the rear of the fuselage.

To estimate σ_1 we use the approach of Section 4.3 employing both the straight optics technique and also the "thin body" approach. In the latter case, however, instead of attempting to predict the oscillatory nature of the return we determine the upper bound to the oscillations. Due to the presence of the fins this oscillatory nature of the return from the "fuselage" is expected to be disrupted except for the rear quartering aspects.

In estimating the response from the fin edges we first model them with thin wires and then employ the material of Section 4.4 of Reference 9 to obtain the estimates of σ_i ($i = 2, 3, 4$ and 5). In each case we determine, for given θ, ϕ_i, and ϕ_r, the "wire aspect angle" (the angle between the wire and the direction of incidence) and the wire polarization angles (this is the angle between the polarization direction and the plane determined by the wire and the direction of incidence). With regard to the leading edges of the vertical fins we note that for our range of aspects the returns from the upper and lower fins will always be "in phase". This is also true for the trailing edges of the vertical fins for $0 < \theta < \pi/2$. The leading edges of the horizontal fins will be "in phase" for $\theta = 0$ but as θ increases the "far" fin will be in shadow and thus can be neglected.

It is known that the return from wires is very dependent on the length of the wire, especially for wires whose lengths are between $\lambda/2$ and 2λ and we

also note from Figure 4.3-1 that it is somewhat difficult to estimate the "effective" length of the wire-like edges of these fins. (An examination of the actual model used in the experimental tests confirmed this fact and also pointed up certain minor differences in the fins themselves.) By examination of Figure 4.3-1 together with a study of the model itself we find that the leading edges are effectively about 1.25 λ in length and the trailing edges about 1.5 λ in length (to be considered as effectively two edges of length $3\lambda/4$ when viewed from the forward quarter). It is realized that these estimates of edge length are quite rough; however, examination of the broadside and average wire response curves in Figures 4.4-6 and 4.4-5 of Reference 9 indicates that at least in the average sense and at the broadside aspect we can expect these edges to scatter somewhat like wires of the above specified lengths. The choice of these wire lengths, i.e., 1.5 λ, 1.25 λ, and 0.75 λ are convenient since the angular distributions of the responses for these wires are given graphically in Section 4.4 of Reference 9.* To be more specific with regard to the above statements we see that the broadside and average returns of wires whose lengths range from about 1.4 λ to 1.6 λ do not vary by more than about a factor of two; thus for 3 db-type estimates it is reasonable to use a 1.5 λ wire to model any edge in the length range from 1.4 λ to 1.6 λ.

---

* It should be pointed out that the graph of the angular response for the 1.25 λ wire shown in Figure 4.4-4 of Reference 9 involves a typographical error; the range should be from 0 to .04 rather than from 0 to 0.4 as indicated. That is, the vertical scale is too large by a factor of ten.

Similar arguments hold for the 1.25 λ and 0.75 λ cases.

For the flat plate contributions we determine the flat plate area of each fin (assuming the entire fin to be flat) and employ the optics approach to estimate the cross section contribution, i.e., we make use of the $4\pi \left[A/\lambda\right]^2$ formula with A being the flat plate area. This contribution only occurs for $\theta = 90^o$ at which aspect we have a large return from the effective cylinder. We employ optics as in the "without fins" case but here we observe that the fins reduce the effective cylinder length to 9.1 in. Taking into account the relative positions of the fins and the cylinder for $\theta = 90^o$ we consider relative phase in estimating the broadside response.

Performing the above steps we have at each θ and for each pair, ϕ_i and ϕ_r, the average cross section expressed as $\sum_{i=1}^{6} \sigma_i$. We also can consider a type of theoretical maximum obtained by assuming all contributions to be in phase, namely the expression $(\sum_{i=1}^{6} \sqrt{\sigma_i})^2$. At some aspects, where there is only one dominant contributor, or at which relative phase was considered (i.e., at $\theta = 90^o$) these two estimates would not differ; at other aspects, however, these two, $\sum \sigma_i$ and $(\sum \sqrt{\sigma_i})^2$, will provide us with estimates of the average cross section and an upper bound. Such estimates have been computed and they are displayed in Figures 4.4-1 through 4.4-6 where the estimates are compared with the experimental data. As in the previous section all results are expressed in db relative to the sphere return of the experimental data. The existence of two "average" estimates for

$120^{o} < \theta < 180^{o}$ is due to the two interpretations given to σ_1 mentioned at the beginning of this section.

With regard to the phase angles which were measured we shall restrict our attention to the nose-on, broadside, and tail-on cases where we would expect the first five to be of the form ϕ_0 with the sixth of the form $\pi + \phi_0$. Table 4.4 displays the measured values compared with this estimate. We note that with all of the amplitudes involved being reasonably large these measured values agree as expected with the theory.

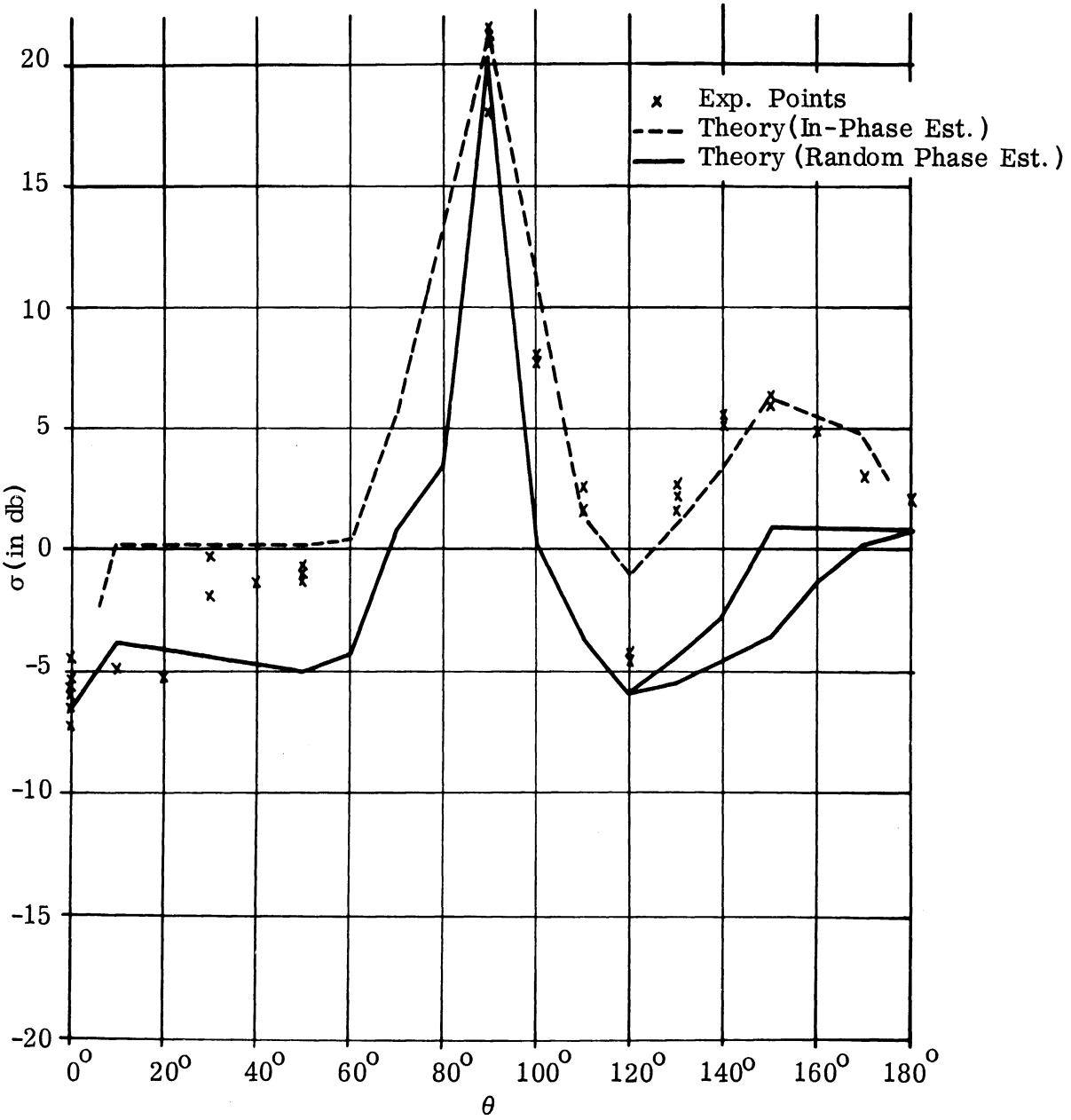

FIGURE 4.4-1: MISSILE WITH FINS - THEORY AND EXPERIMENT FOR $\phi_i = \phi_r = \pi/2$

(0 db $\longleftrightarrow$ 3 in.^{2}, $\lambda = 1.22''$)

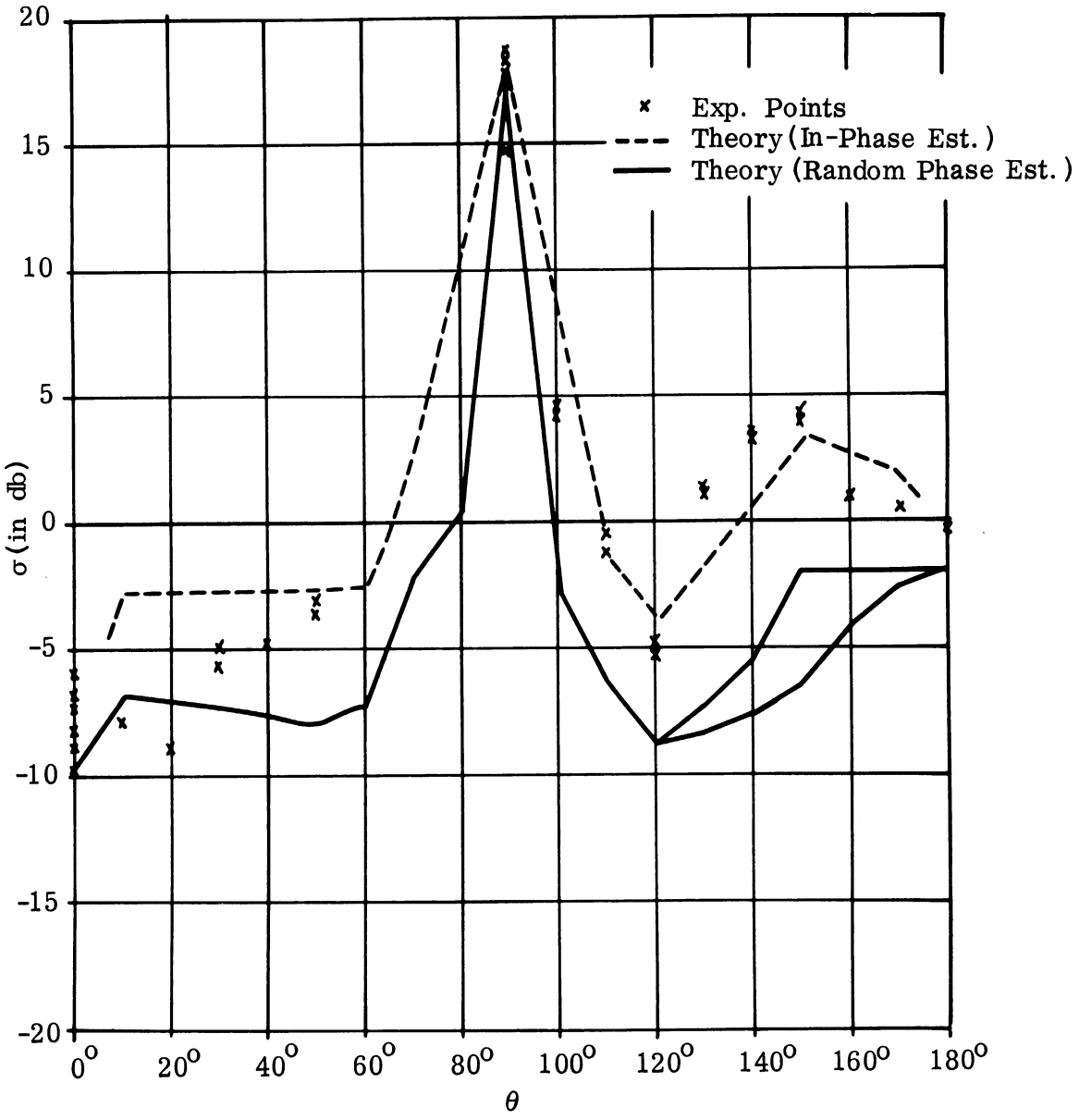

FIGURE 4.4-2: MISSILE WITH FINS - THEORY AND EXPERIMENT FOR $\phi_i = \pi/2$ AND $\phi_r = \pi/4$
(0 db $\leftrightarrow$ 3 in.^{2} $\lambda = 1.22$ in.)

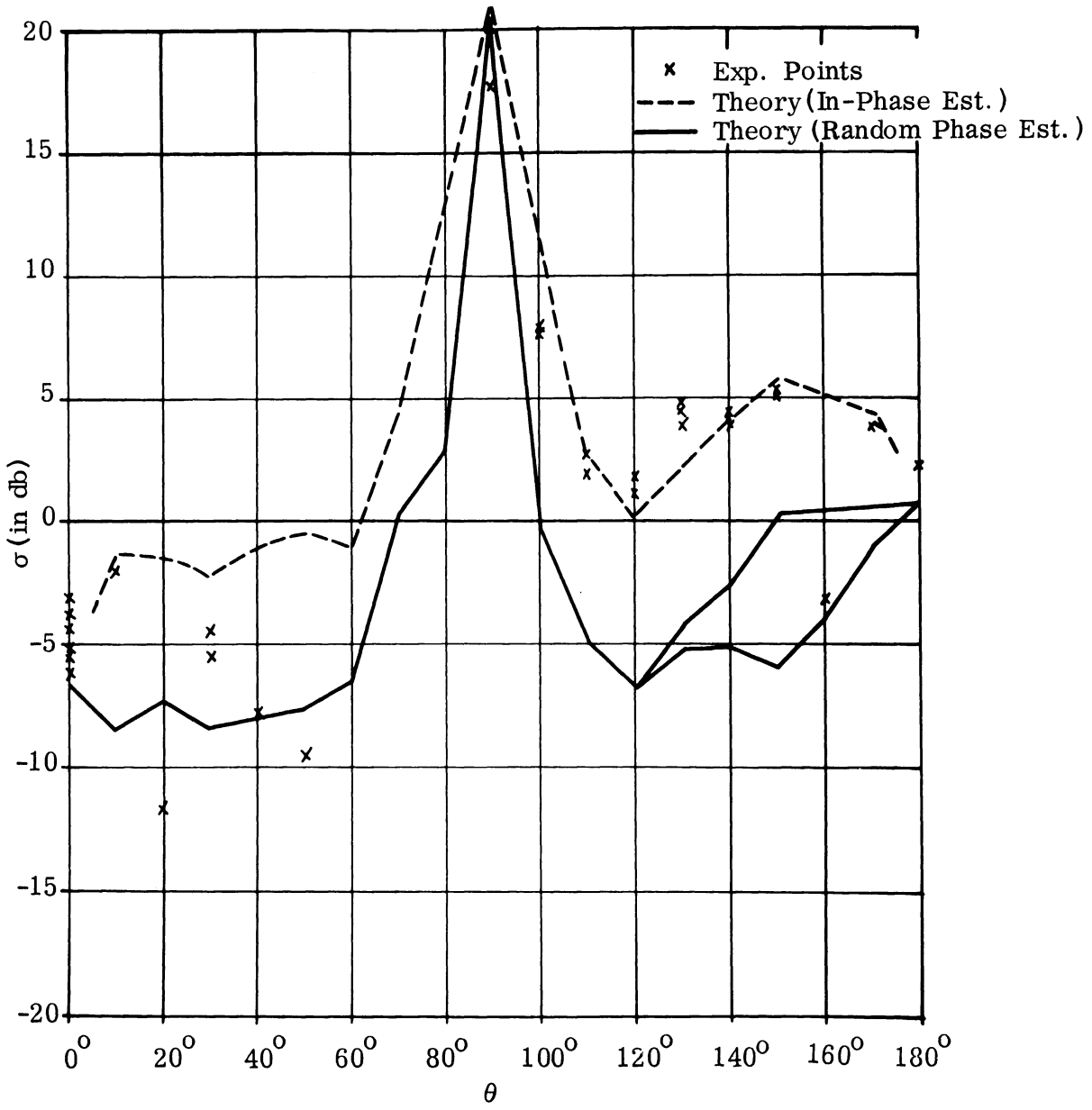

FIGURE 4.4-3: MISSILE WITH FINS - THEORY AND EXPERIMENT FOR $\phi_i = \phi_r = \pi/4$

(0 db $\leftrightarrow$ 3 in.^{2}, λ = 1.22 in.)

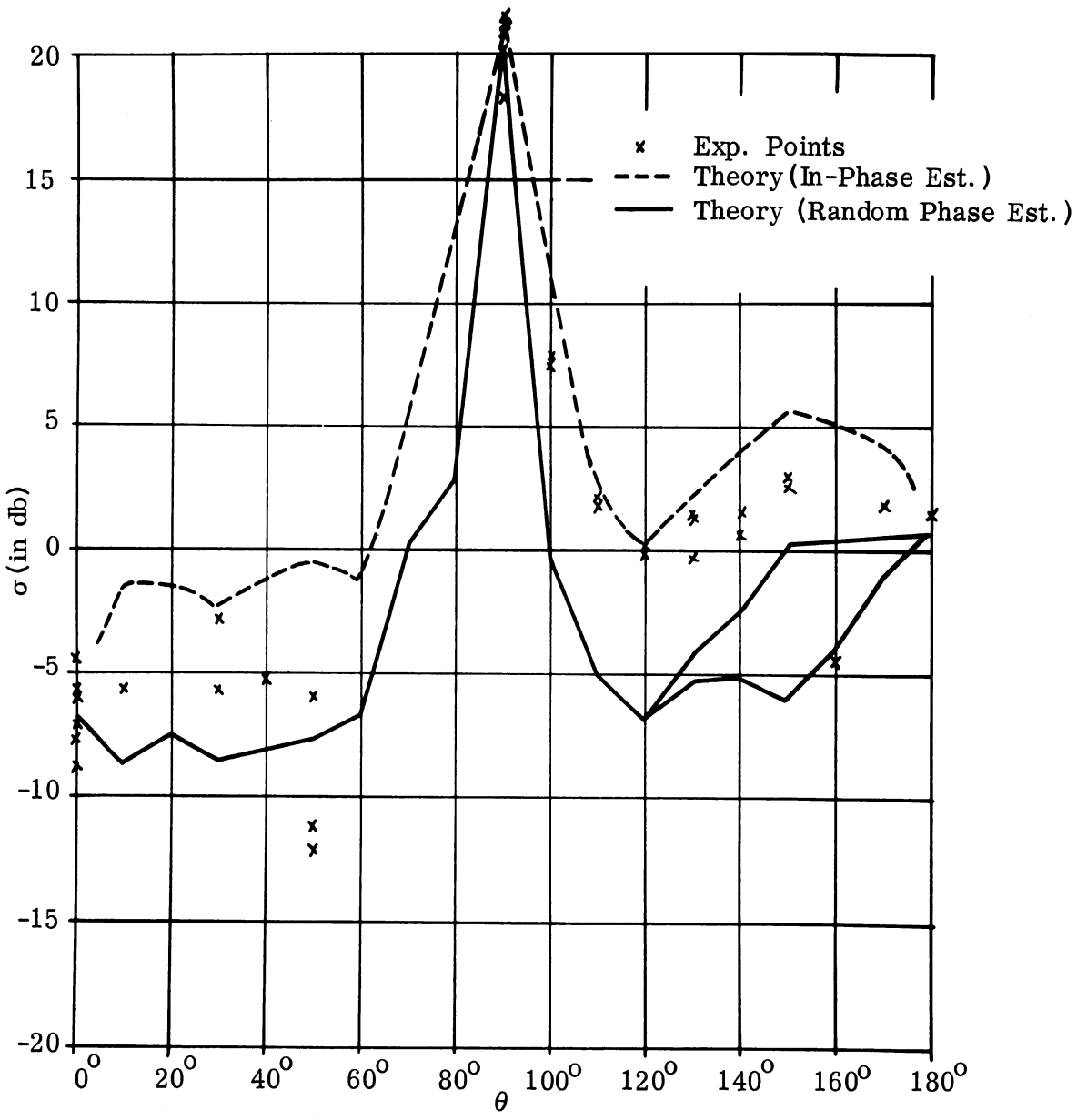

FIGURE 4.4-4: MISSILE WITH FINS - THEORY AND EXPERIMENT FOR $\phi_i = \phi_r = 3\pi/4$

(0 db $\longleftrightarrow$ 3 in.^{2}, $\lambda = 1.22$ in.)

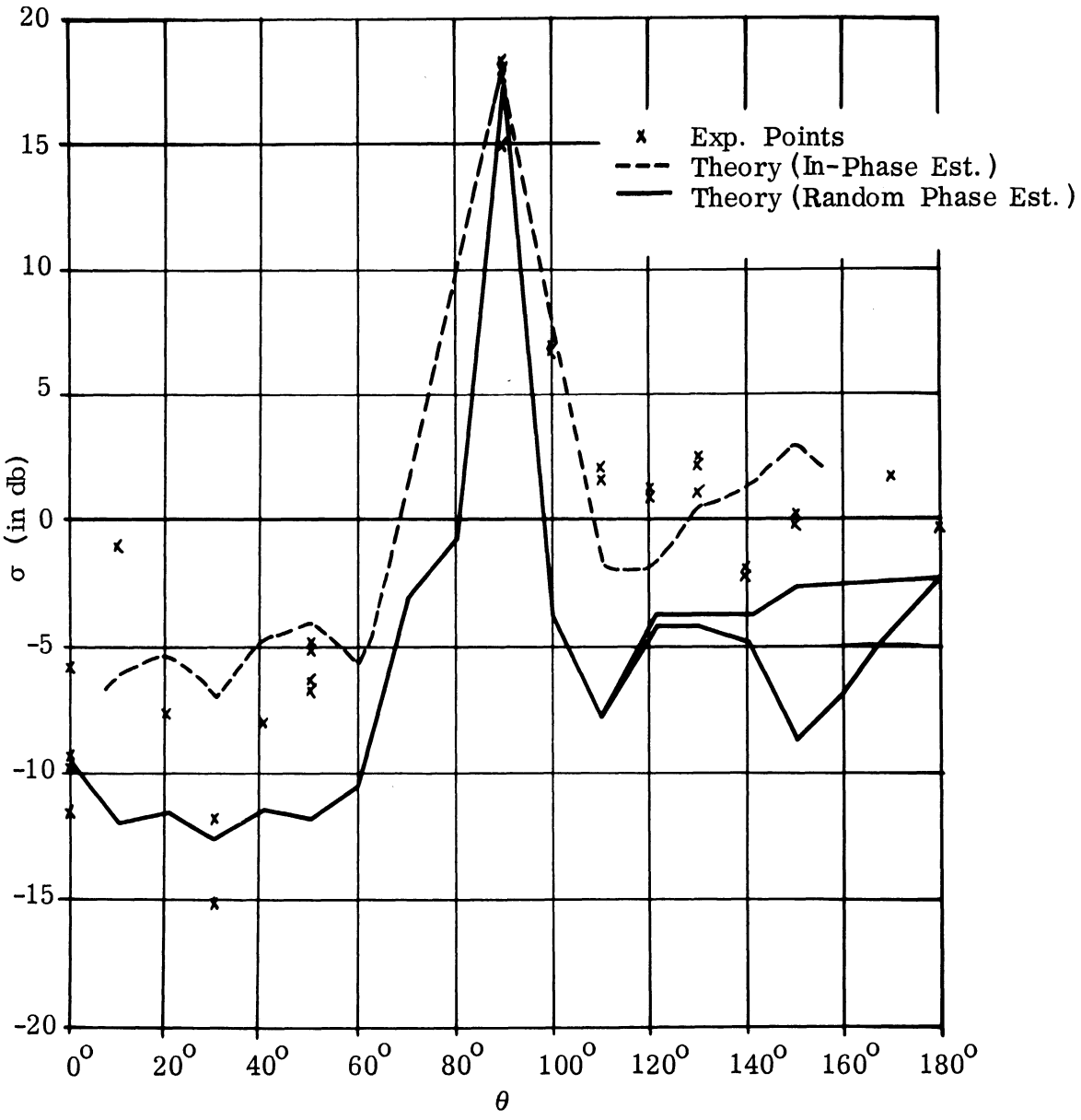

FIGURE 4.4-5: MISSILE WITH FINS - THEORY AND EXPERIMENT FOR $\phi_i = 0$ AND $\phi_r = \pi/4$
(0 db $\leftrightarrow$ 3 in.^{2}, λ = 1.22 in.)

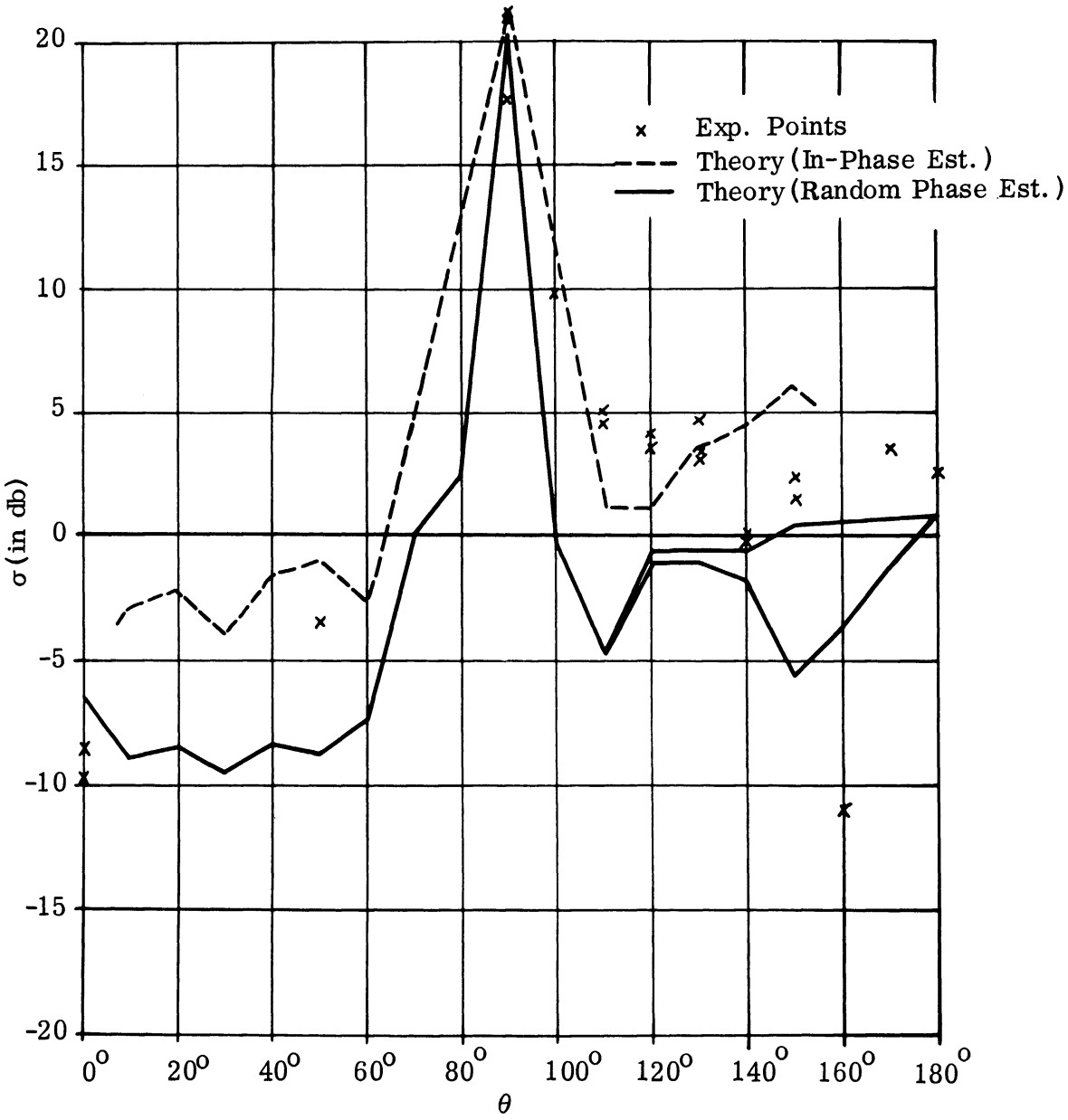

FIGURE 4.4-6: MISSILE WITH FINS - THEORY AND EXPERIMENT FOR $\phi_i = 0$ AND $\phi_r = \pi$

(0 db $\leftrightarrow$ 3 in.^{2}, $\lambda = 1.22$ in.)

Run No	Aspect θ	Relative Phase Angle (in Degrees)					
	ϕ_i =	$\pi/2$	$\pi/2$	$\pi/4$	0	$3\pi/4$	0
	ϕ_r =	$\pi/2$	$\pi/4$	$\pi/4$	$\pi/4$	$3\pi/4$	π
10	0^o	1	2	2	2	-7	-184
11	0^o	2	2	2	2	-7	-189
12	90^o	4	4	-1	-4	-4	174
17	90^o	1	4	1	-4	-2	177
18	90^o	3	4	1	-1	-3	187
19	90^o	3	3	1	-5	-1	174
38	180^o	0	0	1	0	-1	182
	Theory	0	0	0	0	0	+180

TABLE 4.4: MEASURED PHASE ANGLES - MISSILE WITH FINS - THEORY AND EXPERIMENT

Section V

PREDICTION OF SIZE AND SHAPE FROM MATRIX DATA

It is the eventual purpose of this study to evolve a relatively straightforward method by which scattering matrix measurements can be made to yield information on the size and shape of a target as well as information on the orientation of the target's axis relative to its mass-center trajectory. As a preliminary effort, which serves to illustrate the procedure, we have studied three problems which we could refer to as "war games". In these "games" a member of the theoretical group was given a set of experimental data including matrix measurements and asked to make an estimate of size and shape. In each case we have a problem which simulates a simplified field-type problem.

The simplifications and over-all assumptions made for each of the games include the following: It is assumed, in the "game", that the target was not precessing as it moved along its trajectory and that the trajectory information is good enough to yield accurate aspect information. That is, the aspect angle in degrees off nose-on is known. We also assume that our knowledge of the trajectory and/or the ionospheric effects is good enough so that we can be sure that the $\sigma(H, H^{-})$ measurements were made with the $\vec{E}$-vector in the plane of the target axis and the direction of incidence (or that the required corrections had been made). We realize that these are quite extensive assumptions, but for the first set of laboratory "war-game" problems they are appropriate.

In discussing these "games" we shall speak in terms of model sizes rather than the simulated full-scale situations. The application to the corresponding full-scale problem will be discussed but as stated above we shall speak only in terms of the model measurements themselves.

5.1 Problem No. 1

War game No. 1 was evolved from the data obtained for the finless missile model discussed in Section 4.3. A junior member of the Laboratory (E. LeBaron) was given the continuous plot of σ(VV) vs. θ shown in Figure 3.2-2 and the matrix data at $\theta = 90^{o}$. He was not informed as to what model was involved. He was also told to assume that the body was one of revolution and that velocity, etc., data implied that it was a missile type configuration either without fins or with very small fins.

His analysis went as follows: The σ(VV) and σ(HH) returns were sufficiently similar in the 90^{o} matrix data to indicate that optics reasoning should be a reasonable procedure at that aspect while the large narrow peak at 90^{o} implied that the main portion of the target might be a cylinder. At $\theta = 90^{o}$ the broadside peak for a cylinder is given by $2\pi \ell^2 a/\lambda$, or in this case $\left[5.15\, a\ell^2\right]$ in^2 where ℓ is the length and a is the radius of the cylinder. The continuous plot shows σ(VV) to be about 18.5 $\pm$ 1 db above the sphere return, or about 215 $\pm$ 45 in^2 and this implies that $a\ell^2 \approx (41.7 \pm 8.7)$ in^3.

Employing the methods of relative phase calculation discussed in Section 6 (pp. 107 -116) of Reference 9 it is noted that:

(1) the angle locations of the first three nulls away from the broadside peak imply that $\ell \approx$ 5.8", 8.1", and 8.9" respectively,

(2) the angle locations of the first three peaks away from the broadside peak imply that ℓ is approximately 7.6", 8.6" and 9.1" respectively.

Assuming a 0.5^{o} error in the location of these nulls and peaks he thus concluded that $5" < \ell < 10"$, which from the previous analysis would indicate that $0.41" < a < 1.64"$.

At 180^{o} the return is relatively broad $\approx 180^{o} \pm 24^{o}$ and large, (5 db above the sphere). $\sigma(180^{o}) \approx (3.16)\, 3 \approx 9.5$ in^2. Since the flat plate return is $4\pi(\pi a^2)^2/\lambda^2 \gg \sigma(180^{o})$, it follows that $\underline{a \geq .58 \text{ in.}}$ If the return from the back is (5 $\pm$ 1) db and if the rear is a flat plate, then $7.5 \text{ in}^2 < \sigma(180^{o}) < 12.0 \text{ in}^2$ and thus $.55" < a_{min} < .61"$.

If it is assumed that the back has a spherical cap, we can inquire what dimensions would give the measured return. For a sphere $\sigma = \pi R^2 = \sigma(180^{o})$ = 7.5 to 12.0 in^2 or $1.55" < R < 1.95"$. If the maximum effective angle ($\theta' \approx 24^{o}$) occurs at $\sin \theta' = \frac{a}{R}$ then $.62" < a < .76"$ and now one could limit the cylinder radius by $.55" < a < .76"$. This limit on "a" leads to a limit on ℓ (since $a\ell^2 =$ 43.7 $\pm$ 8.7) of $7" < \ell < 10"$.

The dip at zero degrees indicates that the object has a pointed or relatively sharply curved nose. Because the cross section is on the average larger

for $\sim 75^{o} < \theta < 90^{o}$ than it is for $90^{o} < \theta < \sim 105^{o}$ it is likely that the nose is conical or ogival. Because of the relatively small dimensions of any feasible nose there is no way of saying definitely whether it is an ogive or a cone or a collection of conical segments.

If we assume that the 1.1 db difference between vv and hh polarization cross sections displayed in the matrix data is significant, then from Mentzer (Ref. 10) we judge that $ka \approx 2.9$ or $a \approx .56''$. This then leads to the general conclusion that the back is very close to a flat plate and that the radius, a, is close to the minimum a of .55 in; then approximately $.55'' < a < .57''$, and $8'' < \ell < 10''$ with the general shape like that shown below:

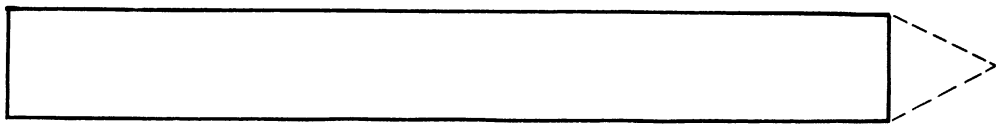

The above completes the analysis, and reference to Figure 4.3-1 will indicate the degree of success. We see that the actual values were a = 0.53" and ℓ = 10.6". One would conclude that this was a successful analysis.

5.2 Problem No. 2

Problem No. 2 involved the simulation of a simultaneous measurement of a given target at two frequencies. These two models of the same shape were referred to as "Baker" and "Charlie" and the problem was to determine what differences (if any) existed between this shape and the warhead. Both models (Baker and Charlie) were measured at 9700 Mc but it was stated that the simulated frequency was 0.3 F for Baker and 0.1 F for Charlie where F was the frequency of the nose-cone measurements discussed in Sections III and IV. Thus, if this shape were the nose-cone then we would have measurements of the shape shown in Figure 4.2-1 simulated at 2910 Mc (Baker) and 970 Mc (Charlie), i.e., Baker would be a 3/10-scale model and Charlie would be a 1/10 - scale model of the configuration of Figure 4.2-1. The analysis is directed toward testing out the assumption that Baker and Charlie were in fact "nose-cone" models.

Plots of the model measurements are shown in Figures 5.2-1 and 5.2-2; these display $\sigma(V, V)$ vs. θ. The matrix data obtained are shown in Table 5.1; these measurements were made at aspects leading to relative peaks in the pattern for the Baker model. (The experimentalist stated that the "large peak" aspect of $\theta = 80^{\circ}$ to 81° was to be assumed the same as the 77.7° location of the peak for the nose-cone model of Sections III and IV.)

The individuals who analyzed the data (J. Crispin with the assistance of D. Raybin) concluded that Baker and Charlie were, in fact, models of the

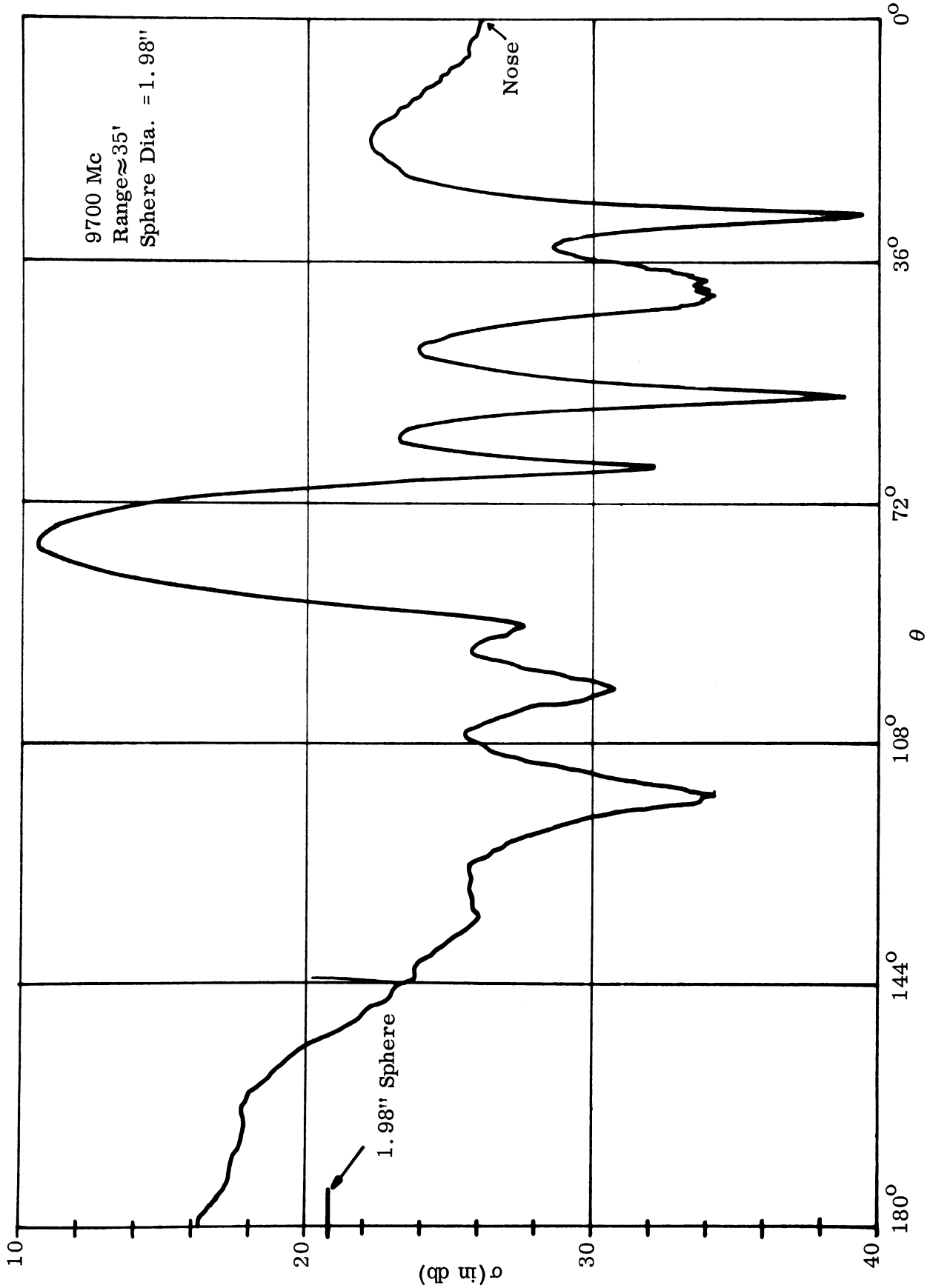

FIGURE 5.2-1: $\sigma(V, V)$ VS. θ FOR THE MODEL "BAKER"

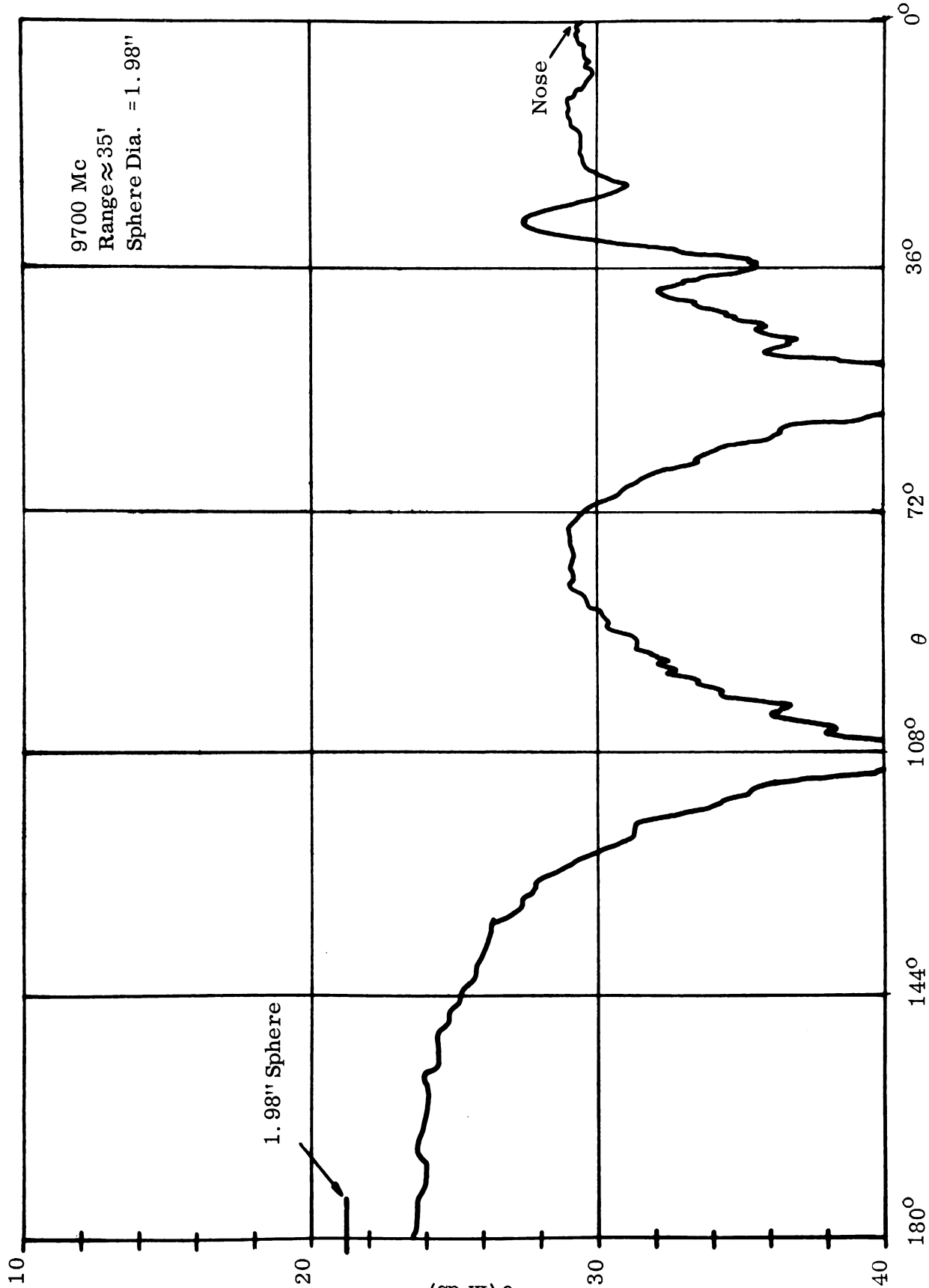

FIGURE 5.2-2: $\sigma(V, V)$ VS. θ FOR THE MODEL "CHARLIE"

Model	Aspect	σ (in db rel. to sphere)*						Rel. Phase Angles (deg.)					
		VV	VA	AA	HA	BB	HH^-	VV	VA	AA	HA	BB	HH^-
BAKER	55°	-3.8	-6.6	-3.5	-4.6	-2.8	-2.0	144	142	141	132	139	315
	66°	-7.9	-10.1	-5.0	-6.8	-6.2	-4.0	4	6	4	3	5	182
	81°	10	7	10.6	7.9	10.4	11.0	36	35	32	29	33	208
	97°	-3.8	-7.4	-5.3	-7.9	-4.2	-6.4	237	237	236	240	236	50
	109°	-4.4	-7.5	-4.6	-8.7	-5.3	-5.9	347	350	359	8	356	191
CHARLIE	54°	-11.7	-14.9	-25.3	-25.8	-21.4	-18.9	97	80	131	309	111	66
	65°	-13.4	-15.5	-10.0	-10.1	-12.8	-6.3	355	351	307	290	309	112
	80°	-7.6	-11.8	-5.9	-6.2	-5.9	-2.7	262	256	236	235	241	51
	96°	-7.1	-8.7	-6.9	-12.5	-7.6	-5.8	120	120	121	125	117	285
	108°	-9.3	-11.9	-15.2	-26.1	-14.6	-26.3	40	35	31	-5	21	163

*sphere dia. = 1.98"

TABLE 5.1: MEASUREMENT DATA FOR MODELS "BAKER" AND "CHARLIE" AT 9700 MC

nose-cone shape of Figure 4.2-1 or that differences between the Baker-Charlie shape and this nose-cone were not significant. This conclusion is based on the following four points.

(1) Cross Section at the Normal Aspect: The cross section of a truncated cone at the normal aspect ($\theta \approx 79^{o}$) is given by $(\text{dimension})^3/\lambda$ as can be seen from Reference 9. Thus, a 3/10-scale model should have a return which is about 15 db below the cross section of the full-scale model and a 0.1-scale model should have a cross section which is 30 db below the full-scale model. (We are considering the shape of Figure 4.2-1 as the full-scale configuration.) Referring all data obtained in the laboratory to db relative to the return from a 1.98" diameter sphere we find for $\sigma(H,H)$ that the nose cone cross section is 25 db, for Baker it is 11 db, and for Charlie it is -3 db, (relative to the sphere return) i.e., the differences are 14 db and 28 db rather than the 15 and 30 db values listed above. (The $\sigma(HH)$ values are used since we would expect these to be closer to the optics predictions than $\sigma(VV)$ for the small Charlie model.) Thus, examination of the normal aspect indicates that Baker and Charlie may be the nose cone.

(2) The Tail-On Aspect: If Baker and Charlie are models of the nose cone, then the tail-on cross section should be given approximately by πR^2 where R is the radius of the rear spherical cap. Thus, in the model measurements

we could expect the Baker return to be about 11 db below, and the Charlie return to be about 20 db below the nose cone cross section given in Section III. Referring to Figures 5.2-1 and 5.2-2 and referring all data to the 1.98" diameter sphere return we find that these three values are respectively 17, 5, and -3 db (relative to the sphere return) for the nose cone , Baker, and Charlie, i.e., the differences are 12 and 20 db as compared to the predicted 11 and 20 db. Thus Baker and Charlie" look like" the nose cone for the tail-on aspect.

(3) Location of Peaks: Reference to Figure 3.2-3 indicates that the first peak in front of the normal peak for that nose cone model is about 5.75^{o} away from the normal. Reference to Figure 5.2-1 indicates that the similar peak for Baker is about 16^{o} away from the normal. If Baker were in fact a 1/N-scale model of the nose cone model, then these relative peaks (assumed to be due to "in phase" relations) should satisfy the relation $N \sin(5.75^{o}) = \sin(16^{o})$, i.e., $N = 2.76$. Since the assumption is a 3.33 to 1 relation in size, we see that again the conclusion that Baker and Charlie are smaller models of the nose cone shape is verified (or, to be more precise, not significantly contradicted) since 3.33 and 2.76 are the same to one significant figure.

(4) Relative Magnitude of Peaks: For the nose cone shape one would expect the amplitude of the first peak in front of the normal peak to be larger than

the amplitude of the first peak to the rear of the normal peak; this is observed for the Baker model. The Charlie model is a little too small for this characteristic to be positively identifiable.

Nose-on calculations could be made for Baker and Charlie; however, it is not expected that calculations would be sufficiently precise to pin down the nature of the front spherical cap which point (4) above implies may be present in the Baker-Charlie shape. Therefore, it was concluded that the Baker-Charlie configuration was basically the Jupiter nose-cone shape with the reservation that the spherical cap in the nose could have a slightly different radius.

This conclusion was presented to R. E. Hiatt, who conducted the experiments, after which the shape was made known to those who had attempted the diagnosis. Hiatt informed those who performed the analysis that the Baker-Charlie configuration was in fact the nose cone. Thus, the analysis of the experimental data was correct.

5.3 Problem No. 3

Problem No. 3 involved the measurements of Model "Dog" and Model "Easy" with $\lambda = 1.22"$. Here it was the task of the theoretical group* to determine what differences existed (if any) in the two models and what could be gleaned about the models from the data provided. The information provided is

* This study was conducted by J. Crispin with the assistance of D. Raybin.

as shown in the Table 5.2, and the plots of σ(vv) vs. θ are displayed in Figures 5.3-1 and 5.3-2.

To compensate for some of the minor measurement inaccuracies, those performing the analysis were informed that both "Dog" and "Easy" were symmetric fore and aft - something that is suggested by the plot of σ(vv) vs. θ for "Dog" in Figure 5.3-1. The pattern exhibited in Figure 5.3-1 is suggestive of a regular body and the first shapes which come to mind are a cylinder, an ogive, and a prolate spheroid.

The matrix data on Dog implies the return is essentially independent of polarization (at least for θ within 20^o of broadside, thus optics methods should be appropriate. Attempting to determine something about the length of the body we note that the locations of successive peaks at θ = 19, 32, 42, 50, 58, and 65 degrees in Figure 5.3-1 imply that $5.6'' < \ell < 6.2''$. The successive peaks at θ = 104, 107, 110, and 113 degrees in the figure, however, imply that $\ell \approx 12 \pm 1$ inches. Thus we can only conclude that $5.6'' < \ell < 13''$.

The broadside return for Dog implies that $\sigma(90^o) \approx 85$ in^2, thus if the body were a cylinder (radius a and length ℓ) then $a\ell^2 = 16.5$ in^3 and with ℓ bounded as shown above we would have $.09'' < a < .53''$. The smaller values of a in this range should lead to a polarization dependence at $\theta = 90^o$ (there is none) and values of a in the 0.5" range would imply a much larger nose-on return than is displayed in Figure 5.3-1. Thus, it is unlikely that Dog is

Model	Aspect	σ (in db rel. to sphere)*						Rel. Phase Angles (deg.)					
		VV	VA	AA	HA	BB	HH	VV	VA	AA	HA	BB	HH
DOG	90°	10.9	8.1	10.8	8.1	10.4	10.9	351	351	341	331	340	150
	76.5° } 113.5° }	-3.3	-6.0	-3.0	-5.8	-3.3	-2.8	293	296	288	276	276	90
	70° } 110° }	-9.2	-11.2	-8.0	-9.6	-9.7	-8.5	343	351	338	324	327	132
EASY	90°	-1.1	-3.4	-3.2	-2.4	-2.8	+0.9	88	94	142	193	153	13
	76° 104°	1.7	-0.9	-4.9	-11.4	-7.8	-10.7	110	110	124	253	126	83
	45° 135°	0	-2.0	-4.2	-5.2	-3.4	-0.7	148	143	181	243	204	68

* 2.945" dia. sphere

TABLE 5.2: MEASUREMENT DATA FOR MODELS "DOG" AND "EASY" AT 9700 MC

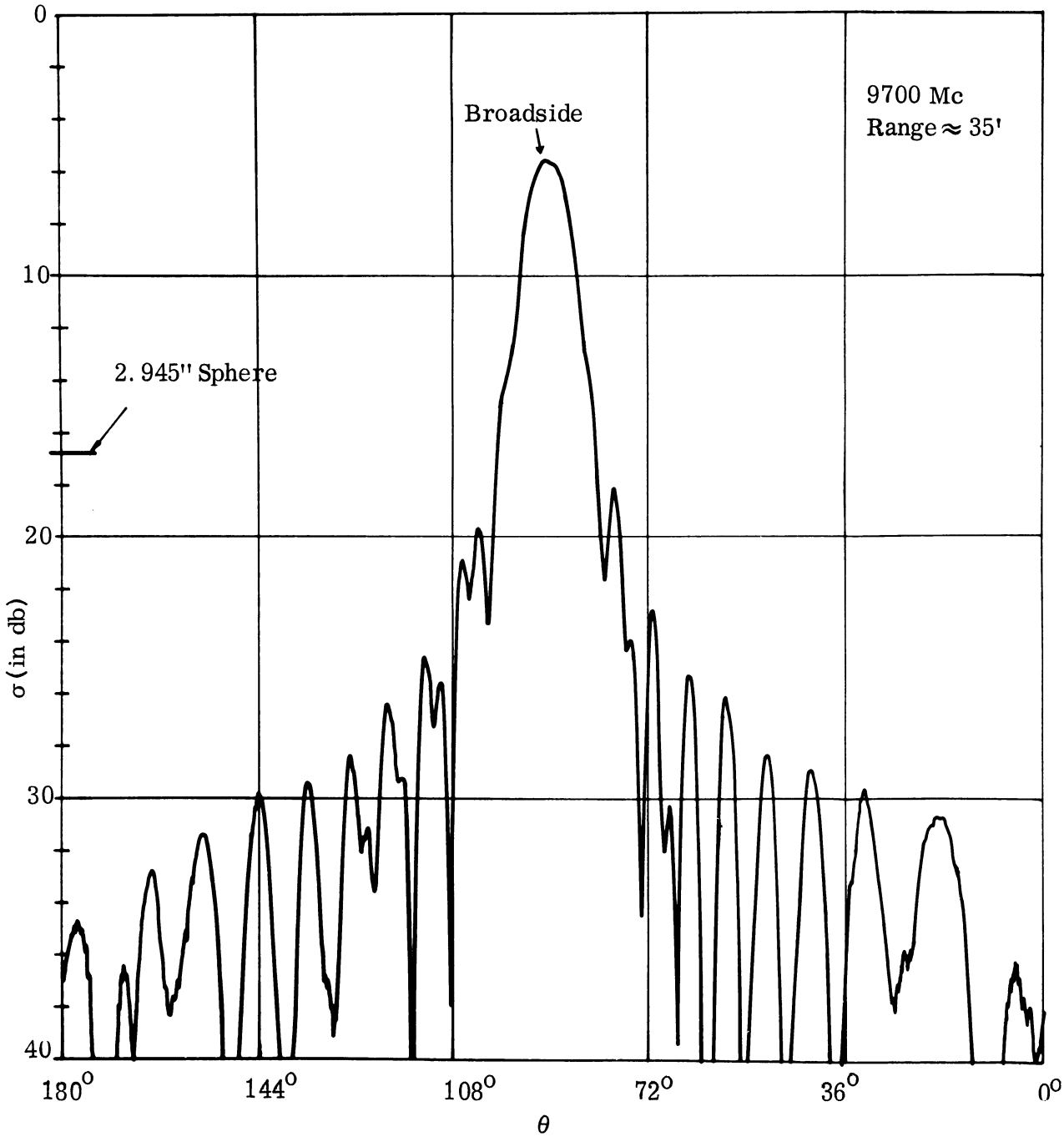

FIGURE 5.3-1: σ(V, V) VS. θ FOR THE MODEL "DOG"

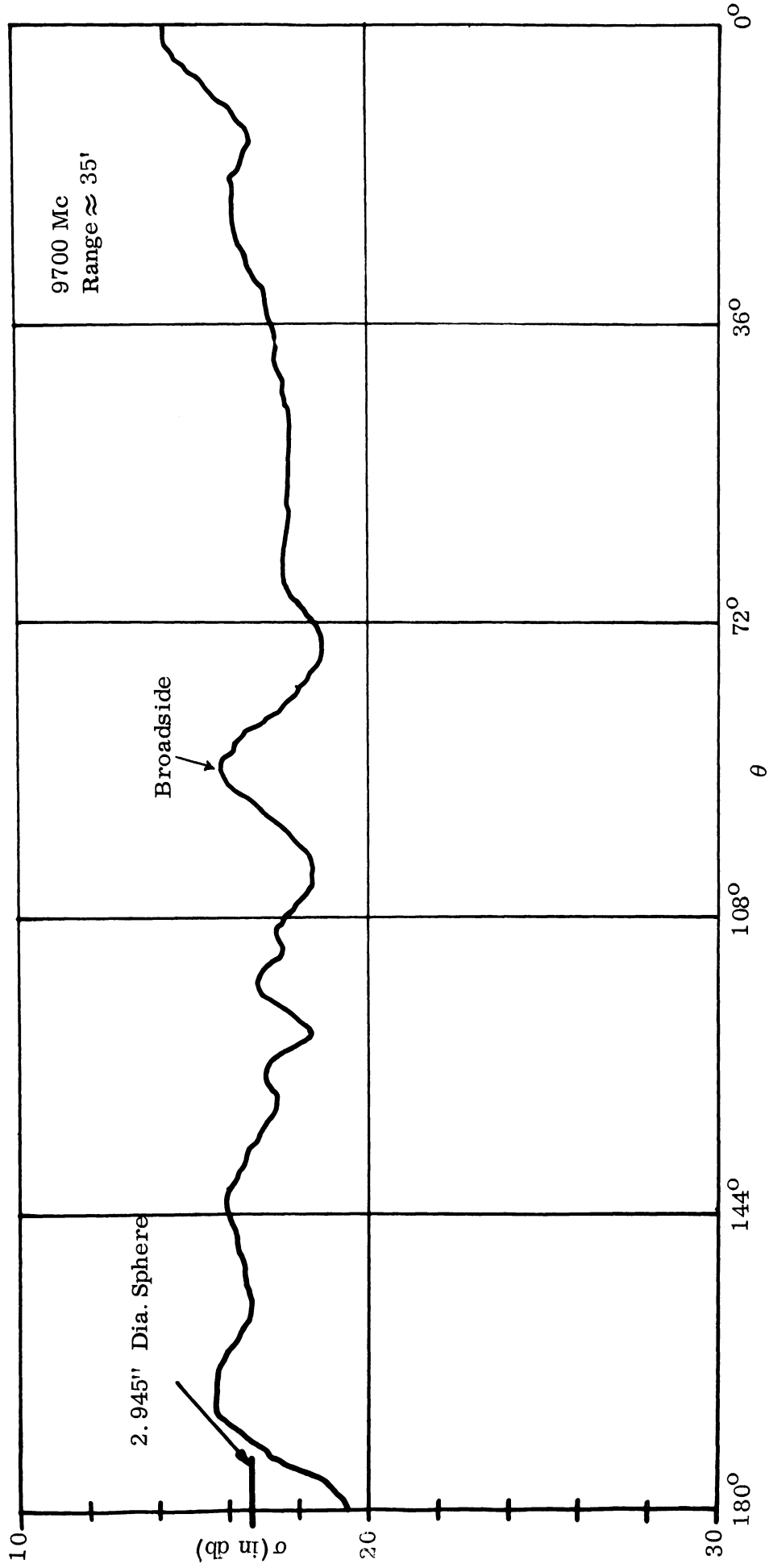

FIGURE 5.3-2: $\sigma(V, V)$ VS. θ FOR THE MODEL "EASY"

a simple cylinder. (It could be a cylinder capped by cones at either end, but this is also unlikely since no sharp cone-like peaks are readily observed.)

The ogive possibility leads to the assumption that $\pi a\, R = 85\ in^2$ where 2a is the maximum thickness and R is the large radius of curvature. The length (ℓ) of the ogive is expressed in terms of a and R by the relation $(\ell/2)^2 + a^2 = 2a\, R$. The pattern shown in Figure 5.3-1 implies that if the object is an ogive the half-nose angle (α) is between 10^o and 18^o. Since the ogive is such that $\sin\alpha = \ell/2R$ and $1 - \cos\alpha = a/R$, estimates of a and ℓ can be obtained. These estimates are shown in the following table (a and R in inches):

α	a	R	ℓ
10^o	0.64	42.5	14.8
18^o	1.15	23.5	8.35

The ogive possibility could be investigated more adequately if we had a plot of σ(HH) vs. θ for here we would expect (if it were an ogive) a relatively large peak at $\theta \approx 10$ to 18 degrees.

If we assume that the body is a prolate spheroid (semi-major axis = c, semi-minor axis = b) then we would have $\pi c^2 = 85\ in^2$, i.e., c = 5.2", thus a body 10.4" long. This is within the range $5.6" < \ell < 13"$ found above. A quick optics check on the cross section values at $\theta = 76.5^o$ and 70^o indicates

that $b \approx .56''$. Thus a possibility is a spheroid about 10.4" long and about 1.1" in diameter.

In summary, then, Dog could be

(1) an ogive of half-angle between 10 and 18 degrees and 8 to 14 inches long,

(2) a prolate spheroid of length about 10.4" and maximum thickness 1.1", or

(3) a cylinder capped fore and aft with ogives or cones.

Either (1) or)2) seems the most likely but additional data at another frequency would be required for more complete diagnosis. In any event, a body of length 9 ± 4 inches is clearly indicated.*

With regard to the model Easy, we have data at only one frequency on an object whose value for σ(VV) is insensitive to changes in θ (see Fig. 5.3-2), but for which σ(HH) is quite sensitive to changes in θ (see Table 5.2). It could be a small scale model of Dog or one of the other models; data at least for one more frequency and σ(HH) vs. θ plots would really be necessary to determine this shape.

Upon completion of this analysis, R. E. Hiatt informed those who performed the analysis that "Dog" was a prolate spheroid of length 12" and thickness 1.2". Model Easy was a "Jack" of arm length 3". The diagnosis on "Dog" was thus reasonably satisfactory considering that data at only one frequency were available. Knowing the shape of Easy we can see that a plot

---

* The existence of the more closely bunched peaks for $\theta > 90^{\circ}$ in Figure 5.3-1 indicates that ℓ is probably in the range from 9 to 13 inches.

of σ(HH) vs. θ would have indicated that the σ(HH) at 0^{o} is the same as σ(HH) at 90^{o} and would have been a great help in identification. It might be noted that the optics techniques of Reference 9 would have implied that this Jack should have a σ(VV) value of approximately 2.86 in^2 independent of θ while the data of Figure 5.3-2 displays a variation of about 3 db from the sphere return, the cross section of the sphere being about 6.8 in^2 at this wavelength.

5.4 Possible Future Laboratory Problems

There are an almost unlimited number of simulated diagnostic games of this type which can be devised. One might consider the problem of determining tumbling and precessing rates knowing the configuration or determining these motion parameters without information on the configuration. It is felt that a systematic program of this type would be extremely informative in developing systematic diagnostic methods.

It seems clear that the matrix approach to electromagnetic diagnostics is a good one and that very good information on size and shape and target motion can be so obtained. The above "games" have illustrated how good estimates of size and shape can sometimes be made with less radar data than the method calls for in general; the Model Easy "games" illustrated that in other cases information at only one frequency is not enough.

ACKNOWLEDGEMENTS

The authors would like to express their thanks to C. W. Williams of the Chrysler Missile Division for providing the configuration data for the nose cone and to several other members of the Radiation Laboratory for their assistance: T. E. Hon, D. L. Pepper, and M. A. Siegman for their assistance in the laboratory measurements; B. Ullman and H. Hunter for their assistance in the analysis of the data; and E. I. Le Baron and D. M. Raybin for their participation in the "games" discussed in Section V.

APPENDIX

Experimental Determination of a Scattering Matrix

Summary

The purpose of this appendix is to discuss the relationships which must exist between various measurements of the far-zone field scattered by an object which is struck by a plane-polarized electromagnetic wave, and to illustrate how the complete information on the scattered field received for any polarization of transmitter and receiver may be expressed in terms of a scattering matrix and how this matrix may be derived from certain measurements of field intensity and phase.

The physical setup which concerns us consists of a transmitter which sends out a plane-polarized wave of specified frequency and which can be rotated about the line of propagation, i.e., beam axis; a target which scatters the transmitted beam, located at sufficient distance from the transmitter so that the far-zone assumptions are valid; and a receiver which is effectively superimposed on the transmitter but which can be rotated independently about the line which joins it to the target. In this situation both the transmitted and received fields will be essentially transverse and the orientations of the transmitter and receiver can be specified in terms of the directions of the electric vectors. In general, at wavelengths of the order of magnitude of the target dimensions, the intensity of the field received from a particular target at a particular frequency and amplitude of the

incident field will vary with the orientations of transmitter and receiver in a manner which is characteristic of the target and frequency. (Here the target is assumed fixed with respect to location of transmitter and receiver. If the target is a movable body, the variation referred to will depend also on the aspect it presents to the transmitter-receiver.)

It follows from the essential nature of the field equations that this polarization dependence will be linear, and consequently it can be described completely in terms of a two-dimensional matrix, which is known as the scattering matrix and which may be defined in the following manner.

Since the field at the transmitter-receiver location is transverse, the electric and magnetic vectors of both the transmitted (incident) and received (scattered) fields lie in the plane normal to the line of sight to the target, or target direction, and therefore each can be expressed as a linear combination of two arbitrary basis vectors in this plane. For simplicity and uniformity we choose the horizontal and vertical directions for these basis vectors (assuming the target direction is horizontal) and designate them by $\hat{p}_h$ and $\hat{p}_v$. The electric (or magnetic) vectors of the incident and scattered fields can be expressed in terms of the basis vectors thus (for the electric vectors)

$$\vec{E}^i = E_h^i \hat{p}_h + E_v^i \hat{p}_v$$

$$\vec{E}^s = E_h^s \hat{p}_h + E_v^s \hat{p}_v ,$$

Since both vectors are expressible in terms of the same basis, there is a linear transformation which converts one into the other. This is most conveniently specified as a matrix, which is called the scattering matrix, and which depends, as previously indicated, on the target characteristics and wavelength.

Specifically, we write the transformation in the form

$$\begin{aligned} E_h^s &= S_{hh} E_h^i + S_{hv} E_v^i \\ E_v^s &= S_{vh} E_h^i + S_{vv} E_v^i \end{aligned} \qquad \text{(A-1)}$$

which is equivalent to the matrix form

$$\begin{pmatrix} E_h^s \\ E_v^s \end{pmatrix} = \begin{pmatrix} S_{hh} & S_{hv} \\ S_{vh} & S_{vv} \end{pmatrix} \begin{pmatrix} E_h^i \\ E_v^i \end{pmatrix} , \qquad \text{(A-2)}$$

in which the square matrix on the right-hand side is the scattering matrix. Once the elements of this matrix are known, it is clear that the horizontal and vertical components of the scattered electric vector are given immediately in terms of those of the incident vector. Furthermore the reciprocity theorem, which states that the field measurements will be unaltered if the transmitter and receiver are interchanged, and which certainly holds in the laboratory experiments considered here, assures that the matrix is symmetric, i.e., $S_{vh} = S_{hv}$, so that only three

quantities are necessary for complete knowledge of the matrix. These three quantities are directly determinable, in theory at least, by three measurements*, one with both transmitter and receiver oriented horizontally, one with both oriented vertically, and one with one horizontal and the other vertical. However, this is not the only set of measurements which is sufficient to determine the matrix. Since any two non-collinear basis vectors span the space in question, namely the plane normal to the target direction, it follows that knowledge of the components of a vector referred to one basis determines the components in any other basis provided the relation between the two bases is given. For example, suppose we consider a basis consisting of the vectors $\hat{p}_a$ and $\hat{p}_b$, which are inclined at an angle α with respect to $\hat{p}_h$ and $\hat{p}_v$ respectively. Then the components of the vector $\vec{E}^s$ referred to the new basis are given in terms of those in the old basis by the equations

$$\begin{aligned} E^s_a &= E^s_h \cos\alpha + E^s_v \sin\alpha \\ E^s_b &= -E^s_h \sin\alpha + E^s_v \cos\alpha . \end{aligned} \qquad \text{(A-3)}$$

These can be combined with Equation (A-1) to express E^s_a and E^s_b in terms of E^i_h and E^i_v as follows:

$$E^s_a = (\cos\alpha\, S_{hh} + \sin\alpha\, S_{vh})\, E^i_h + (\cos\alpha\, S_{hv} + \sin\alpha\, S_{vv})\, E^i_v$$

$$E^s_b = (-\sin\alpha\, S_{hh} + \cos\alpha\, S_{vh})\, E^i_h + (-\sin\alpha\, S_{hv} + \cos\alpha\, S_{vv})\, E^i_v$$

* Measuring both amplitude and phase of each complex number.

or in matrix form

$$\begin{pmatrix} E^s_a \\ E^s_b \end{pmatrix} = \begin{pmatrix} S_{ah} & S_{av} \\ S_{bh} & S_{bv} \end{pmatrix} \begin{pmatrix} E^i_h \\ E^i_v \end{pmatrix} \tag{A-4}$$

where

$$\begin{aligned} S_{ah} &\equiv \cos\alpha\, S_{hh} + \sin\alpha\, S_{vh} \\ S_{av} &\equiv \cos\alpha\, S_{hv} + \sin\alpha\, S_{vv} \\ S_{bh} &\equiv -\sin\alpha\, S_{hh} + \cos\alpha\, S_{vh} \\ S_{bv} &\equiv -\sin\alpha\, S_{hv} + \cos\alpha\, S_{vv} \end{aligned} \tag{A-5}$$

This new scattering matrix, which results from the rotation of the basis for the scattered wave, can be considered as the (matrix) product of the original scattering matrix and the matrix of the rotation, i. e.

$$\begin{pmatrix} S_{ah} & S_{av} \\ S_{bh} & S_{bv} \end{pmatrix} = \begin{pmatrix} \cos\alpha & \sin\alpha \\ -\sin\alpha & \cos\alpha \end{pmatrix} \cdot \begin{pmatrix} S_{hh} & S_{hv} \\ S_{vh} & S_{vv} \end{pmatrix} , \tag{A-6}$$

which is the matrix form of the set of equations (A-5).

There is still another scattering matrix of interest, which expresses the a and b components of the scattered wave in terms of the corresponding ones for the incident wave, in analogy with equations (A-1) and (A-2). Thus

$$\begin{aligned} E^s_a &= S_{aa} E^i_a + S_{ab} E^i_b \\ E^s_b &= S_{ba} E^i_a + S_{bb} E^i_b \end{aligned} \tag{A-7}$$

or

$$\begin{pmatrix} E_a^s \\ E_b^s \end{pmatrix} = \begin{pmatrix} S_{aa} & S_{ab} \\ S_{ba} & S_{bb} \end{pmatrix} \begin{pmatrix} E_a^i \\ E_b^i \end{pmatrix} \quad . \tag{A-8}$$

The three scattering matrices appearing in Equations (A-2), (A-4) and (A-8) are clearly not independent and are, in fact, essentially equivalent in the sense that knowledge of one of the three plus the angle α determines the other two. For in analogy with Equation (A-3) we can write for the incident field

$$\begin{pmatrix} E_a^i \\ E_b^i \end{pmatrix} = \begin{pmatrix} \cos\alpha & \sin\alpha \\ -\sin\alpha & \cos\alpha \end{pmatrix} \begin{pmatrix} E_h^i \\ E_v^i \end{pmatrix} , \tag{A-9}$$

which combined with (A-4), (A-6) and (A-8) yields

$$\begin{pmatrix} S_{ah} & S_{av} \\ S_{bh} & S_{bv} \end{pmatrix} \begin{pmatrix} E_h^i \\ E_v^i \end{pmatrix} = \begin{pmatrix} S_{aa} & S_{ab} \\ S_{ba} & S_{bb} \end{pmatrix} \begin{pmatrix} \cos\alpha & \sin\alpha \\ -\sin\alpha & \cos\alpha \end{pmatrix} \begin{pmatrix} E_h^i \\ E_v^i \end{pmatrix} = \begin{pmatrix} \cos\alpha & \sin\alpha \\ -\sin\alpha & \cos\alpha \end{pmatrix} \begin{pmatrix} S_{hh} & S_{hv} \\ S_{vh} & S_{vv} \end{pmatrix} \begin{pmatrix} E_h^i \\ E_v^i \end{pmatrix} \tag{A-10}$$

and since the components E_h^i and E_v^i are independent variables, the vector (or column matrix $\begin{pmatrix} E_h^i \\ E_v^i \end{pmatrix}$ may be in effect cancelled in each member of (A-10) to leave

$$\begin{pmatrix} S_{ah} & S_{av} \\ S_{bh} & S_{bv} \end{pmatrix} = \begin{pmatrix} S_{aa} & S_{ab} \\ S_{ba} & S_{bb} \end{pmatrix} \begin{pmatrix} \cos\alpha & \sin\alpha \\ -\sin\alpha & \cos\alpha \end{pmatrix} = \begin{pmatrix} \cos\alpha & \sin\alpha \\ -\sin\alpha & \cos\alpha \end{pmatrix} \begin{pmatrix} S_{hh} & S_{hv} \\ S_{vh} & S_{vv} \end{pmatrix} \quad . \tag{A-11}$$

It should be noted that the elements S_{ij} of the scattering matrices are in general complex quantities, each one involving an amplitude and a phase. The above relations hold also if the rotation performed on the axes is complex. Such would be the case if transmitter and receiver were separated by a distance appreciable in relation to the target range, or if the distance of either or both from the target were altered by an amount appreciable in terms of the wavelength. In the present circumstance neither of these conditions is considered, and the angle α is taken as a real quantity.

Upon carrying out the matrix multiplications indicated in Equation (A-11) and equating the corresponding elements of the resulting 4 x 4 matrices it is seen that these matrix equations are equivalent to the following system of algebraic equations:

$$\begin{aligned}
S_{ah} &= S_{aa}\cos\alpha - S_{ab}\sin\alpha = S_{hh}\cos\alpha + S_{vh}\sin\alpha \\
S_{av} &= S_{aa}\sin\alpha + S_{ab}\cos\alpha = S_{hv}\cos\alpha + S_{vv}\sin\alpha \\
S_{bh} &= S_{ba}\cos\alpha - S_{bb}\sin\alpha = -S_{hh}\sin\alpha + S_{vh}\cos\alpha \\
S_{bv} &= S_{ba}\sin\alpha + S_{bb}\cos\alpha = -S_{hv}\sin\alpha + S_{vv}\cos\alpha .
\end{aligned} \tag{A-12}$$

This system consists formally of 8 equations in the 12 elements S_{ij} of the scattering matrices. However, as noted previously, two of the matrices are symmetric; i.e., $S_{hv} = S_{vh}$ and $S_{ab} = S_{ba}$. Furthermore, considering the righthand equalities, if we eliminate S_{aa} between the first two and S_{bb} between the second

two, the resulting expressions are identical, which reduces the number of equations to seven involving the ten values S_{ij}. These are conveniently listed in the following form (though of course there are many possible alternatives),

$$
\begin{aligned}
S_{ah} &= S_{hh}\cos\alpha + S_{vh}\sin\alpha \\
S_{av} &= S_{hv}\cos\alpha + S_{vv}\sin\alpha \\
S_{bh} &= -S_{hh}\sin\alpha + S_{vh}\cos\alpha \\
S_{bv} &= -S_{hv}\sin\alpha + S_{vv}\cos\alpha \\
S_{aa} &= S_{hh}\cos^2\alpha + S_{hv}\sin 2\alpha + S_{vv}\sin^2\alpha \\
S_{ab} &= -\frac{1}{2}S_{hh}\sin 2\alpha + S_{vh}\cos 2\alpha + \frac{1}{2}S_{vv}\sin 2\alpha \\
S_{bb} &= S_{hh}\sin^2\alpha - S_{vh}\sin 2\alpha + S_{vv}\cos^2\alpha.
\end{aligned}
\qquad \text{(A-13)}
$$

These may be treated as fourteen real equations in the twenty real quantities which specify the ten complex elements. Knowledge of six of these real quantities (or alternatively three complex ones) should then be sufficient to determine all the rest. However, it is clear that not every such set is sufficient. For example, if we know three complex quantities all of which appear in one of the three-term equations of (A-13), we can determine one more element, but nothing further. Any set of three elements which do not all appear in one three-term equation is sufficient to determine the system in general, though for certain values of α some of the coefficients vanish and this rule does not hold.

If we consider the real and imaginary parts of the complex elements S_{ij} individually, a similar situation prevails. Since the coefficients in the Equations (A-13) are limited to real numbers, there are two separate and formally identical systems for the real and imaginary parts. Each system is determined by any set of three quantities not all of which appear in any one three-term equation. It is not necessary to know the corresponding sets in the two systems.

In terms of the phases and amplitudes of the elements, the situation is more complicated. Here the determination of the system involves solution of quadratic and inverse trigonometric equations, which in general yield extraneous values of the amplitudes and phases. Unless the correct values can be selected on physical grounds, at least one extra measurement is usually required to remove the ambiguity. In this regard, it should also be noted that an absolute phase of one element alone has no meaning in relation to the scattering matrix, and that knowledge of the phase of an element implies knowledge of the difference between this phase and that of another element arbitrarily chosen as the basis of reference. It follows that knowledge of five real quantities, amplitudes and/or phases, should be sufficient to determine the system, since the absolute phases are of no concern. Again it is clear that not every set of five quantities is sufficient, since if all five appear in one three-term equation, the most that can be determined are two more phases or amplitudes. As noted in Section II it would

suffice to measure $|S_{hh}|$, $|S_{vv}|$, $|S_{hv}|$, and any two of the phases ϕ_{hh}, ϕ_{vv}, and ϕ_{hv}, with the elements S_{ij} written $S_{ij} = |S_{ij}| e^{i\phi_{ij}}$. If α, i.e. the angle specifying the direction a, is $\pi/4$, then given any five of the following six quantities: $|S_{ah}|$, $|S_{av}|$, $|S_{hh}|$, $|S_{vv}|$, ϕ_{hh}, ϕ_{vv}, where the two phases are given in terms of some arbitrary third phase, which we may take to be that of S_{hv} for convenience, it is possible to determine phases and amplitudes of all the rest of the elements appearing in Equations (A-13) (up to the ambiguity in sign mentioned previously).

To show this we first observe that the righthand sides of Equations (A-13) contain only the three elements S_{hh}, S_{vv}, and S_{hv}, so that once these are known completely, all the rest of the elements are given explicitly. The only remaining problem is to determine $|S_{hv}|$ and whichever component of S_{hh} or S_{vv} is not given, if any. The first two of Equations (A-13) will yield this information in any case. We write these in squared form in order to deal with phases and amplitudes directly, thus

$$2|S_{ah}|^2 = |S_{hh}|^2 + |S_{hv}|^2 + 2|S_{hh}\,S_{hv}| \cos(\phi_{hh} - \phi_{hv}) \qquad \text{(A-14)}$$

$$2|S_{av}|^2 = |S_{hv}|^2 + |S_{vv}|^2 + 2|S_{hv}\,S_{vv}| \cos(\phi_{hv} - \phi_{vv}). \qquad \text{(A-15)}$$

No matter which of the above six quantities is lacking in the given data, one or the other of these equations will serve to determine it, and the remaining one will give $|S_{hv}|$, provided always that extraneous roots can be eliminated.

In the absence of physical arguments to indicate which roots are valid, the question can be settled in general by employing additional equations, which may of course require more data.

If the measured phases are given in terms of some phase other than ϕ_{hv}, certain other manipulations are required. For example, if ϕ_{ah} or ϕ_{av} is used as the reference quantity, then certain equations of (A-13) may be rearranged before squaring so that only the given phase differences appear explicitly. Instead of (A-14) we might have, for instance,

$$2\left|S_{hv}\right|^2 = \left|S_{ah}\right|^2 + 2\left|S_{hh}\right|^2 - 2\sqrt{2}\left|S_{ah}\,S_{hh}\right|\cos\left(\phi_{ah} - \phi_{hh}\right). \quad \text{(A-16)}$$

If neither ϕ_{ah} nor ϕ_{av} is used as reference, then other equations of (A-13) or possibly combinations of these must be employed. No general scheme presents itself for handling an arbitrary case of this sort, and the possibilities are too numerous for individual treatment here. We proceed instead to establish another theorem which is of some practical importance, and which depends on the following considerations.

The energy density of the scattered field per unit time at a given point in the far zone is a function of the scattering characteristics and aspect of the scatterer and of the intensity and polarization of the incident field. This energy density is proportional to the quantity $\left|\vec{E}^S\right|^2$, and a measure of it is the radar cross section σ, which may be defined by the expression

$$\sigma = \lim_{r \to \infty} \left\{ 4\pi r^2 \left| \frac{\vec{E}^s}{\vec{E}^i} \right|^2 \right\} . \qquad \text{(A-17)}$$

The measured value of this quantity will of course depend on the orientation of the receiver with respect to the polarization direction of the scattered wave, and this in turn, as well as the amplitude of the latter, depends on the amplitude and polarization of the incident wave. Assuming the incident amplitude is unity i.e. $\left|\vec{E}^i\right| = 1$, we can write the measured cross section as a function of the two polarization directions as follows:

$$\sigma_{jk} = \lim_{r \to \infty} 4\pi r^2 \left| \vec{E}^s_k \cdot \hat{p}_j \right|^2 \qquad \text{(A-18)}$$

where $\hat{p}_j$ is a unit vector in the direction of the receiver polarization, and $\vec{E}^s_k$ is the electric vector of the scattered field produced by an incident wave of unit amplitude with electric vector in the direction $\hat{k}$. The quantity $\vec{E}^s_k \cdot \hat{p}_j$ is, according to the notation used earlier, exactly E^s_j which by Equation (A-4) with a = j we can write as

$$E^s_j = S_{jh} E^i_h + S_{jv} E^i_v . \qquad \text{(A-19)}$$

But since the relation between a and the hv basis was arbitrary, we can just as well consider a basis parallel and perpendicular to k, i.e. let h = k, whereupon E^i_h becomes $E^i_k = 1$ and $E^i_v = 0$, so that $E^s_j = S_{jk}$. The measured cross section

(A-18) thus becomes

$$\sigma_{jk} = \lim_{r\to\infty} 4\pi r^2 \left| S_{jk} \right|^2 . \qquad \text{(A-20)}$$

Now if we consider any direction ℓ perpendicular to j we can substitute this direction for b in Equation (A-4), which then becomes

$$\begin{pmatrix} E^s_j \\ E^s_\ell \end{pmatrix} = \begin{pmatrix} S_{jk} S_{jm} \\ S_{\ell k} S_{\ell m} \end{pmatrix} \begin{pmatrix} 1 \\ 0 \end{pmatrix} = \begin{pmatrix} S_{jk} \\ S_{\ell k} \end{pmatrix} \qquad \text{(A-21)}$$

where m is perpendicular to k. By Equations (A-17), (A-20) and (A-21) we can now write

$$\sigma = \lim_{r\to\infty} 4\pi r^2 \left| \vec{E}^s \right|^2 = \lim_{r\to\infty} 4\pi r^2 \left[\left| S_{jk} \right|^2 + \left| S_{\ell k} \right|^2 \right] \qquad \text{(A-22)}$$

$$= \sigma_{jk} + \sigma_{\ell k} .$$

But this quantity, as observed earlier, depends only on the characteristics of scatterer and transmitted field and not on receiver polarization. We thus have: Given a scatterer of fixed aspect and a transmitted field of fixed amplitude and polarization the sum of the measured cross sections for any two orthogonal receiver polarizations is constant.

The fact is of course useful as a simple check on the consistency of cross section data measured in the laboratory. A more comprehensive check,

which involves the phases of the measured fields as well as the amplitudes, is afforded by Equations (A-13). If more quantities are measured than the minimum number required to determine the system, then one or more of these equations or at least an equation derivable from them must be satisfied identically by the measured values. The more measured values available, the more equations involving only these quantities should be derivable, though the functional relation between these two numbers and the number of quantities in each equation may be complicated. For the case of the investigation actually carried out, a procedure was developed as follows.

In this investigation, phase and amplitude measurements of the scattered fields for various bodies were made with six different polarization combinations, namely vv, hh, aa, ah, av, and bb, where the angle α, i.e. angle between a and h directions, was 45^{o}. With this many quantities available, a rather large number of equations may be derived which involve only these quantities. For example if we seek all such equations having four terms, we would have 15 equations. In the case at hand certain coefficients vanish, leaving three equations identical and with only three non-zero terms. Thus, the consistency check was conducted with 13 equations, those listed in Section III (Equation 3-1). The treatment of these equations is described in Section III.

REFERENCES

1. M. L. Barasch, W. E. Burdick, J. W. Crispin, Jr., B. A. Harrison, R. E. Kleinman, R. J. Leite, D. M. Raybin, T. B. A. Senior, K. M. Siegel, and H. Weil, "Studies in Radar Cross Sections XXIX - Determination of Spin, Tumbling Rates, and Sizes of Satellites and Missiles", University of Michigan Report No. 2758-1-T (April 1959). SECRET

2. A. L. Maffett, M. L. Barasch, W. E. Burdick, R. F. Goodrich, W. C. Orthwein, C. E. Schensted and K. M. Siegel, "Studies in Radar Cross Sections XVII - Complete Scattering Matrices and Circular Polarization Cross Sections for the B-47 Aircraft at S-band", University of Michigan Report No. 2260-6-T (June 1955). CONFIDENTIAL

3. H. Brysk, "Measurement of the Scattering Matrix with an Intervening Ionosphere", Communications and Electronics, 611 (1958).

4. K. M. Siegel, "Increasing the Effective Dynamic Range of a Radar". Paper presented at AIEE Great Lakes District Meeting, East Lansing (May 5-7, 1958).

5. "Radio Observations of the Russian Earth Satellite", Mullard Radio Astronomy Observatory, Cambridge, Nature, 180, 879 (1957).

6. K. M. Siegel, M. L. Barasch, J. W. Crispin, Jr., R. F. Goodrich, A. H. Halpin, A. L. Maffett, W. C. Orthwein, C. E. Schensted, and C. J. Titus, "Studies in Radar Cross Sections XVIII - Airborne Passive Measures and Countermeasures", University of Michigan Report No. 2260-29-F (January 1956). SECRET

7. E. M. Kennaugh, A. F. Buttler and L. S. Taylor, "Effects of the Type of Polarization on Echo Characteristics", OSURF 389-9 (16 June 1951).UNCLASSIFIED

8. "Project Michigan - Radar and Communications", University of Michigan Report 2144-30-P (January 1955). SECRET

9. J. W. Crispin, Jr., R. F. Goodrich, and K. M. Siegel, "A Theoretical Method for the Calculation of the Radar Cross Section of Aircraft and Missiles", University of Michigan Report No. 2591-1-H, (July 1959). UNCLASSIFIED

10. J. R. Mentzer, Scattering and Diffraction of Radio Waves, Pergamon Press (1955).

11. K. M. Siegel, M. L. Barasch, J. W. Crispin, Jr., W. C. Orthwein, I. V. Schensted, and H. Weil, "Studies in Radar Cross Sections XIV - Radar Cross Section of a Ballistic Missile", University of Michigan Report No. UMM-134 (September 1954). SECRET

The University of Michigan, Ann Arbor, Michigan
THE MEASUREMENT AND USE OF SCATTERING MATRICES
J. W. Crispin Jr., R. E. Hiatt, R. B. Sleator
and K. M. Siegel

Radiation Laboratory Report No. 2500-3-T, February, 1961, 123 pp., Aeronutronic Purchase Order No. SC - 11334, Unclassified Report.

An experimental and theoretical investigation of the reflection characteristics of an IRBM type missile is described. The complete scattering matrix was determined for several aspects for the Jupiter C with and without the tail fins and for the Jupiter C nose cone. Good agreement was found between experimental and theoretical data. Experimental data from "unknown" models was analyzed to determine the possibility of identifying a target by means of scattering matrix data.

Unclassified

1. Scattering Matrices
2. P. O. No. SC-11334
3. Aeronutronic a division of Ford Motor Co. Space Technology Operations Newport Beach, California

The University of Michigan, Ann Arbor, Michigan
THE MEASUREMENT AND USE OF SCATTERING MATRICES
J. W. Crispin Jr., R. E. Hiatt, R. B. Sleator
and K. M. Siegel

Radiation Laboratory Report No. 2500-3-T, February, 1961, 123 pp., Aeronutronic Purchase Order No. SC - 11334, Unclassified Report.

An experimental and theoretical investigation of the reflection characteristics of an IRBM type missile is described. The complete scattering matrix was determined for several aspects for the Jupiter C with and without the tail fins and for the Jupiter C nose cone. Good agreement was found between experimental and theoretical data. Experimental data from "unknown" models was analyzed to determine the possibility of identifying a target by means of scattering matrix data.

Unclassified

1. Scattering Matrices
2. P. O. No. SC-11334
3. Aeronutronic a division of Ford Motor Co. Space Technology Operations Newport Beach, California

The University of Michigan, Ann Arbor, Michigan
THE MEASUREMENT AND USE OF SCATTERING MATRICES
J. W. Crispin Jr., R. E. Hiatt, R. B. Sleator
and K. M. Siegel

Radiation Laboratory Report No. 2500-3-T, February, 1961, 123 pp., Aeronutronic Purchase Order No. SC - 11334, Unclassified Report.

An experimental and theoretical investigation of the reflection characteristics of an IRBM type missile is described. The complete scattering matrix was determined for several aspects for the Jupiter C with and without the tail fins and for the Jupiter C nose cone. Good agreement was found between experimental and theoretical data. Experimental data from "unknown" models was analyzed to determine the possibility of identifying a target by means of scattering matrix data.

Unclassified

1. Scattering Matrices
2. P. O. No. SC-11334
3. Aeronutronic a division of Ford Motor Co. Space Technology Operations Newport Beach, California

The University of Michigan, Ann Arbor, Michigan
THE MEASUREMENT AND USE OF SCATTERING MATRICES
J. W. Crispin Jr., R. E. Hiatt, R. B. Sleator
and K. M. Siegel

Radiation Laboratory Report No. 2500-3-T, February, 1961, 123 pp., Aeronutronic Purchase Order No. SC - 11334, Unclassified Report.

An experimental and theoretical investigation of the reflection characteristics of an IRBM type missile is described. The complete scattering matrix was determined for several aspects for the Jupiter C with and without the tail fins and for the Jupiter C nose cone. Good agreement was found between experimental and theoretical data. Experimental data from "unknown" models was analyzed to determine the possibility of identifying a target by means of scattering matrix data.

Unclassified

1. Scattering Matrices
2. P. O. No. SC-11334
3. Aeronutronic a division of Ford Motor Co. Space Technology Operations Newport Beach, California

The University of Michigan, Ann Arbor, Michigan
THE MEASUREMENT AND USE OF SCATTERING MATRICES
J. W. Crispin Jr., R. E. Hiatt, R. B. Sleator
and K. M. Siegel

Radiation Laboratory Report No. 2500-3-T, February, 1961, 123 pp., Aeronutronic Purchase Order No. SC - 11334, Unclassified Report.

An experimental and theoretical investigation of the reflection characteristics of an IRBM type missile is described. The complete scattering matrix was determined for several aspects for the Jupiter C with and without the tail fins and for the Jupiter C nose cone. Good agreement was found between experimental and theoretical data. Experimental data from "unknown" models was analyzed to determine the possibility of identifying a target by means of scattering matrix data.

Unclassified

1. Scattering Matrices
2. P. O. No. SC-11334
3. Aeronutronic a division of Ford Motor Co. Space Technology Operations Newport Beach, California

The University of Michigan, Ann Arbor, Michigan
THE MEASUREMENT AND USE OF SCATTERING MATRICES
J. W. Crispin Jr., R. E. Hiatt, R. B. Sleator
and K. M. Siegel

Radiation Laboratory Report No. 2500-3-T, February, 1961, 123 pp., Aeronutronic Purchase Order No. SC - 11334, Unclassified Report.

An experimental and theoretical investigation of the reflection characteristics of an IRBM type missile is described. The complete scattering matrix was determined for several aspects for the Jupiter C with and without the tail fins and for the Jupiter C nose cone. Good agreement was found between experimental and theoretical data. Experimental data from "unknown" models was analyzed to determine the possibility of identifying a target by means of scattering matrix data.

Unclassified

1. Scattering Matrices
2. P. O. No. SC-11334
3. Aeronutronic a division of Ford Motor Co. Space Technology Operations Newport Beach, California

The University of Michigan, Ann Arbor, Michigan
THE MEASUREMENT AND USE OF SCATTERING MATRICES
J. W. Crispin Jr., R. E. Hiatt, R. B. Sleator
and K. M. Siegel

Radiation Laboratory Report No. 2500-3-T, February, 1961, 123 pp., Aeronutronic Purchase Order No. SC - 11334, Unclassified Report.

An experimental and theoretical investigation of the reflection characteristics of an IRBM type missile is described. The complete scattering matrix was determined for several aspects for the Jupiter C with and without the tail fins and for the Jupiter C nose cone. Good agreement was found between experimental and theoretical data. Experimental data from "unknown" models was analyzed to determine the possibility of identifying a target by means of scattering matrix data.

Unclassified

1. Scattering Matrices
2. P. O. No. SC-11334
3. Aeronutronic a division of Ford Motor Co. Space Technology Operations Newport Beach, California

The University of Michigan, Ann Arbor, Michigan
THE MEASUREMENT AND USE OF SCATTERING MATRICES
J. W. Crispin Jr., R. E. Hiatt, R. B. Sleator
and K. M. Siegel

Radiation Laboratory Report No. 2500-3-T, February, 1961, 123 pp., Aeronutronic Purchase Order No. SC - 11334, Unclassified Report.

An experimental and theoretical investigation of the reflection characteristics of an IRBM type missile is described. The complete scattering matrix was determined for several aspects for the Jupiter C with and without the tail fins and for the Jupiter C nose cone. Good agreement was found between experimental and theoretical data. Experimental data from "unknown" models was analyzed to determine the possibility of identifying a target by means of scattering matrix data.

Unclassified

1. Scattering Matrices
2. P. O. No. SC-11334
3. Aeronutronic a division of Ford Motor Co. Space Technology Operations Newport Beach, California